Insights into the reactivity of H_2CO_3 and its derivatives in bulk water, water clusters, and at the air/water interface: Ab initio molecular dynamics and metadynamics studies

by

Mirza Galib

A thesis submitted in partial fulfillment of the requirements for the degree of

Doctor of Philosophy

Department of Chemistry

University of Alberta

Abstract

H_2CO_3 can decompose into CO_2 in water either via the water route ($H_2CO_3 \rightleftharpoons CO_2 + H_2O$) or the hydroxide route ($H_2CO_3 + H_2O \rightleftharpoons CO_2 + OH^- + H_3O^+$). The water route reactions play a fundamental role in the global carbon cycle, and the hydroxide route reactions play an important role in the regulation of blood pH and the transport of CO_2 during respiration. Despite the plethora of experimental work on these reactions in water, a microscopic understanding of the underlying mechanisms was lacking due to a shortage of theoretical work. In this thesis, we employed Car-Parrinello molecular dynamics and metadynamics to ascertain the microscopic mechanisms and compute the free energy changes and barriers of a series of reactions involving H_2CO_3, HCO_3^-, and CO_2 in bulk water, water clusters, and at the air/water interface in order to shed much needed light on these reactions.

Before delving into the reactivity of H_2CO_3 in water, we investigated the energetics and mechanisms of the conformational changes of the cis-cis (CC), cis-trans (CT), and trans-trans (TT) conformers of H_2CO_3 in water. The free energy barriers/changes for the various conformational changes via the change in one of the

two dihedral angles were calculated and contrasted with the previously calculated values for the gas phase.

We then investigated the energetics and mechanisms of the dissociation ($H_2CO_3 \rightleftarrows HCO_3^- + H^+$) and hydroxide-route decomposition ($HCO_3^- \rightarrow CO_2 + OH^-$) of all three conformers of H_2CO_3 in water. The CT and TT conformers were found to undergo decomposition in water via a two-step process: dissociation followed by decomposition. This is in contrast with the concerted mechanism proposed for the gas phase, which involves a dehydroxylation of one of the OH groups and a simultaneous deprotonation of the other OH group to yield CO_2 and H_2O. Our calculated pK_a values and decomposition free energy barriers for the CT and TT conformers are consistent with the experimental values.

The decomposition of H_2CO_3 in different-sized water clusters was investigated to determine whether the concerted or step-wise mechanism predominates in bulk water. We found that in the small clusters (containing 6 and 9 water molecules), the decomposition occurs via a concerted proton shuttle mechanism involving a cyclic transition state, whereas in the larger clusters (containing 20 and 45 water molecules), the decomposition follows a two-step mechanism involving a solvent-separated HCO_3^-/H_3O^+ ion pair intermediate. The larger clusters contain a sufficient number of water molecules to fully solvate the H_3O^+ intermediate, a prerequisite for the step-wise reaction. Our results demonstrated that the decomposition of H_2CO_3 predominantly occurs via the step-wise mechanism in bulk water.

The dissociation of H_2CO_3 at the air/water interface was then studied. Our results

indicated that H_2CO_3 dissociates faster at the water surface than in bulk water, in contrast to recent experiments and simulations which have shown that HNO_3 has a lower propensity to dissociate at the water surface than in bulk water. We found that, at the water surface, there is a more structured solvation environment around H_2CO_3 than in bulk water, which leads to a decrease in the dissociation energy barrier via a stabilization of the transition state relative to the undissociated acid.

We then investigated the hydration of CO_2 to form HCO_3^- (i.e., CO_2 + 2 $H_2O \rightarrow HCO_3^- + H_3O^+$) at the air/water interface. We found that CO_2 is weakly solvated, even more so than in the bulk due to a deficiency of water molecules at the surface. Both the reaction mechanism and dissociation energy barrier were found to be similar to those in bulk water. Although the energy barrier was initially expected to be different, our result was not surprising given the fact that CO_2 is weakly solvated in both environments.

The insights gained from this thesis have implications on understanding CO_2 and H_2CO_3 chemistry in a variety of environments encountered in atmospheric and geological chemistry and set the stage for further kinetic and thermodynamic studies in a wide range of aqueous environments with different morphologies and compositions.

Acknowledgement

I would like to express my deepest gratitude to my supervisor, Dr. Gabriel Hanna, for his excellent guidance, patience, support and providing me with a beautiful atmosphere for doing research. This was an exciting journey which began five years back with Dr. Hanna and now it is coming to an end for new beginnings. It was my pleasure to have such an effective and engaging guide throughout my PhD research.

I would also like to thank the members of my supervisory committee Dr. Mariusz Klobukowski and Dr. Frederick West for their sincere monitoring, cooperation, and advices. I also would like to thank Dr. Yunjie Xu and Dr. Jack Tuszynski for their valuable suggestions and encouragements.

I would like to thank my fellow group members, Farnaz Shakib and Franz Martinez, who were always good friends and helpful group mates.

Special thanks to the National Science and Engineering Research Council of Canada (NSERC) and University of Alberta Chemistry department for their funding, without which, nothing would be possible. I am also grateful to Compute Canada which provided the computational resources necessary for my project.

Finally, I would like to thank my wife, Mashuda Amatullah. She was always there encouraging me with trust, love, and smiling beauty.

Contents

List of Figures

List of Tables

Abbreviations

AIMD	ab initio molecular dynamics
BLYP	Becke-Lee-Yang-Parr functional
CBS	complete basis set method
CC	cis-cis
CPCM	conductor-like polarizable continuum model
CPMD	Car-Parrinello molecular dynamics
CT	cis-trans
CV	collective variable
DFT	density functional theory
fs	femtosecond
MD	molecular dynamics
MTD	metadynamics
ps	picosecond
SFG	sum frequency generation
TT	trans-trans

Chapter 1

Introduction

1.1 Basics of carbonic acid chemistry

The acid-base chemistry of carbonic acid (H_2CO_3) has received much attention over the years due to its importance in many environmental, industrial, and biological processes[4–8]. H_2CO_3 forms by the reaction of CO_2 with either water (known as the water route) or with the hydroxide ion (known as the hydroxide route). The corresponding reverse reactions are the decompositions of H_2CO_3 into CO_2 and H_2O and CO_2 and OH^-, respectively. In the presence of water, H_2CO_3 may also undergo dissociation into HCO_3^- and H_3O^+. These reactions are summarized below:

$$\mathrm{CO_2(aq) + H_2O \rightleftharpoons H_2CO_3} \tag{1.1}$$

$$\mathrm{CO_2(aq) + OH^- \rightleftharpoons HCO_3^- \rightleftharpoons H_2CO_3} \tag{1.2}$$

$$\mathrm{H_2CO_3 + H_2O \rightleftharpoons HCO_3^- + H_3O^+} \tag{1.3}$$

The water route reactions play a fundamental role in the global carbon cycle, i.e., atmospheric CO_2 dissolves into the ocean → a fraction of the dissolved CO_2 reacts with water to form H_2CO_3 → H_2CO_3 dissociates into HCO_3^- and H_3O^+, thereby increasing the acidity of the ocean[9, 10], The hydroxide route reactions, with the aid of carbonic anhydrases (which increase the rate of hydroxylation of CO_2 by a factor of 70), play an important role in the regulation of blood pH and in the transport of CO_2 during respiration[11–13]. The pK_a value for the dissociation of H_2CO_3 was originally determined to be 6.4 (based on electromotive force and conductance measurements), suggesting that H_2CO_3 is a weak acid [14–16]. However, it was later found that this value does not correspond to the true pKa of H_2CO_3, since it includes the equilibrium of CO_2 with H_2O:

$$CO_2(aq) + 2H_2O \rightleftharpoons H_2CO_3 + H_2O \rightleftharpoons HCO_3^- + H_3O^+ \tag{1.4}$$

The true pKa was later determined to be $3.4 - 3.8$ via stopped flow spectrophotometric measurements[17] and IR pump-probe spectroscopy [18], which revealed that H_2CO_3 could play a larger role in the acidification of water than originally thought.

1.2 Conformational changes of H_2CO_3 in water

H_2CO_3 can exist in three conformers [cis-cis (CC), cis-trans (CT) and trans-trans (TT)] in both the gas phase and in water (see Fig. 1.1 for a depiction of the conformers).

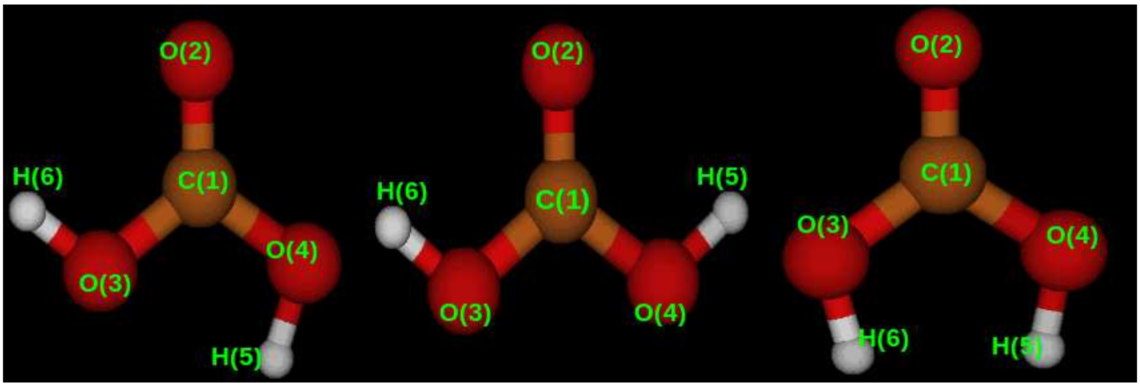

FIGURE 1.1: The three conformers of H_2CO_3. Left: Cis-trans (CT) conformer. Center: Trans-trans (TT) conformer. Right: Cis-cis (CC) conformer.

Fourier-transform microwave spectroscopy has positively identified CT and TT conformers in the gas phase[19, 20]. These conformers can be distinguished from one another via their two dihedral angles, defined by the relative positions of atoms O(2)-C(1)-O(4)-H(5) and O(2)-C(1)-O(3)-H(6) (see Fig. 1.1).

Using ab-inito metadynamics, it was found that in the gas phase the CC conformer is the least stable (7.9 kcal/mol higher in energy than the CT conformer) and the TT conformer is the most stable (only 1.5 kcal/mol lower in energy than the CT conformer)[1]. However, in the aqueous phase, their relative stabilities are expected to change due to interactions with the water molecules. In a CBS-QB3 study with CPCM continuum solvation, the order of stability of the three conformers with respect to the decomposition products (i.e., CO_2 and H_2O) was found to be CC $<$ CT $<$ TT, as in the gas phase[21]. However, the conformational free energy changes and barriers in water had not been previously calculated. Therefore, calculations of the free energy changes and barriers for the interconversions between all three conformers in the presence of explicit water molecules was warranted.

1.3 Dissociation and decomposition of H_2CO_3 in various aqueous environments

In the early 1960s, Eigen[22] proposed that the decomposition of H_2CO_3 in bulk water can occur via two different pathways, viz., a concerted pathway that does not involve a stable intermediate:

$$H_2CO_3 \rightleftharpoons CO_2 + H_2O \tag{1.5}$$

and a step-wise pathway that first involves the dissociation into stable HCO_3^- and H_3O^+ ions, followed by the decomposition into CO_2 and H_2O:

$$H_2CO_3 + H_2O \rightleftharpoons HCO_3^- + H_3O^+ \rightleftharpoons CO_2 + 2H_2O \tag{1.6}$$

Despite the fact that numerous experiments have been performed over the years to probe the kinetics and thermodynamics of the decomposition of H_2CO_3 in water, [17, 18, 23–30] they did not explicitly pin down the elementary steps of the decomposition mechanism. The dissociation and decomposition reactions of H_2CO_3 in the gas phase and in water have also been studied by theoretical techniques[1–3, 21, 31–38] . Previous quantum chemical[31, 33] and CPMD/metadynamics studies[1] have found that in the gas phase, H_2CO_3 decomposes into CO_2 and H_2O via a concerted mechanism, in which the C-O and O-H bonds break and the new O-H bond forms simultaneously. The energy barrier of this process was calculated to be $39 - 43$ kcal/mol[1, 31, 33], indicating that H_2CO_3 is kinetically stable in the gas phase (even at 300 K). However, quantum chemical studies have shown that in the presence of three water molecules, one of the hydroxyl hydrogens transfers to the other hydroxyl oxygen through a chain of two water molecules and then the C-O bond breaks, yielding a concerted pathway to the production of CO_2 and H_2O[34, 36]. The calculated energy barrier in the presence of these three water molecules was found to be $\sim$21 kcal/mol, approximately half of the gas phase barrier[34]. Despite this substantial reduction in the barrier, the calculated decomposition rate constant was still $\sim$50 times smaller than the experimentally measured rate constant of 10 s^{-1} at 293 K[34]. Therefore, the next logical step was to introduce more water molecules into the simulation for a more realistic treatment of the hydrogen bonding interactions in an effort to further bridge the gap between the experiment and theory. In this connection, CPMD/metadynamics simulations (involving 63 water molecules and periodic boundary conditions) were performed and the results suggested that the decomposition occurs via a step-wise pathway, first involving the formation of a stable HCO_3^-/H_3O^+ ion pair and then the breakage of the C-O bond in HCO_3^- to yield CO_2 and H_2O[2]. In addition, the dissociation of H_2CO_3 and its reverse reaction have been investigated by constrained ab initio molecular dynamics (involving 37 water molecules and periodic boundary conditions)[3]. In both studies, the authors calculated pK_a values of 3.4-3.7, which are in good agreement with the experimental value of 3.45 obtained in Ref. [18]. In light of all these studies, it became clear that further studies were needed to ascertain which mechanism dominates in bulk water. In addition, since the hydroxide route plays an essential role in human respiration[13], detailed theoretical studies which elucidate the mechanisms, energetics, and kinetics of these reactions are warranted.

Understanding the reactivity of H_2CO_3 in water clusters is also important since CO_2, H_2CO_3, and aqueous clusters are prevalent in the atmosphere. Reactions in clusters can be significantly different from those in bulk water due to differences in the solvation environment around the reactants[39–43]. In the upper troposphere, reactions between CO_2 and water clusters can form H_2CO_3 which then can undergo dissociation and decomposition[5]. Solid H_2CO_3 can also form in the upper troposphere from the reaction of mineral dust particles containing $CaCO_3$ and HCl[44]. Below 240 K, it does not undergo decomposition even under high relative humidities[44] and can sublime to form gaseous H_2CO_3[5]. Moreover, studying the reactions of H_2CO_3 in water clusters of increasing size can aid in understanding the transition from its gas to bulk phase reactivity[45–50]. Quantum chemical studies of CO_2-H_2O clusters have been conducted to investigate their stability and the possibility of binary nucleation in the atmosphere and their reactions[36, 51, 52]. However, little attention has been given to the decomposition reactions of H_2CO_3 in water clusters. Therefore, comprehensive studies of the mechanisms, energetics, and kinetics of these reactions are warranted, especially in light of the increasing levels of CO_2 in the atmosphere.

When H_2CO_3 (or any other acid gas molecule for that matter) approaches a water droplet or an aerosol in the atmosphere, it first comes into contact with its surface. Since, in general, the nature of the solvation at a heterogeneous interface can differ substantially from that in a homogeneous bulk medium[53–56], the energetics and kinetics of the dissociation and decomposition of H_2CO_3 at the air/water interface can change dramatically, especially given that hydrogen bonding interactions are known to play an instrumental role in these processes in bulk water. For example, X-ray photoelectron spectroscopy showed that HNO_3's degree of dissociation decreases by $\sim 20\%$ on the surface of water relative to in bulk water[43]. This study was accompanied by ab initio molecular dynamics simulations which found that the solvation environment around HNO_3 at the water surface is more structured than in bulk water, and could thereby stabilize the undissociated HNO_3. Another ab initio molecular dynamics study showed that HNO_3 remains undissociated on the surface of a water slab throughout a 20 ps simulation, suggestive of a more stable HNO_3 at the surface and a higher dissociation energy barrier than in the bulk (cf. in bulk, HNO_3 was found to dissociate within 0.5 ps)[42]. A classical molecular dynamics study of the hydration structure of NO_3^- revealed that the hydrogen bond distances between an oxygen of NO_3^- and adjacent water hydrogens increase at the surface compared to in the bulk (∼1.95 Å vs. ∼1.87 Å), suggesting that NO_3^- is preferentially stabilized in the bulk than at the surface[57]. Although these results can explain the shift in the equilibrium at the surface favouring HNO_3 over NO_3^-, it is not clear why the dissociation barrier increases at the surface. Hence, it is important to understand how the reactivity of H_2CO_3 changes at such a heterogeneous interface, especially in light of the increasing CO_2 levels in the atmosphere. To date, no experimental or theoretical studies of the dissociation and decomposition of H_2CO_3 at the air/water interface have been carried out. Therefore, studies that probe the kinetics, energetics, and nature of the hydrogen bonding interactions between the acid, its conjugate base, and the water surface are required.

1.4 Hydration of CO_2 at the air/water interface

The uptake of CO_2 by atmospheric aerosols and water bodies plays an important role in their acidification[9, 30, 53–55]. The reaction of CO_2 with H_2O in the gas phase and in bulk water has been investigated both theoretically[1–3, 21, 31–38, 58] and experimentally[17, 23–30]. The CO_2/H_2O interface has also been studied using classical and ab initio molecular dynamics under low CO_2 pressure conditions[59–61], clathrate hydrate-forming conditions[62–65], and supercritical and subcritical

CO_2 conditions[66–68]. Vibrational sum frequency generation (SFG) spectroscopy confirmed the formation of hydration products of CO_2 at the air/water interface, but the mechanisms and kinetics of the formation reactions were not elucidated[54]. Therefore, a detailed investigation of CO_2 hydration at the air/water interface, its first point-of-contact with an aerosol or water pool, is crucial for understanding its affect on the acidity of such particles.

1.5 Simulation methods

Advances in high performance computing architectures with massively parallel capabilities have made molecular dynamics (MD) simulation a standard tool in chemistry and biology over the last couple of decades. Nowadays, MD simulations can routinely probe atomic and molecular motions in systems involving thousands of atoms over nanosecond timescales. Traditionally, MD solves the classical equations of motion for all particles present in a system using pre-defined analytical potentials describing the interactions between them[69–72]. With the aid of statistical mechanics, one can then compute a host of equilibrium and dynamical properties of a system (e.g., free energies, diffusion constants, densities, heat capacities, vibrational spectra, etc.), which can then be compared with their corresponding experimental values. In contrast to full quantum dynamics simulations, classical MD can treat much larger systems within a reasonable amount of time and can yield thermodynamic information for condensed phase systems. However, the reliability of a classical MD simulation depends largely on the potential (or force field) from which the forces are calculated. Since chemical reactions in the condensed phase involve bond breaking/forming and electronic polarization effects, the choice of a suitable force field that can properly account for such effects is of paramount importance. Traditional MD, which typically employs *non-reactive* empirical force fields, is not capable of incorporating such effects. In light of this, ab initio molecular dynamics (AIMD) was developed, wherein the problem of finding the correct *reactive* force field is solved by computing the forces on-the-fly from ab initio electronic structure calculations[73–75]. More specifically, the time-independent Schrödinger equation is solved for the ground state electronic wave function to yield the potential energy surface on which the nuclei evolve according to the classical equations of motion. Therefore, the often tedious problem of parametrizing an analytical force field is circumvented, making AIMD an attractive technique for investigating chemical reactions in condensed phase environments. On the other hand, however, AIMD is much more computationally expensive than classical MD since the ground state electronic wave function is re-optimized at each time step due to the changing nuclear positions.

The need to re-optimize the ground state electronic wave function was overcome by an extended Lagrangian technique named Car-Parrinello molecular dynamics (CPMD)[76]. In CPMD, the evolution of the electronic orbitals is treated classically. A fictitious mass is assigned to the electronic orbitals and the forces on the orbitals are calculated by taking the functional derivative of the Lagrangian with respect to the orbitals. The Car-Parrinello Lagrangian, L_{CP}, has the following form:

$$\mathrm{L_{CP}}[\mathrm{R^N}, \dot{\mathrm{R}}^{\mathrm{N}}, \{\Phi_\mathrm{i}\}, \{\dot{\Phi}_\mathrm{i}\}] = \sum_\mathrm{I} \frac{1}{2}\mathrm{M_I}\dot{\mathrm{R}}_\mathrm{I}^2 + \sum_\mathrm{i} \mu\langle\dot{\Phi}_\mathrm{i}|\dot{\Phi}_\mathrm{i}\rangle - \xi^{\mathrm{KS}}[\{\Phi_\mathrm{i}\}, \mathrm{R^N}] \tag{1.7}$$

where M and R denote the masses and positions of the N nuclei, respectively, μ is the mass of the fictitious particles, Φ is the electronic orbital, and ξ^{KS} is the Kohn-Sham energy. The nuclei evolve at the simulation temperature $\propto \sum_I \frac{1}{2}M_I\dot{R}_I^2$, whereas a sufficiently low fictitious temperature $\propto \sum_i \mu\langle\dot{\Phi}_i|\dot{\Phi}_i\rangle$ is assigned to the electronic degrees of freedom such that the instantaneous energy of the electronic subsystem remains close to the minimum energy on the exact ground state surface (i.e., such that adiabaticity is not broken). Therefore, if one optimizes the wave function for the initial nuclear configuration, it is expected to remain close to the original ground state throughout the simulation, thereby avoiding the need for wave function re-optimization at each time step. Although this trick makes CPMD faster than regular AIMD, it remains computationally expensive for exploring rare events, i.e., chemical reactions with high energy barriers relative to k_bT. To observe a handful of reactive crossings (from reactant/product → product/reactant) of a barrier that is a handful of k_bT high, it may take hundreds of nanoseconds, which would take a great deal of computational time even on multiple (relatively fast) processors. Therefore, to efficiently compute free energy surfaces for systems with high reaction barriers using CPMD, one has to resort to enhanced sampling techniques.

One method that has proven especially useful for studying rare events in condensed phase and biological systems is metadynamics[77–79]. In metadynamics, history-dependent biasing potentials are added periodically to the system's natural potential over the course of a trajectory in order to discourage the system from revisiting points in the configurational space and thereby drive the system over an energy barrier and into a neighbouring well. The metadynamics Lagrangian, L_{MTD}, has the following form:

$$\mathrm{L_{MTD}} = \mathrm{L_{CP}} + \frac{\mathrm{m}}{2}\sum_{\alpha}\dot{\mathrm{s}}_{\alpha}^{2} - \frac{\mathrm{k}}{2}\sum_{\alpha}[\mathrm{S}_{\alpha}(\mathrm{r}) - \mathrm{s}_{\alpha}]^{2} - \mathrm{V}(\mathrm{t},\mathrm{s}) \tag{1.8}$$

where L_{CP} is the CPMD Lagrangian, $S_\alpha(r)$ is the coordinate of collective variable α, s_α is the coordinate of the fictitious particle that couples to collective variable α, m is the mass of this fictitious particle, and k is the harmonic spring constant. $V(t, s)$ is the history-dependent biasing potential acting on the fictitious particles, which is given by

$$\mathrm{V}(\mathrm{t},\mathrm{s}) = \mathrm{W}\sum_{\mathrm{i}}\exp\{-\frac{(\mathrm{s}-\mathrm{s}^{\mathrm{i}})^{2}}{2(\Delta\mathrm{s}')^{2}}\}\exp\{-\frac{[(\mathrm{s}^{\mathrm{i}+1}-\mathrm{s}^{\mathrm{i}})\cdot(\mathrm{s}-\mathrm{s}^{\mathrm{i}})]^{2}}{2(\Delta\mathrm{s}'')^{4}}\} \tag{1.9}$$

where W is the Gaussian height, $s = \{s_1, s_2, \ldots\}$ is a vector of variables corresponding to the fictitious particle coordinates, s^i is a vector of the values of the fictitious particle coordinates at metadynamics step i, and $\Delta s'$ and $\Delta s''$ are Gaussian widths. When all of the potential wells have been filled with these Gaussians, the free energy as a function of the fictitious particle coordinates may be calculated from the total biasing potential added, i.e.,

$$\mathrm{F(s)} = -\lim_{\mathrm{t}\to\infty} \mathrm{V(t,s)} \tag{1.10}$$

If a suitable choice of collective variables is made to monitor the progress of the reaction, the mechanism deduced from a metadynamics simulation is considered to be a probable reaction pathway. However, since metadynamics is a fictitious dynamics, it is not possible to extract any real temporal information from a trajectory.

1.6 Outline of thesis

In this work, we have used CPMD and metadynamics to investigate the mechanisms and energetics of chemical and physical processes involving H_2CO_3 and CO_2 in a host of environments. Namely, we have studied the conformational changes of H_2CO_3 in bulk water, the hydroxide route decomposition of H_2CO_3 in bulk water, the water route decomposition in different-sized water clusters, the dissociation of H_2CO_3 at the air/water interface, and the hydration of CO_2 at the air/water interface.

In Chapter 2, we studied the energetics and mechanisms of the conformational changes of H_2CO_3 in bulk water. We employed CPMD and metadynamics simulations involving the CT, CC, and TT conformers of H_2CO_3 in a box of 45 water molecules with periodic boundary conditions. We were interested in determining how the mechanisms, free energy barriers, and free energy changes differ in bulk water compared to the gas phase.

In Chapter 3, we describe CPMD and metadynamics simulations aimed at understanding the dissociation and decomposition of the various conformers of H_2CO_3 in bulk water via the hydroxide route. These simulations involved a H_2CO_3 molecule in a box of 45 water molecules with periodic boundary conditions, thereby providing a bulk solvation environment around the H_2CO_3. Specifically, we investigated the mechanisms and energetics of the dissociation and decomposition of the various conformers of H_2CO_3 and calculated the pK_a of each conformer.

In Chapter 4, we investigated the energetics and mechanisms for the decomposition of H_2CO_3 in water clusters of various sizes (viz., 6, 9, 20, and 45 water molecules) using CPMD in conjunction with metadynamics. Our goals were to pin down the mechanism (whether concerted, step-wise, or both) for the water route decomposition of H_2CO_3 in bulk water and to shed light on the differences between the gas, cluster, and bulk phase decomposition mechanisms. Systematically increasing the size of the clusters allowed us to gain insights into the roles of solvation and hydrogen bonding on the mechanisms of the reactions.

In Chapter 5, we investigated the dissociation of H_2CO_3 at the air/water interface and the hydrogen bonding of the acid and its conjugate base with the interfacial waters by CPMD and metadynamics. This was done to understand how the mechanism, kinetics, and energetics of the dissociation differ at the water surface from in the bulk, and thereby shed light on the implications of these differences on the dissociation of H_2CO_3 at the surface of atmospheric water droplets and aerosols. In these simulations, an H_2CO_3 molecule was initialized in various orientations on and near the surface of a water slab and the ensuing dissociation reactions were studied and their free energy barriers calculated/estimated. An analysis of the solvation and hydrogen bonding environments around H_2CO_3 and its conjugate base enabled us to explain the origin of the differences between the dissociation energy barriers at the surface and in the bulk.

In Chapter 6, we investigated the solvation environment of CO_2 at the surface of water by CPMD and explored the reaction mechanisms and energetics of its hydration with the aid of metadynamics. In these simulations, a CO_2 molecule was initialized in parallel and perpendicular orientations near the surface of a water slab. Our aim was to determine if and how the mechanism and energetics of the hydration reaction change at the air/water interface in the limit of low CO_2 pressure.

In Chapter 7, the main results of this thesis are summarized and some prospective future work is discussed.

Chapter 2

Mechanistic insights into the conformational changes of carbonic acid in water

(Portions of this chapter are reproduced in part with permission from Ref. [58], Copyright ©2011 American Chemical Society.)

2.1 Introduction

Reactions of H_2CO_3 in aqueous environments are important in many chemical, biological, and environmental processes[4–8]. For example, the dissociation/decomposition of H_2CO_3 in water are fundamental reactions in the global carbon cycle. When atmospheric CO_2 dissolves in the oceans to form H_2CO_3, H_2CO_3 dissociates into bicarbonate (HCO_3^-) and carbonate (CO_3^{-2}) ions, thereby increasing the acidity of the oceans[9, 10]. In order to better understand ocean acidification, a detailed knowledge of the microscopic mechanisms, energetics, and kinetics of these reactions is required.

H_2CO_3 has three conformers, namely, the CT, TT, and CC conformers (see Fig. 1.1 in Chapter 1), which differ from each other in the relative orientation of the hydroxyl groups[1]. These conformers may be quantitatively distinguished from one another via their two dihedral angles defined by the relative positions of atoms O(2)-C(1)-O(4)-H(5) and O(2)-C(1)-O(3)-H(6) (see Fig. 1.1 in Chapter 1). In a previous ab-inito metadynamics study of gas-phase H_2CO_3[1], it was found that amongst the three conformers, the CC conformer is the least stable (7.9 kcal/mol higher in energy than the CT conformer) and the TT conformer is the most stable (only 1.5 kcal/mol lower in energy than the CT conformer). However, there is some uncertainty as to how their relative stabilities change in the aqueous phase due to the interactions with water molecules[21, 37]. In Ref. [21], the order of stability was found to be CC $<$ CT $<$ TT using the CBS-QB3 method with CPCM continuum solvation. The free energy barriers for the CT → CC and the CT → TT conformational changes were determined to be 9.9 and 8.1 kcal/mol, respectively, in the gas phase. However, the free energy changes and barriers in the aqueous phase have not been previously calculated using an explicit solvent.

In this chapter, we have carried out CPMD simulations in conjunction with the metadynamics technique for constructing free energy surfaces, in order to study the mechanisms and energetics of the conformational changes of the TT, CT, and CC conformers of aqueous H_2CO_3. In order to obtain a more accurate picture of the catalytic role played by water in reactions involving the conformatinal changes, all of our simulations started with one H_2CO_3 molecule explicitly solvated with 45 water molecules. Since, unbiased CPMD would be an inefficient way for exploring the reaction dynamics and calculating free energies for these conformational changes due to their relatively high free energy barriers, we have employed metadynamics technique in order to circumvent this problem. The remainder of this chapter is organized as follows: The computational details are outlined in Sec. 2.2, the results are presented and discussed in Sec. 2.3, and the main conclusions are summarized in Sec. 2.4.

2.2 Computational details

We have studied the conformational changes of all three conformers of H_2CO_3 (see Fig. 1.1 in Chapter 1) in water employing Car-Parrinello molecular dynamics (CPMD)[76] in conjunction with metadynamics[77]. The conformational changes in the gas phase have been previously studied using these approaches[1]. CPMD, an ab-initio MD technique, solves the time-independent Schrodinger equation for the ground state electronic wavefunction (within the Kohn-Sham formulation of density functional theory) to yield the potential energy surface on which the nuclei evolve according to Newton's equations of motion. In contrast to classical MD employing standard non-reactive empirical potentials, this method is capable of treating bond breaking and formation since the potential is calculated on-the-fly. Since the conformational changes have high energy barriers compared to k_BT, we used metadynamics to overcome these barriers in relatively short CPMD simulations and to calculate free energy profiles. This technique has been extensively reviewed[78–82], so we only give a brief explanation in Appendix A.

Our simulations were carried out using version 3.13.2 of the CPMD software [83] on a system consisting of a single molecule of H_2CO_3 with 45 water molecules in a cubic cell with periodic boundary conditions and an edge length of 11.3 Å. These parameters give rise to a number density of 0.033 molecules/Å^3, which is consistent with the experimental density of water (i.e., 1 g/cm^3). The starting configurations for the CPMD runs were taken from the final equilibrated configurations of 100 ps classical MD simulations using the SPC[84] and Dreiding[85] force field parameters. Further equilibrations of 10 ps were performed using CPMD, followed by 15 ps CPMD/metadynamics production runs. In order to generate different initial conditions, we randomized the coordinates and resampled the velocities from a previously equilibrated set of initial conditions, which was followed by further equilibration for 10 ps. These new initial conditions were then used to generate ensembles of trajectories for each conformer. The valence electrons were treated within the DFT formalism employing the BLYP functional[86, 87]. The BLYP functional has been successfully used recently in the study of the hydrogen bonding (H-bonding) properties[37] and the formation of H_2CO_3 in water[2]. Ultrasoft pseudopotentials[88, 89] were used to describe the interaction of the core electrons with the valence electrons and the nuclei. A plane wave basis set with a cutoff of 40 Ry was employed to expand the Kohn-Sham orbitals. A fictitious electron mass of 600 a.u. and a time step of 4 a.u. (or 0.1 fs) were used. A temperature of 315 K for the ions and a fictitious kinetic energy of 0.06 a.u. for the electronic degrees of freedom were controlled using Nose-Hoover thermostats. Bulk translations and rotations of the system were removed every 100 time steps. It should be noted that using the above parameters, functional, and pseudopotential, we were able to reproduce the various radial distribution functions for all three conformers calculated in Ref. [37].

For the metadynamics simulations, the CVs used were the two dihedral angles between the C=O group and the two O-H groups of H_2CO_3. In order to build up the history-dependent potential, Gaussian hills with heights of 0.56475 kcal/mol for the CC → CT → TT conformational changes (see Fig. 2.1 (upper panel)) and 0.31375 kcal/mol for the TT → CT conformational change (see Fig. 2.1 (lower panel)) were added every 20 MD steps. The kinetic and potential energy parameters corresponding to the fictitious particles which couple to each collective variable were $\mu = 40$ hartee × (a.u./radians)^2 and $k = 0.02$ hartee/radians^2, respectively. The velocities of the fictitious particles were rescaled periodically in order to maintain their temperature within a range around 315 K.

It should be noted that since the history-dependent biasing potential is accumulated iteratively over the course of a metadynamics simulation, the system tends to escape from any well via the lowest free energy saddle point. Therefore, metadynamics is not only useful for calculating free energies, but also for exploring reaction mechanisms[82]. However, its reliability strongly depends on the choice of the CVs. If an appropriate set of CVs is employed, metadynamics can give rise to reasonable reaction pathways and shed light on new intermediates.

2.3 Results and discussion

2.3.1 Conformational changes of carbonic acid in water

In the gas phase, the inter-conversion between the H_2CO_3 conformers occurs only via a change in one of the two dihedral angles[1] [defined by O(2)-C(1)-O(4)-H(5) and O(2)-C(1)-O(3)-H(6)], since an intra-molecular proton transfer is not feasible due to its high energy barrier[31]. Hence, in this metadynamics study, we have used these two dihedral angles as the CVs in order to investigate the conformational changes in water as the dihedral angles change. Using these two CVs, we ran several metadynamics trajectories starting from different initial conditions for the CC and the TT conformers. The evolution of the CVs as a function of the number of Gaussian hills added throughout a representative metadynamics run starting from the CC and TT conformers is plotted in Fig. 2.1. In the case of the CC conformer [see Fig. 2.1 (upper panel)], we see that after the addition of 9600 Gaussian hills, the O(2)-C(1)-O(4)-H(5) dihedral angle changes from 180° to 0 °, while the other dihedral angle remains fixed at 180°, i.e., the CC conformer has overcome the barrier and converted to the CT conformer. After the addition of 21253 more Gaussian hills, the O(2)-C(1)-O(3)-H(6) dihedral angle changes from 180° to 0°, i.e., the CT conformer has overcome the barrier and converted to the TT conformer. In the case of the metadynamics simulation starting from the TT conformer [see Fig. 2.1 (lower panel)], we see that after the addition of 15537 Gaussian hills, the O(2)-C(1)-O(4)-H(5) dihedral angle changes from 0° to 180°, while the other dihedral angle remains fixed at 0°, i.e., the TT conformer has overcome the barrier and converted to the CT conformer.

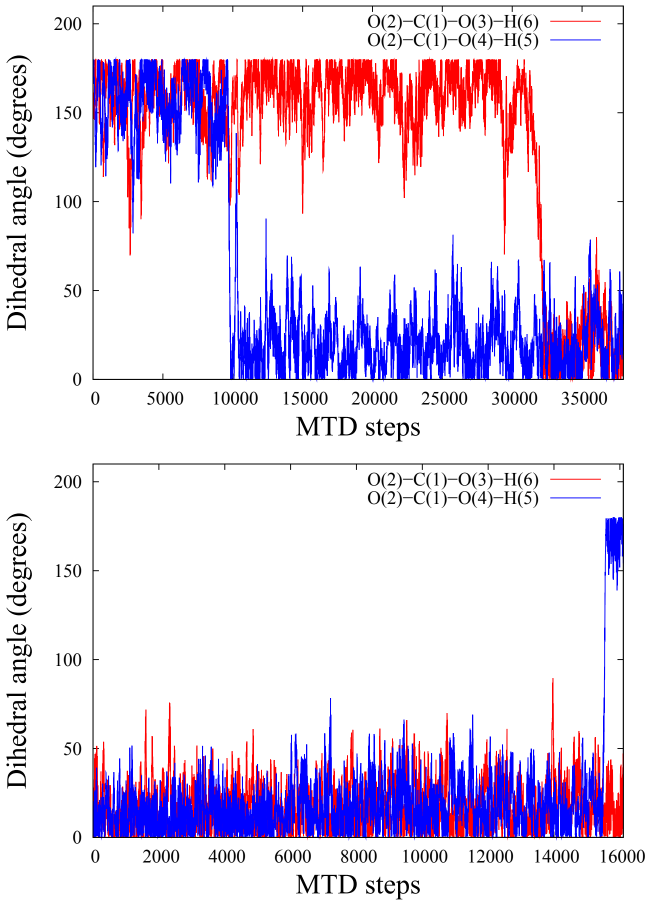

Figure 2.1: Representative metadynamics trajectories of the two dihedral angles along various conformational changes. Upper panel: CC → CT → TT. Lower panel: TT → CT. Note that each metadynamics (MTD) step = 20 CPMD steps.

Figure 2.2 shows the free energy profiles for the conformational changes depicted in Fig. 2.1 as a function of the two auxiliary variables corresponding to the fictitious particles that couple to their respective dihedral angles.

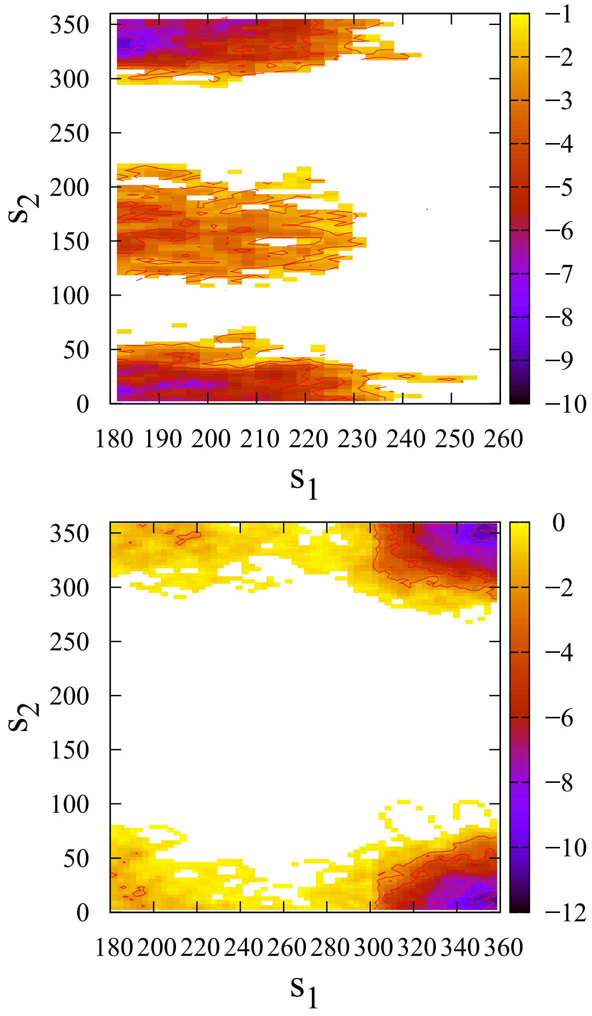

FIGURE 2.2: Free energy surfaces (in kcal/mol) as a function of the two auxiliary variables corresponding to the dihedral angles for the various conformational changes of H_2CO_3. CC → CT → TT. Lower panel: TT → CT. Note that the metadynamics simulations were stopped as soon as the trajectories reached the product wells.

The dihedral angles range from $-180°$ to $+180°$ (where the $\pm 180°$ configurations are identical), but the auxiliary variables range from 0° to 360° (where the 0° and 360° configurations are identical). However, due to inversion symmetry, we have reduced the space of one of the dihedral angles to $\{0, 180°\}$, and consequently the space of the corresponding auxiliary variable reduces to $\{180, 360°\}$. The well located near $\{s_1, \mathrm{s}_2\}$=$\{190°, 190°\}$ corresponds to the CC conformer, near $\{s_1, \mathrm{s}_2\}$=$\{190°, 350°\}$

and {190°, 20°} correspond to the CT conformer, and near $\{s_1, s_2\}=\{350°, 20°\}$ and {350°, 350°} correspond to the TT conformer.

The free energy changes and barriers for all of these conformational changes, averaged over our ensemble of five metadynamics runs, are summarized and compared with the corresponding gas-phase values in Table 2.1.

Conformational change	Free energy barrier (kcal/mol)	Free energy change (kcal/mol)
CC $\longrightarrow$ CT	3.9 (≈2)	–
CT $\longrightarrow$ CC	7.5 (9.9)	3.6 (7.9)
CT $\longrightarrow$ TT	9.0 (8.1)	–
TT $\longrightarrow$ CT	11.5 (9.6)	2.5 (1.5)

TABLE 2.1: Free energy barriers and changes from metadynamics calculations for the conformational changes of H_2CO_3 in water. The values within the brackets are the corresponding gas-phase values from Ref. [1].

We see that the TT conformer is the most stable conformer in water, as it was found to be in the gas phase. Moreover, it becomes slightly more stable in water than in the gas phase in comparison to the CT conformer, i.e., in the gas phase the TT conformer was 1.5 kcal/mol lower in energy than the CT conformer, whereas we found the energy difference between them to be 2.5 kcal/mol (cf. 0.3 kcal/mol in Ref. [21]) in water. Like in the gas phase, the CC conformer is the least stable conformer in water, but it is only 3.6 kcal/mol higher in energy than the CT conformer (cf. 1.9 kcal/mol in Ref. [21]), whereas the energy difference between them was found to be 7.9 kcal/mol in the gas phase. Thus, the use of the CPCM solvation model in Ref. [21] seems to underestimate the relative energy differences.

2.3.2 Error estimation

We estimated the error in our metadynamics simulations according to the procedure used in Refs. [82, 90] to be 1.9 kcal/mol. We also calculated the standard deviations for the free energy barriers based on our ensemble, which is 1.6 kcal/mol. The size of the metadynamics error may be reduced by using smaller Gaussian hills and a lower frequency of hill additions, at the expense of a longer simulation time.

2.4 Conclusions

The mechanisms and energetics of the conformational changes of H_2CO_3 in water via the hydroxide route have been investigated using CPMD in conjunction with metadynamics. The various energy barriers for the conformational changes involving a change in one of the dihedral angles were calculated. We found that the barrier for CC → CT is 3.9 kcal/mol, which is about twice that of the gas phase value due to the formation of H-bonds with adjacent water molecules, whereas the barrier for CT → CC decreases by $\approx$ 2 kcal/mol relative to that of the gas phase possibly since intermolecular H-bonding with neigbouring water molecules reduces the strength of the intramolecular H-bond between H(5) and O(3). In the cases of the CT → TT and TT → CT changes, the energy barriers do not change significantly in water compared to the gas phase. This is most likely due to the fact that the dihedral angle changes are primarily influenced by the intramolecular H-bonds, which are present in both phases. Like in the gas phase, the TT and CC conformers of H_2CO_3 were found to be the most and least stable in water, respectively. However, the CC → CT free energy change was found to be 3.9 kcal/mol lower in water than in the gas phase, which indicates that the CC conformer is more stable when solvated by water.

The results presented herein may provide new insights into the understanding of the chemistry of various conformers of H_2CO_3 in bulk water. The tools and approach used in this paper should be particularly useful in studying the energetics and mechanisms of the complete set of reactions carried out by all of the conformers of H_2CO_3 in water. Therefore, this investigation sets the stage for studies of H_2CO_3 reactivity in diverse aqueous environments and under different physical conditions.

Chapter 3

Mechanistic insights into the dissociation and decomposition of carbonic acid in water via the hydroxide route

(Portions of this chapter are reproduced in part with permission from Ref. [58], Copyright ©2011, American Chemical Society.)

3.1 Introduction

An understanding of the acid-base chemistry of carbonic acid (H_2CO_3) in water is important in the study of many environmental, biological, and industrial processes[4–8]. H_2CO_3 is formed when carbon dioxide (CO_2) dissolves in water and reacts reversibly with either water molecules (i.e., water route) or with hydroxide ions (i.e., hydroxide route), the latter predominating at higher pHs. The hydration of CO_2 to form H_2CO_3 and the dehydration of H_2CO_3 to form CO_2 are fundamental reactions in the global carbon cycle. For example, the dissolution of atmospheric CO_2 in water to form H_2CO_3, which then undergoes dissociation to bicarbonate (HCO_3^-) and carbonate (CO_3^{-2}) ions, increases the acidity of the oceans[9, 10]. In light of the increasing levels of CO_2 in the atmosphere from anthropogenic sources, many strategies for sequestering it have been proposed, one of which is injection into the ocean[4, 91]. In order to assess the viability of such an approach, a detailed knowledge of the microscopic mechanisms, energetics, and kinetics of the reactions involving aqueous H_2CO_3 is required. Moreover, the hydroxide route is known to play a fundamental role in the regulation of blood pH and in the transport of CO_2 in biological systems[11–13]. However, this route has yet to be comprehensively investigated theoretically.

H_2CO_3 has been studied in the gas and aqueous phases both theoretically[1–3, 21, 31–37]and experimentally[5, 18–20, 30, 92, 93]. Previous theoretical studies have suggested that H_2CO_3 is kinetically stable in the gas phase, having a high activation barrier of $\approx$ 43 kcal/mol for its decomposition into CO_2 and H_2O[1, 19, 33], whereas in the presence of water the decomposition is greatly accelerated[19]. In the ab-initio metadynamics study of gas-phase H_2CO_3 by Kumar et al.[1], it was found that among the three conformers of H_2CO_3 only the cis-trans (CT) conformer undergoes a direct decomposition into CO_2 and H_2O, whereas the trans-trans (TT) and cis-cis (CC) conformers undergo conformational changes to the CT conformer prior to decomposition. It should be noted that among the three, only the CT and TT conformers have been positively identified experimentally via Fourier-transform microwave spectroscopy[19, 20]. Moreover, in Ref. [35], the energetics of the formation of H_2CO_3 in the aqueous phase via the hydroxide route were calculated using ab-initio molecular dynamics. However, the relative stabilities and dissociation/decomposition mechanisms for all three conformers in water have not yet been thoroughly explored.

Previous quantum chemical studies of H_2CO_3 solvated with a few water molecules have shown that there is a systematic reduction in the energy barrier as the number of water molecules is increased from one to three[34]. In the presence of three water molecules, the energy barrier reduced to 20.9 kcal/mol and the decomposition rate constant increased substantially compared to its gas-phase counterpart, but was still a factor of 50 times smaller than the experimentally measured rate constant of 10 s^{-1} at 293 K [34]. Thus, a calculation of the rate constant for a fully solvated system containing many water molecules, rather than just a few, may be necessary to bridge the gap between the theoretical and experimental rate constants. Over the years, the kinetics of the decomposition of H_2CO_3 in water has been investigated by various experimental techniques[17, 30]. More recently, stopped-flow spectrophotometry was used to measure the rate and equilibrium constants of the various reactions involved in the water and hydroxide routes over a wide range of temperatures[30], providing valuable data for comparison in future theoretical studies.

It has been suggested in Ref. [34] that the decomposition of H_2CO_3 into H_2O and CO_2 is a one-step concerted process. The authors found that the minimum energy path for the dehydration of H_2CO_3 in the presence of water involves the direct participation of one water molecule in a six-membered transition state. However, a recent ab-initio molecular dynamics study[2] has suggested that both the hydration and dehydration of H_2CO_3 are two-step processes, with the dissociation into HCO_3^- and H^+ occurring before the decomposition. The hydration mechanism has been studied directly, but the dehydration mechanism has only been studied in the context of the reverse (hydration) direction. Furthermore, the reactivity of the various H_2CO_3 conformers in water remains to be explored in detail.

The pK_a of aqueous H_2CO_3 has been a subject of debate for many decades due to the presence of dissolved CO_2. A pK_a value of 6.35, which corresponds to the equilibrium involving CO_2, has been commonly reported in chemistry textbooks[33, 93]. However, the true pK_a value, which should not take into account the presence of CO_2, is substantially lower and was determined to be 3.45 from stopped-flow spectrophotometric measurements[17] and also from kinetic fits of ultrafast IR pump-probe data[18]. Several theoretical calculations support these experimental results. Using the CBS-QB3 method with CPCM continuum solvation, pK_a values of 3.8, 3.6, and 2.2 were obtained for the TT, CT, and CC conformers, respectively[21]. Using constrained ab-initio molecular dynamics, pK_a values of 3.11, 2.60, 3.75, and

0.0 were obtained for the TT, CT_1 (i.e., OH pointing away from carbonyl oxygen), CT_2 (i.e., OH pointing towards carbonyl oxygen) and CC conformers of D_2CO_3, respectively[3]. Recently, a pK_a value of 3.7 was calculated using Car-Parrinello molecular dynamics (CPMD) with metadynamics for the CT_2 conformer[2].

In this chapter, we have carried out CPMD simulations in conjunction with the metadynamics technique for constructing free energy surfaces, in order to study the mechanisms and energetics of the dissociation and decomposition of the TT, CT, and CC conformers of aqueous H_2CO_3 associated with the hydroxide route. In order to obtain a more accurate picture of the catalytic role played by water in both the dissociation and decomposition reactions, all of our simulations started with one H_2CO_3 molecule explicitly solvated with 45 water molecules. The energetics of the conformational changes of H_2CO_3 in water were also studied and the pK_a's of these conformers were calculated. The remainder of this chapter is organized as follows: The computational details are outlined in Sec. 3.2, the results are presented and discussed in Sec. 3.3, and the main conclusions are summarized in Sec. 3.4.

3.2 Computational details

We have studied the dissociation/decomposition reactions of all three conformers of H_2CO_3 (see Fig. 1.1 in Chapter 1) in water employing Car-Parrinello molecular dynamics (CPMD)[76] in conjunction with metadynamics[77]. The hydration of CO_2 yielding H_2CO_3[2], auto-ionization in water [94], and the dissociation of some other acids in water such as formic acid [95], acetic acid [96], HCl [97], HBr [98], and HF[99] have been previously studied using these approaches.

In general, the dissociation and decomposition of weak acids have relatively high energy barriers compared to k_BT and, as a result, are considered to be rare events. Therefore, one would have to run very long CPMD trajectories in order to observe these events, which would be computationally very expensive. In order to circumvent this problem, one may use metadynamics to overcome the high energy barriers in relatively short CPMD simulations and also to calculate free energy profiles. A brief explanation of the technique is given in Appendix A.

Our simulations were carried out using version 3.13.2 of the CPMD software [83] on a system consisting of a single molecule of H_2CO_3 with 45 water molecules in a cubic cell with periodic boundary conditions and an edge length of 11.3 Å. These parameters give rise to a number density of 0.033 molecules/Å^3 (consistent with the density of water of 1 g/cm^3) and a H_2CO_3 concentration of 0.07 g/cm^3. The starting configurations for the CPMD runs were taken from the final equilibrated configurations of 100 ps classical MD simulations using the SPC[84] and Dreiding[85] force field parameters. Further equilibrations of 10 ps were performed using CPMD, followed by 15 ps CPMD/metadynamics production runs. In order to generate different initial conditions, we randomized the coordinates and resampled the velocities from a previously equilibrated set of initial conditions, which was followed by further equilibration for 10 ps. These new initial conditions were then used to generate ensembles of trajectories for each conformer. The valence electrons were treated within the DFT formalism employing the BLYP functional[86, 87]. The BLYP functional has been successfully used recently in the study of the hydrogen bonding (H-bonding) properties[37] and the formation of H_2CO_3 in water[2]. Ultrasoft pseudopotentials[88, 89] were used to describe the interaction of the core electrons with the valence electrons and the nuclei. A plane wave basis set with a cutoff of 40 Ry was employed to expand the Kohn-Sham orbitals. A fictitious electron mass of 600 a.u. and a time step of 4 a.u. (or 0.1 fs) were used. A temperature of 315 K for the ions and a fictitious kinetic energy of 0.06 a.u. for the electronic degrees of freedom were controlled using Nose-Hoover thermostats. Bulk translations and rotations of the system were removed every 100 time steps. It should be noted that using the above parameters, functional, and pseudopotential, we were able to reproduce the various radial distribution functions for all three conformers calculated in Ref. [37].

For the metadynamics simulations, the CVs used were the C-O and O-H coordination numbers. Coordination numbers are more convenient CVs than bond lengths for describing bond formation/breaking since they are constructed to be 1 when the bond is intact and 0 when the bond is broken. This was accomplished by defining the coordination numbers in the following way:

$$\mathrm{C_{ij}} = \frac{1 - (\frac{\mathrm{d_{ij}}}{\mathrm{d_0}})^{\mathrm{p}}}{1 - (\frac{\mathrm{d_{ij}}}{\mathrm{d_0}})^{\mathrm{p+q}}} \tag{3.1}$$

where C_{ij} is the coordination number of atom i with respect to atom j, d_{ij} is the instantaneous distance between atoms i and j, d_0 is the distance beyond which the bond breaks, and p and q are parameters chosen such that C_{ij} tends to zero beyond d_0. We have set p=6, q=12, d_0(C-O)=1.80, and d_0(O-H)=1.40. Gaussian hills with heights of 0.1255 kcal/mol were added every 50 MD steps. The kinetic and potential energy parameters corresponding to the fictitious particles were $\mu =$ 40 hartee $\times(a.u.)^2$ and k = 0.2 hartee, respectively. The velocities of the fictitious particles were rescaled periodically in order to maintain their temperature within a range around 315 K.

3.3 Results and discussion

3.3.1 Dissociation and decomposition of carbonic acid

In order to understand the chemistry of H_2CO_3 in water, studies of the mechanism, energetics, and kinetics of its dissociation into HCO_3^- (and subsequently CO_3^{2-}) and decomposition into CO_2 are required. Theoretical investigations can give us insight into these aspects by facilitating the interpretation of experimental data and providing a detailed microscopic picture of the underlying reactions. As mentioned in Sec. 3.1, in the CPMD/metadynamics study by Kumar et al. [1], it was found that the CC and TT conformers in the gas phase do not undergo decomposition, but rather convert to the CT conformer via a change in one dihedral angle before decomposition. They found that the decomposition of the CT conformer occurs via a single-step mechanism. However, in the aqueous phase, the situation is expected to change. For example, Stirling et al.[2] have already found that the CT conformer undergoes decomposition via a two-step mechanism. Hence, several questions arise:

1. Do the TT and CC conformers undergo decomposition in water?
2. If so, do the reactions involving the CT, TT, and CC conformers take place in a single concerted step or via a step-wise mechanism?
3. How do the energetics of these reactions compare?

In the course of studying the conformational changes, we had observed that unbiased CPMD is inefficient for exploring the reactive dynamics of the various conformers. Therefore, we have also employed the metadynamics technique in order to study the dissociation and decomposition reactions. As shown in Fig. 1.1 in Chapter 1, the dissociation and decomposition of H_2CO_3 require the cleavage of two bonds, the O(4)-H(5) and C(1)-O(3)H(6) bonds [or alternatively, the O(3)-H(6) and C(1)-O(4)H(5) bonds]. Thus, the use of two bond lengths or, equivalently, two coordination numbers (see Sec. 3.2) as the CVs is sufficient for exploring the reaction mechanism by metadynamics and for ascertaining whether it is a one-step or multi-step process. For the CT conformer, the two O-H bonds are not equivalent, and therefore has two different ways to undergo bond cleavage: (i) C(1)-O(3)H(6) and O(4)-H(5), and (ii) C(1)-O(4)H(5) and O(3)-H(6)(see Fig. 1.1 in Chapter 1). Thus, we have used two sets of CVs, CV set 1 (or CV_1), corresponding to the C(1)-O(3)H(6) and O(4)-H(5) coordination numbers, and CV set 2 (or CV_2), corresponding to the C(1)-O(4)H(5) and O(3)-H(6) coordination numbers. However, for the TT and the CC conformers, both ways are equivalent (see Fig. 1.1 in Chapter 1). It should be noted that, using the same CVs, the decomposition of the CT conformer in the gas phase was found to take place via a one-step concerted mechanism in which both bonds break simultaneously to yield CO_2 and H_2O [1]. We ran several independent trajectories using these two CVs starting from the CT, TT, and CC configurations. A set of initial conditions was generated for each by randomizing an equilibrated configuration of the system and rescaling the velocities.

3.3.1.1 Dissociation and decomposition of the cis-trans conformer

Figure 3.1 shows snapshots from a representative metadynamics trajectory for the dissociation of a CT H_2CO_3 molecule using CV_1. Initially, the H of the O(4)-H(5) hydroxyl group is involved in a H-bond with a water molecule that is H-bonded to other water molecules [see Fig. 3.1 (top left)]. At $t_{MTD} = 1417$ (where t_{MTD} denotes the the number of Gaussian hills added), we see that the H-bonding distance (i.e., the distance between the donor and acceptor O atoms) becomes shorter, forming a Zundel-like structure [see Fig. 3.1 (top right)]. At $t_{MTD} = 1658$, the O-H bond of H_2CO_3 breaks for the first time due to a solvent fluctuation [see Fig. 3.1 (bottom left)]. Thus, this deprotonation leads to the formation of HCO_3^- and H_3O^+ species. Over the next few hundred metadynamics steps, the proton bounces back and forth between the two species (see Fig. 3.5) until ultimately a proton from the H_3O^+ transfers to an adjacent water molecule via the Grotthuss mechanism. Then, at $t_{MTD} = 2480$, a solvent-separated state forms with one water molecule between the HCO_3^- and H_3O^+ ions [see Fig. 3.1 (bottom right)]. It should be noted that in some of the metadynamics trajectories generated, we also observed that two water molecules separate the ions.

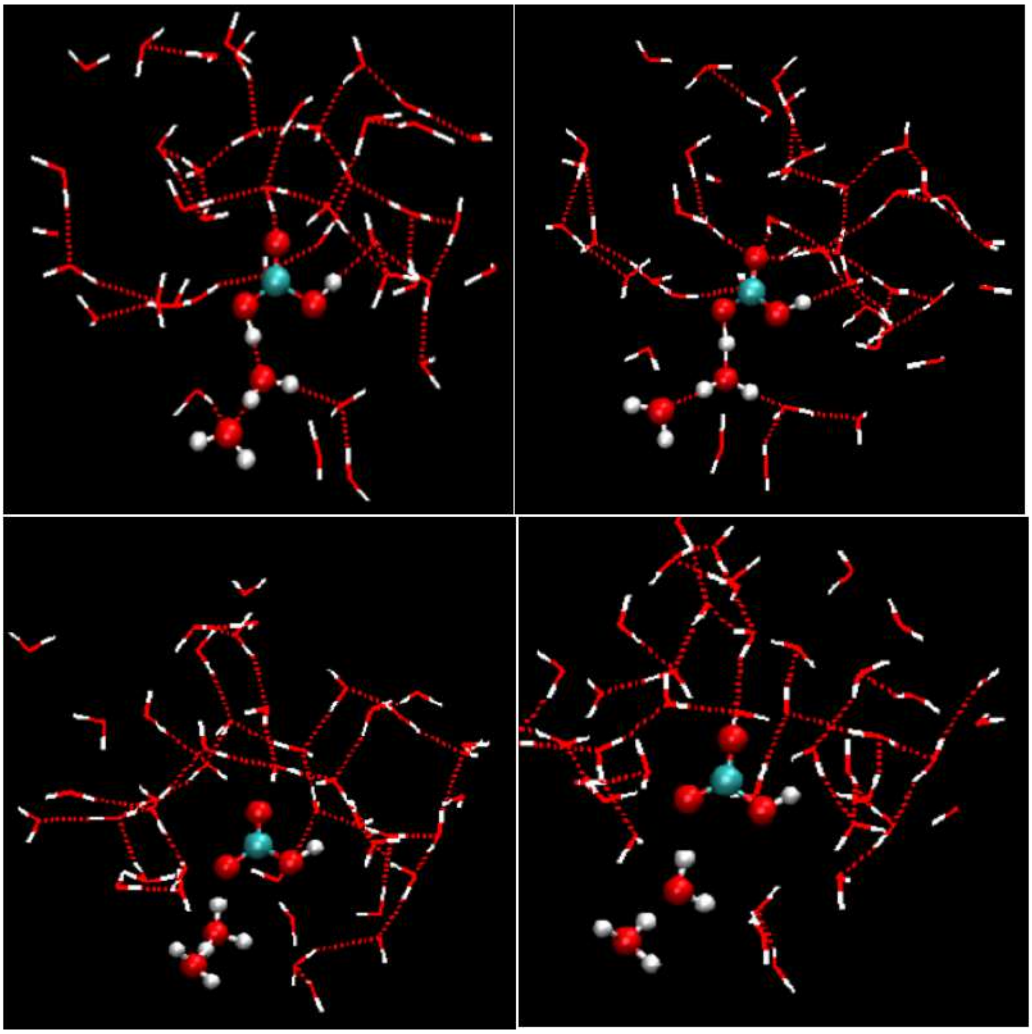

Figure 3.1: Snapshots of the dissociation of the CT conformer along a representative metadynamics trajectory. Top left: H-bond formation between the donor O in H_2CO_3 and acceptor O in an adjacent water molecule. Top right: Formation of a Zundel-like structure. Bottom left: O-H bond of H_2CO_3 breaks, leading to the formation of HCO_3^- and H_3O^+. Bottom right: The excess proton transfers to the next adjacent water molecule, giving rise to a solvent-separated ion pair.

At this point, two possible scenarios are observed within our ensemble of trajectories:

1. If the H-bond wire remains unbroken, the proton returns to the HCO_3^-, yielding H_2CO_3. This is the case for the previously discussed trajectory, where a subsequent protonation occurs (see Fig. 3.2). Deprotonation of H_2CO_3 and reprotonation of HCO_3^- continues to take place as long as the proton wire is

intact, giving rise to HCO_3^- and H_3O^+ ions (i.e., the $H_2CO_3 \rightleftarrows HCO_3^- + H^+$ equilibrium).

2. If the H-bond wire breaks, the proton diffuses into the bulk via the Grotthuss mechanism as shown in Fig. 3.3. The proton wire formed between the solvent-separated H_3O^+ ion and adjacent water molecules [see Fig. 3.3 (center panel)] breaks and the excess proton diffuses into the bulk [see Fig. 3.3 (right panel)].

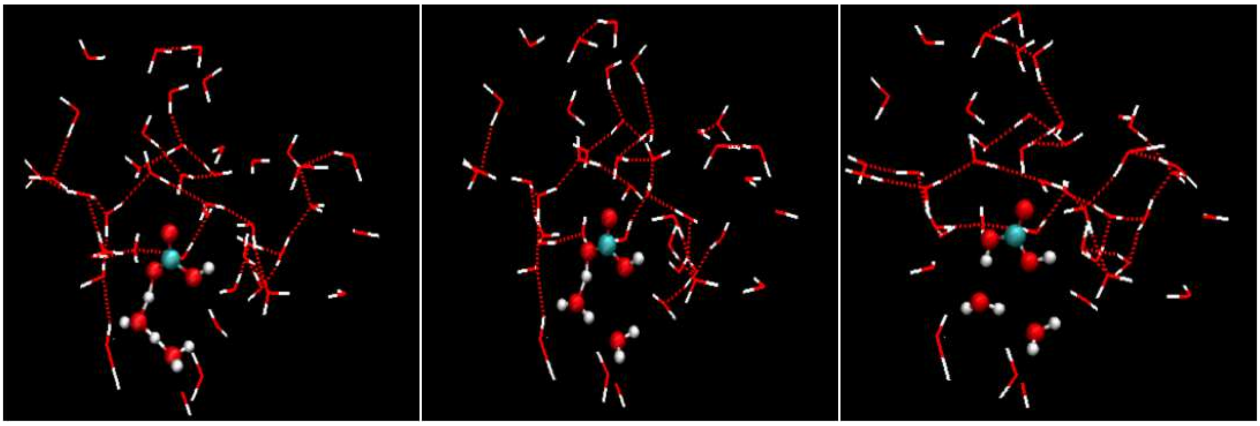

FIGURE 3.2: Snapshots along a representative metadynamics trajectory illustrating scenario 1 for the CT conformer (using CV_1). Left: The excess proton returns to the HCO_3^- along a H-bond wire. Center: Zundel-like intermediate forms. Right: Reprotonation of HCO_3^- yields H_2CO_3.

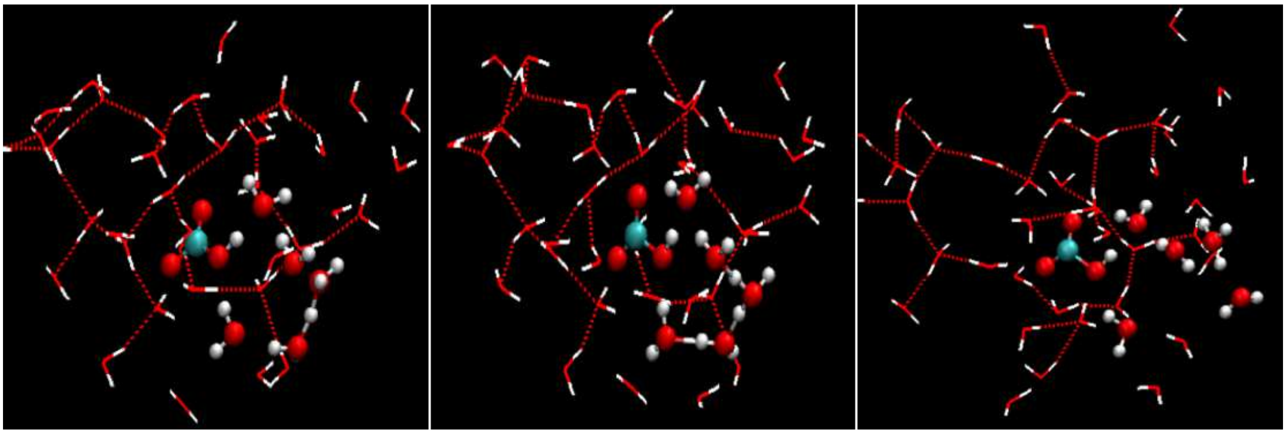

Figure 3.3: Snapshots along a representative metadynamics trajectory illustrating scenario 2 for the CT conformer (using CV_1). Left: H_3O^+ and HCO_3^- ions are separated by two water molecules. Center: Excess proton resides in H-bond wire. Right: H-bond wire breaks down and the excess proton diffuses away from the HCO_3^-.

We have also investigated the dissociation of the CT conformer using CV_2, i.e., the C(1)-O(4)H(5) and O(3)-H(6) coordination numbers. The mechanism for the formation of the solvent-separated state (with one or two water molecules between the two ions) is the same as that observed using CV_1 (see Fig. 3.1). At this point, the two scenarios just described for CV_1 are observed. However, in this case a third scenario is also observed. A H-bond wire is formed which connects the proton to the carbonyl oxygen of H_2CO_3 [i.e., O(2)] and thereby leads to the protonation of this oxygen (see Fig. 3.4). In doing so, the CT conformer converts to the TT conformer.

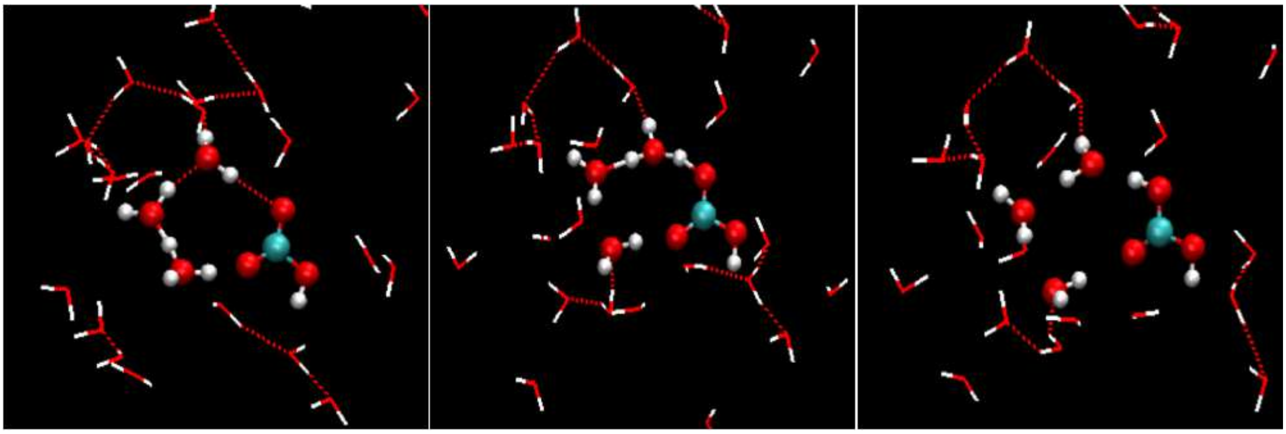

Figure 3.4: Snapshots along a representative metadynamics trajectory illustrating scenerio 3 for the CT conformer (using CV_2). Left: H-bond wire forms. Center: Excess proton transfers along the H-bond wire. Right: Excess proton transfers to O(2) of HCO_3^-, reforming H_2CO_3.

This scenario is not observed with CV_1 due to the large distance between the hydroxyl hydrogen, H(5), and the carbonyl oxygen, O(2). For CV_2, a proton transfer to the carbonyl oxygen takes place due to the fact that H(6) is relatively close to it, facilitating the formation of a H-bond wire connecting the proton through water molecules to O(2). The mechanism observed in this scenario suggests that, unlike in the gas phase, the CT conformer can also undergo a conformational change via an intra-molecular proton transfer from O(3) to O(2) along a H-bond wire. The H-bonds between the H_2CO_3 and nearby H_2O molecules facilitate the proton transfer along a H-bond wire, making this route energetically favourable in the aqueous phase.

In summary, we ran a total of 20 trajectories starting from different initial conditions using CV_1 and 15 trajectories using CV_2. For CV_1, 8 metadynamics trajectories underwent dissociation via the mechanism in scenario 1, and 12 trajectories via the mechanism in scenario 2. For CV_2, 2 trajectories underwent dissociation via the mechanism in scenario 1, 9 trajectories via the mechanism in scenario 2, and 4 trajectories via the mechanism in scenario 3.

Based on the three scenarios, we see that H-bond wires play a key role in the dissociation of CT H_2CO_3. This is also the case in water auto-ionization[94], where a H-bond wire between the solvent-separated OH^- and H_3O^+ ions is involved in the dissociation dynamics. However, in a CPMD/transition path sampling study, it was found that the dissociation of acetic acid in water is not driven by the breaking of a H-bond wire between the ions[96]. The role of H-bond wires in the dissociation of H_2CO_3 has also been observed in a recent CPMD/metadynamics study[2]. However, the equilibrium in scenario 1 was observed through two independent simulations, namely one following the reaction $H_2CO_3 \rightarrow HCO_3^- + H_3O^+$ using one set of CVs, and the other following the reaction $HCO_3^- + H_3O^+ \rightarrow H_2CO_3$ using another set of CVs. Their trajectory was not evolved for a sufficiently long time in order to observe both the forward and reverse reactions in a single run, whereas in our simulations both reactions were observed in a single run and using the same sets of CVs. Moreover, scenario 3 was not observed in their simulations due to their choice of CVs. More specifically, starting from HCO_3^- and H_3O^+, only the reprotonation of the hydroxyl oxygen occurs due to the use of an additional CV (i.e., the distance between H_3O^+ and the hydroxyl oxygen), since their intention was to study the formation of H_2CO_3.

The evolution of the CVs as a function of the number of Gaussian hills added during a representative metadynamics run is plotted in Fig. 3.5. In this figure, the evolution of CV_1 for a trajectory giving rise to scenario 1 is shown. We see that the dissociation begins after the addition of 1417 Gaussian hills, where the magnitude of the fluctuations in the O-H coordination number becomes larger, reflecting the back and forth shuttling of the proton between the donor and acceptor oxygen atoms. After the addition of 2581 hills, the system overcomes the barrier and reaches the product well, giving rise to HCO_3^- and H_3O^+. After the addition of 1785 more hills, the product well becomes filled with hills and the system then crosses back into the reactant well. This dissociation event involves a change in only one CV (i.e., the O-H coordination number), while the other CV (i.e., the C-O coordination number) remains unchanged.

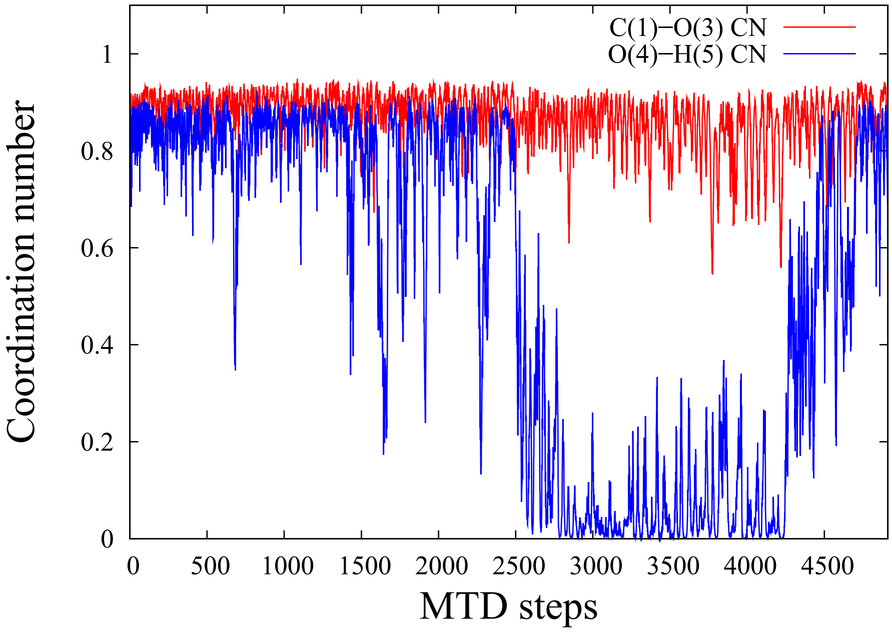

FIGURE 3.5: Representative metadynamics trajectories of CV_1 for the CT conformer, illustrating Scenario 1. Each MTD step = 50 CPMD steps.

The dissociation mechanism involves the formation of two intermediates: first, a proton-shared Zundel-like structure ($HCO_3^{\delta-} \cdots H \cdots {}^{\delta+}OH_2$) forms, which is neither completely covalent nor completely dissociated, followed by the formation of a contact ion pair ($HCO_3^- \cdot H_3O^+$). The formation of these intermediates was observed by analyzing the following:

1. the distance between the proton and the donor O_d (i.e., hydroxyl O in H_2CO_3).
2. the distance between the proton and the acceptor O_a (i.e., O atom in water molecule).

The upper panel of Fig. 3.6 shows the evolution of these distances along the same representative metadynamics trajectory depicted in Fig. 3.5. The O_a-H distance initially fluctuates around 1.7 Å, which corresponds to the first coordination shell of water molecules around H_2CO_3 as seen in the H-O_a radial distribution function[37]. After the addition of 1417 hills, the O_a-H distance decreases and begins to fluctuate around ≈1.5 Å until 2481 hills have been added. During this period, the proton-shared Zundel-like structure exists [see Fig. 3.2 (center panel)]. In this Zundel-like form, HCO_3^- does not give rise to a resonance structure (since the formation of a resonance structure is not energetically favourable)[100], which is consistent with our observation that the C(1)-O(2) and C(1)-O(4) bond lengths are not equal [see Fig. 3.6 (lower panel)]. After the addition of 2481 hills, the O_d-H and O_a-H distances become equal at ≈ 1.2 Å, and the contact ion pair forms. At this point, the two C-O bond lengths become equal and the formation of the resonance structure of HCO_3^- becomes energetically favourable. The contact ion pair is short-lived (separating completely after the addition of 299 more hills) compared to the proton-shared Zundel-like structure. We also investigated the trajectories of these distances for scenario 2 and, like in the case of scenario 1, observed the formation of a Zundel-like intermediate and a contact ion pair.

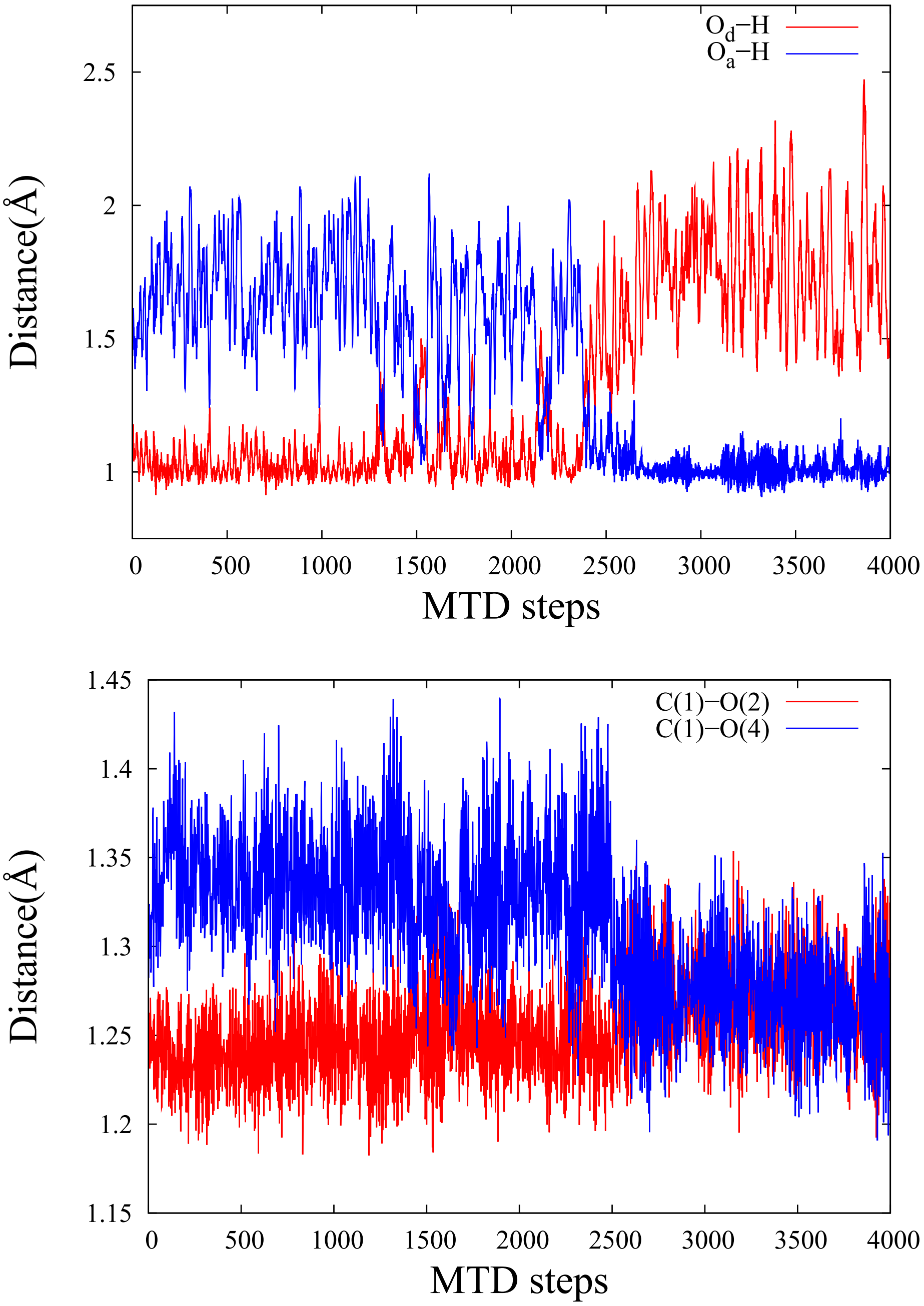

FIGURE 3.6: Representative metadynamics trajectories of various inter-atomic distances for the CT conformer, illustrating Scenario 1. Each MTD step = 50 CPMD steps. Upper panel: Trajectories of the (i) O_a-H distance, the distance between the H(6) in H_2CO_3 and the acceptor oxygen in the adjacent water molecule, and the (ii) O_d-H distance, the O(4)-H(6) distance in H_2CO_3. Lower panel: Trajectories of the C(1)-O(2) and C(1)-O(4) distances.

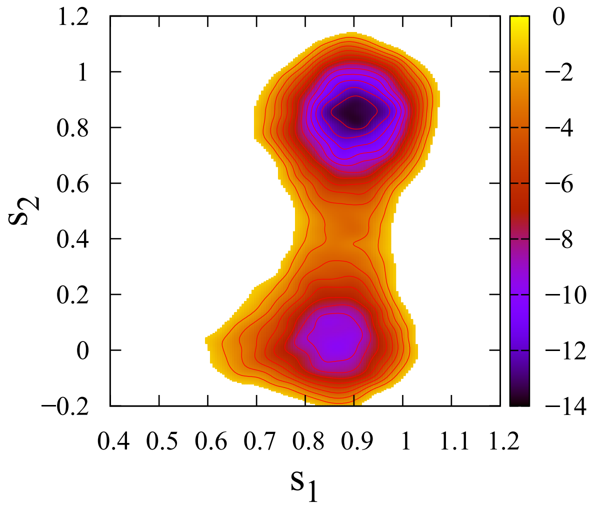

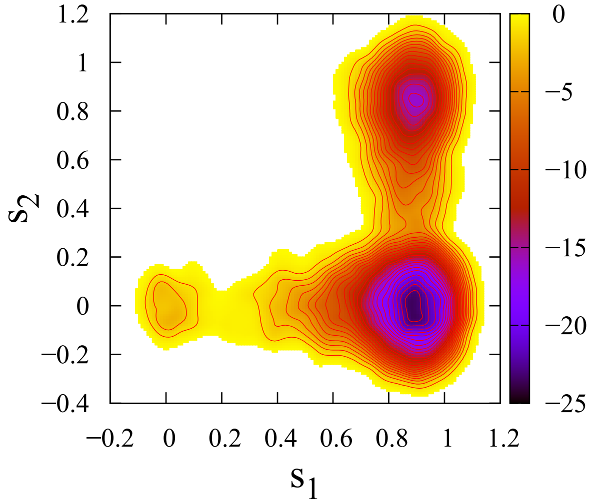

FIGURE 3.7: Free energy surfaces (in kcal/mol) as a function of the two auxiliary variables corresponding to the two coordination numbers in CV_1 for the CT conformer. Upper panel: Dissociation observed in scenario 1. Lower panel: Dissociation and decomposition observed in scenario 2.

The free energy profile for the dissociation (i.e., the $H_2CO_3 \rightleftarrows HCO_3^- + H^+$ equilibrium observed in scenario 1) as a function of the coordinates of the two fictitious particles coupled to the two coordination numbers in CV_1 is shown in Fig. 3.7 (upper panel). The reactant well is located near $\{s_1 = 0.85, s_2 = 0.85\}$ and the product well near $\{s_1 = 0.85, s_2 = 0\}$. The free energy change between the two wells is 3.8

kcal/mol and the free energy barrier for the reactant well is 9.7 kcal/mol (and 5.9 kcal/mol for the product well).

Our free energy change is close to the previously reported value of 3.51 kcal/mol for D_2CO_3, calculated using a constrained ab-initio MD technique[3]. We have also calculated the free energy changes/barriers and the pK_a values for CV_2. The free energy change is 5.5 kcal/mol and the free energy barrier for the reactant well is 9.3 kcal/mol (and 3.8 kcal/mol for the product well), which is slightly lower than previously calculated value for D_2CO_3 [2]. Our calculated pK_as for CT_1 and CT_2 H_2CO_3 are 2.6 and 3.8, respectively, which are very close to the previously calculated values for D_2CO_3[3]. It should be noted that the experimental pK_a for D_2CO_3 was estimated to be ≈ 3.95[18], which is considerably higher than those calculated in Ref. [3]. Table 3.1 summarizes the free energy changes/barriers and pKa values for the dissociation, and also contains the various previously calculated values.

	Free energy barrier (kcal/mol)	Free energy change (kcal/mol)	pK_a
CT_1	9.7	3.8 (3.51)[3]	2.6 (2.60)[3]
CT_2	9.3 (9.5)[2]	5.5 (5.06)[3]	3.8 (3.75)[3]

TABLE 3.1: Free energy barriers/changes and pK_a values corresponding to the dissociation of the CT conformer. The values within the brackets correspond to the results of previous theoretical calculations taken from Refs. [2] and [3].

The lower panel of Fig. 3.7 shows the free energy profile corresponding to scenario 2. In this case, more water molecules separate and solvate the ions, resulting in a product state that is 19 kcal/mol more stable than that in scenario 1. The decomposition of HCO_3^- into CO_2 and OH^- occurs only after the system has undergone scenario 2. This can be seen by examining the representative trajectory presented in Fig. 3.8.

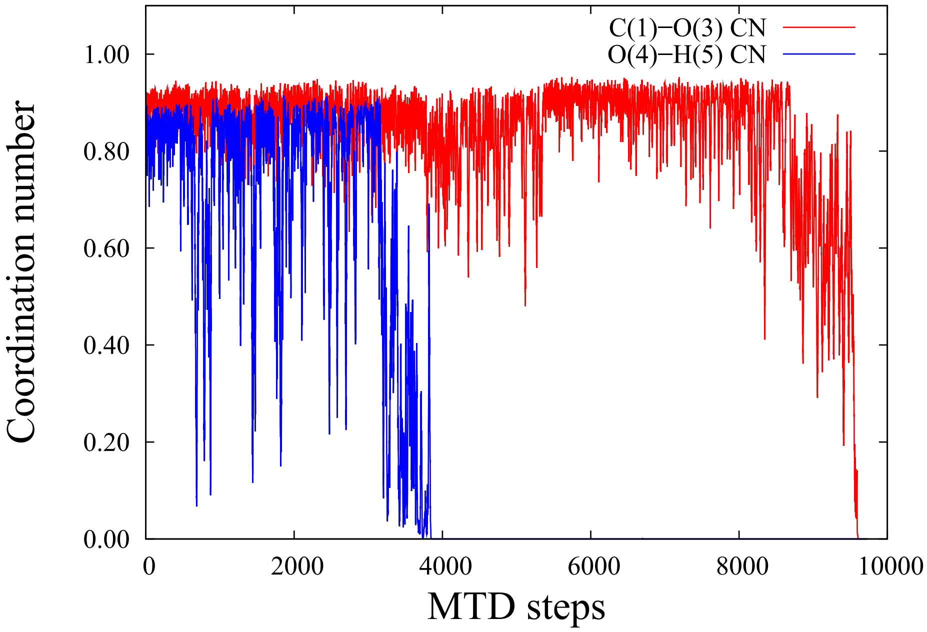

Figure 3.8: Representative metadynamics trajectories of CV_1 for the CT conformer, illustrating scenario 2. Each MTD step = 50 CPMD steps.

After the addition of 8713 hills, the C-O coordination number begins to decrease towards zero and, at zero, the C(1)-O(3) bond breaks, yielding CO_2 and OH^-. This decomposition is the reverse process in the hydroxyl pathway mentioned in Sec. 3.1. This should be contrasted with the reverse process in the water pathway, where the HCO_3^- undergoes a decomposition into CO_2 and H_2O[2]. The proposed mechanism for this process first involves a proton transfer from a H_3O^+ to the hydroxyl oxygen of HCO_3^-, to form a coordinated H_2O and thereby weaken the C-O bond, which eventually breaks to yield CO_2 and H_2O. However, we have found that the decomposition via the reverse hydroxyl pathway follows a different mechanism that does not involve the participation of H_3O^+. Rather, we observe that the C(1)-O(3) bond breaks yielding OH^- and a bent CO_2 moiety, which straightens to form the linear CO_2 molecule as the OH^- diffuses into the bulk (see Fig. 3.9). The OH^- eventually acquires a proton from an adjacent water molecule, which leads to the diffusion of OH^- via a Grotthuss mechanism. The free energy barrier for this decomposition was calculated to be 24.2 kcal/mol (using CV_1) and 26.6 kcal/mol (using CV_2), which are in reasonable agreement with the experimental value of 22.24 kcal/mol, obtained from a spectrophotometric stopped-flow measurement[30].

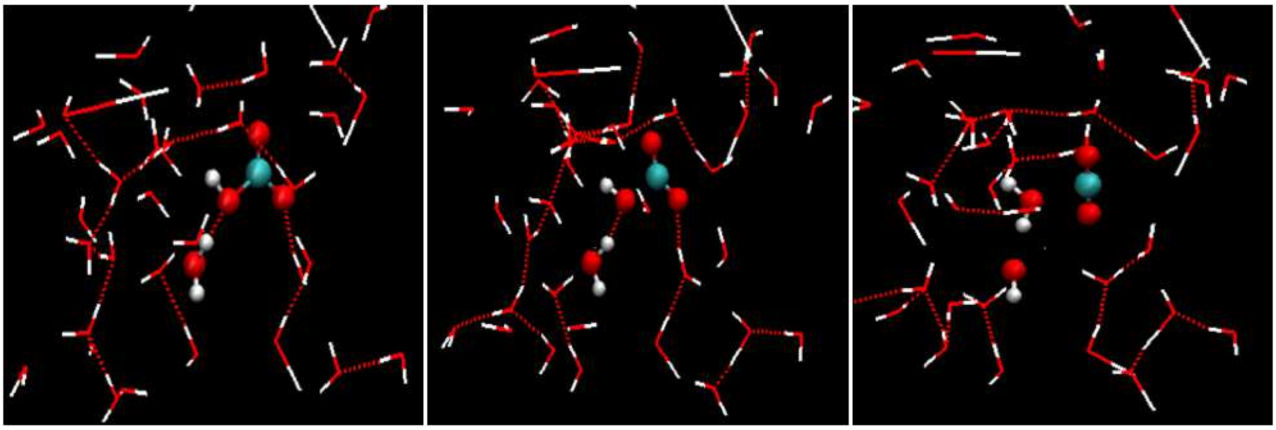

FIGURE 3.9: Snapshots of the decomposition of HCO_3^- along a representative metadynamics trajectory. Left: A H-bond forms between O(3) and an adjacent water molecule. Center: C(1)-O(3) bond breaks. Right: CO_2 moiety straightens out to yield the linear CO_2 molecule.

3.3.1.2 Dissociation and decomposition of the trans-trans conformer

As stated earlier, the TT conformer also plays an important role in aqueous H_2CO_3 chemistry. Unlike the CT conformer, the two O-H bonds in the TT conformer are symmetrical and therefore only one set of CVs [i.e., the C(1)-O(3) and O(4)-H(5) coordination numbers] is required. We ran ten metadynamics trajectories using this set of CVs, starting from the TT conformer. It was found that, unlike in the gas phase, the TT conformer in water first undergoes a direct dissociation into

HCO_3^- and H^+, followed by decomposition into CO_2 and OH^-. In the gas phase, the TT conformer does not readily undergo decomposition via the reverse water route since the combination of the H^+ and OH^- ions to form H_2O and break off CO_2 is energetically unfavorable due to the larger distance between these groups[1]. Therefore, the presence of water allows the TT conformer to undergo decomposition after dissociation, according to the same mechanisms observed in the case of the CT conformer. In addition, after the dissociation takes place, the formation of H-bond wires leads to the same three scenarios we observed in the case of the CT conformer.

The free energy profiles for the dissociation and decomposition reactions were calculated as a function of the coordinates of the two fictitious particles s_1 and s_2, which couple to the C(1)-O(3) and O(4)-H(5) coordination numbers, respectively. Figure 3.10 (upper panel) shows the free energy profile for scenario 1, corresponding to the reversible reaction $H_2CO_3 \rightleftarrows HCO_3^- + H^+$. The free energy change between the two wells is 4.4 kcal/mol and the free energy barriers for the reactant and product wells are 8.4 and 4.0 kcal/mol, respectively. Our value for the free energy change is close to the previously reported value of 4.20 kcal/mol for TT D_2CO_3, calculated using a constrained ab-initio MD technique[3]. A free energy change of 4.4 kcal/mol yields a pK_a value of 3.0, which again is close to the previously reported value of 3.11 for TT D_2CO_3 [3]. This value should be contrasted with the pK_as of the CT conformer, which are 2.6 and 3.8 for CT_1 and CT_2, respectively.

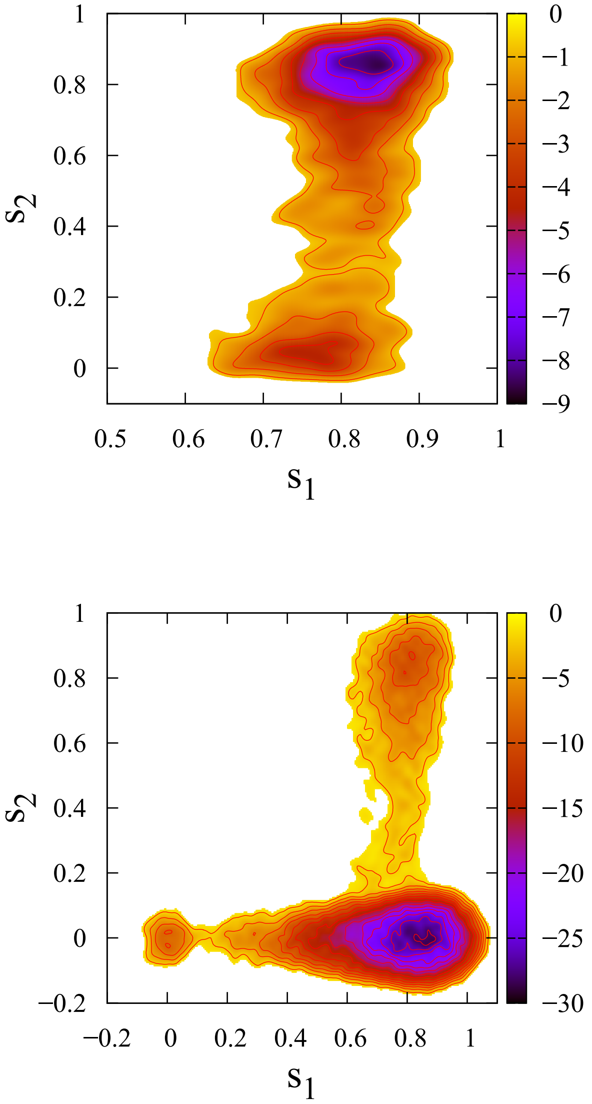

Figure 3.10: Free energy surfaces (in kcal/mol) as a function of the two auxiliary variables corresponding to the two coordination numbers for the TT conformer. Upper panel: Dissociation observed in scenario 1. Lower panel: Dissociation and decomposition observed in scenario 2.

Thus, we see that the acidity of the TT hydroxyl groups lies in between those of the two different hydroxyl groups in the CT conformer. Figure 3.10 (lower panel) shows the free energy profile corresponding to scenario 2. In this case, the product state at $\{s_1 = 0.85, s_2 = 0\}$ is 22.23 kcal/mol more stable than that in scenario 1, whereas in the case of the CT conformer, this product state is 18.3 and 22.4 kcal/mol more stable for CV_1 and CV_2, respectively. The free energy barrier for the decomposition was calculated to be 26.2 kcal/mol, which is in reasonable agreement with the overall experimental value of 22.24 kcal/mol [30].

3.3.1.3 Dissociation and decomposition of the cis-cis conformer

The two O-H groups in the CC conformer are equivalent, like in the case of the TT conformer, and therefore only one set of CVs [i.e., the C(1)-O(3) and O(4)-H(5) coordination numbers] is required. We ran 15 metadynamics trajectories using this set of CVs, starting from the CC conformer. It was found that the CC conformer undergoes dissociation into HCO_3^- and H^+ via the previously observed mechanism, which is then followed by a reprotonation of O(4) or O(2) to yield either the CT or TT conformer. This is similar to what happens in scenario 3 in the cases of the CT and TT conformers. Therefore, like in the gas phase, the CC conformer was found not to directly undergo a decomposition into CO_2 and OH^-, but rather undergoes a conformational change to the CT or TT conformer first. However, unlike in the gas phase, the mechanism for the conformational change is an intra-molecular proton transfer along a H-bond wire, which is then followed by re-dissociation and decomposition.

3.3.2 Error estimation

The errors in our metadynamics simulations were estimated using the procedure given in Refs. [82, 90]. This procedure has also been used in Ref. [2], where the authors report an error bar of 1.5 kcal/mol. We obtained error bars of 1.3 kcal/mol based on our ensembles of trajectories. It should be noted that the size of the error bars may be reduced by decreasing the height of the Gaussian hills and the frequency at which they are added, at the cost of increasing the simulation time. Some possible sources of error in these types of simulations have already been discussed in Ref. [2]. The standard deviation was also calculated to be 1.1 kcal/mol based on our ensemble of trajectories.

3.4 Conclusions

The mechanisms and energetics of the dissociation, and decomposition of H_2CO_3 in water via the hydroxide route have been investigated using CPMD in conjunction with metadynamics. Unlike in the gas phase, both the CT and TT conformers were found to undergo decomposition via a two-step process: first, dissociation of H_2CO_3 into HCO_3^- and H^+, followed by the decomposition of HCO_3^- into CO_2 and OH^-. The CC conformer does not undergo a direct decomposition, but first converts to either the CT or TT conformer prior to decomposition. The dissociation mechanism for the TT conformer is the same as that for the CT conformer, but just has different energetics. More specifically, the dissociation equilibrium involves the formation and subsequent breakage of a H-bond wire with a neighbouring water molecule. During this process, two intermediates were observed: (1) a proton-shared Zundel-like structure ($HCO_3^{\delta-}\cdots H\cdots{}^{\delta+}OH_2$), and (2) a contact ion pair ($HCO_3^-{\cdot}H_3O^+$). The decomposition of HCO_3^- involves the breaking of the C-OH bond yielding OH^- and a bent CO_2 moiety, which straightens to form CO_2 as the OH^- diffuses away into the bulk. The OH^- eventually acquires a proton from an adjacent water molecule, which leads to the diffusion of OH^- via the Grotthuss mechanism. Unlike in the case of the water route dehydration, H_3O^+ does not take part in the decomposition via the hydroxide route.

Our metadynamics simulations yielded dissociation free energy barriers of 9.7 and 9.3 kcal/mol for the CT_1 and CT_2, respectively, and 8.4 kcal/mol for the TT conformer. The calculated free energy changes were 3.8 and 5.5 kcal/mol for CT_1 and CT_2, respectively, and 4.4 kcal/mol for the TT conformer, which correspond to pK_a values of 2.6, 3.8 and 3.0, respectively. This trend in the pK_a's is in agreement with a recent constrained ab-initio MD calculation [3], but different from an ab-initio gas-phase calculation [21] with an implicit solvent which found that the TT conformer is less acidic than CT_2. Therefore, a dynamical treatment with an explicit solvent is required to properly describe the aqueous system. Our values are also supported by the recent experimental measurement of the pK_a of H_2CO_3, which yielded a value of 3.45 [18], and thereby suggest that the presence of all three conformers in water contribute to the overall pK_a. The decomposition free energy barrier was found to be 24.2 and 26.6 kcal/mol for the CT conformer using CV_1 and CV_2, respectively, and 26.2 kcal/mol for the TT conformer, which are in decent agreement with the experimentally measured value of 22.24 kcal/mol at 298 K [30] for the hydroxide route. Our values slightly overestimate the experimental decomposition free energy barrier because the actual temperature in our simulations was most likely lower than 298 K (albeit the simulation temperature was 315 K), as previous CPMD studies have indicated that higher simulation temperatures are required to reproduce the correct behaviour at lower temperatures[101].

The results presented herein may provide new insights into the understanding of blood pH regulation and CO_2 transport in living systems, for example. The tools and approach used in this paper should be particularly useful in studying the energetics and kinetics of the complete set of reactions carried out by H_2CO_3 and its derivatives in water. In particular, since the previously calculated rate constants for the decomposition of H_2CO_3 via the water route are in major disagreement with experiment, these tools may be used to more accurately calculate this rate constant. This investigation also sets the stage for studies of H_2CO_3 reactivity in diverse aqueous environments and under different physical conditions, which will have important implications in understanding the role of H_2CO_3 in biological systems and in the development of CO_2 sequestration technologies.

Chapter 4

Role of hydrogen bonding in the decomposition of H_2CO_3 in water clusters

(Portions of this chapter are reproduced in part with permission from Ref. [102], Copyright ©2014, American Chemical Society.)

4.1 Introduction

Reactions of acid gases with water clusters are ubiquitous in atmospheric and environmental chemistry[42, 43, 55, 103–112] . Due to the nature of the hydrogen bonding environment around the reactants, reactions in water clusters can be significantly different than those in the gas phase and in bulk water. Even a single water molecule can considerably stabilize the structures of the reactants, products, and transition states relative to their gas phase counterparts[113]. The interplay between forces in the interior and at the surface of a cluster makes reactions in clusters differ from those in bulk water[39–43]. Moreover, since the size of a cluster may be varied to gain control over a reaction, understanding the transition between the properties of isolated and fully solvated reactants is of great importance [45–50].

Studying the stability of carbonic acid (H_2CO_3) in water clusters is important for understanding its effects on the atmosphere. In the upper troposphere, solid carbonic acid can be produced by the reaction of mineral dust particles containing $CaCO_3$ and acids like HCl[44]. Spectroscopic studies have shown that this solid H_2CO_3 remains intact below 240 K and under high relative humidities[44], and can therefore sublime to gaseous H_2CO_3[5]. H_2CO_3 may also form in the upper troposphere by the reaction of CO_2 and H_2O in a water cluster[5]. In both cases, H_2CO_3 can then react with water to undergo dissociation and decomposition. Thus, in light of the environmental issues related to increasing atmospheric CO_2 levels, it is important to understand the reactivity of H_2CO_3 in water clusters. The energetics, kinetics, and mechanisms of the decomposition of H_2CO_3 in the gas phase and in bulk water have been investigated both experimentally[5, 18–20, 30, 92, 93], and theoretically[1–3, 21, 31–38, 58] but relatively little attention has been given to the decomposition of H_2CO_3 in water clusters[51, 52]. In fact, to date, no molecular dynamics studies of the decomposition of H_2CO_3 in water clusters at atmospherically relevant temperatures have been performed. The reactivity of H_2CO_3 in water clusters is expected to be different from that in the gas phase and in bulk water due to differences in the hydrogen bonding interactions between H_2CO_3 and the neighbouring water molecules. Therefore, molecular dynamics studies of H_2CO_3 in water clusters are warranted.

Studying the decomposition of H_2CO_3 in water clusters is also important for gaining deeper insight into the differences between the decomposition mechanisms in the gas phase, small water clusters, and bulk water. A previous quantum chemical study has shown that H_2CO_3 is kinetically stable in the gas phase, having a high decomposition energy barrier of 43.55 kcal/mol[33]. However, in the presence of just three water molecules, quantum chemical calculations have shown that the energy barrier is substantially lower (by 22.7 kcal/mol) than in the gas phase[34]. In bulk water, recent ab initio metadynamics simulations[2, 38, 58] involving tens of water molecules have also revealed that the energy barriers encountered are lowered in the presence of water, but the details of the energetics are quite different than those in Ref. 34. With regards to the mechanisms, H_2CO_3 decomposes into H_2O and CO_2 via a concerted mechanism in the gas phase[1, 31, 33], whereas in bulk water, it has been proposed that the decomposition may occur either via a concerted mechanism[22, 34, 36] or a sequential mechanism[2, 22, 58, 114]. The concerted mechanism involves the transfer of one of the hydroxyl hydrogens to the other hydroxyl oxygen through a chain of two water molecules, which is accompanied by a concurrent breakage of the C-O bond to yield CO_2 and H_2O. In contrast, the sequential mechanism initially involves the formation of metastable HCO_3^- and H_3O^+ intermediates, followed by the breakage of the C-OH bond to release CO_2. It should be noted that kinetic data from a wide variety of experiments aimed at determining the rate of H_2CO_3 decomposition in water have been analyzed in terms of the concerted proton shuttle mechanism [17, 23–30], even though it was not evident from the results that the reaction only follows this route, if at all.

In order to resolve this mechanistic debate and shed light on the differences between the gas, cluster, and bulk phase decomposition mechanisms, we have investigated the energetics and mechanisms for the decomposition of H_2CO_3 in water clusters of varying size (viz., 6, 9, 20, and 45 water molecules) using ab initio molecular dynamics. More specifically, CPMD simulations in conjunction with metadynamics were used to construct the free energy surfaces and map out the mechanisms along collective variables appropriate for the decomposition of H_2CO_3 into H_2O and CO_2. The effects of cluster size on the mechanism and energetics of the decomposition were investigated, the solvation structures of the reaction intermediates were elucidated, and the concerted versus step-wise mechanistic debate was resolved. The remainder of this paper is organized as follows: The computational details are outlined in Sec. 4.2, the results are presented and discussed in Sec. 4.3, and the main conclusions are summarized in Sec. 4.4.

4.2 Computational details

We investigated the mechanisms and energetics for the decomposition of H_2CO_3 in water clusters of various sizes using Car-Parrinello molecular dynamics (CPMD)[76]. Since the energy barriers associated with these reactions both in the gas and condensed phases are too high to explore using CPMD, we employed metadynamics[77] in conjunction with CPMD to efficiently study the mechanisms and calculate the free energy surfaces. CPMD and metadynamics have been previously used to study the dissociation and/or decomposition of weak acids such as H_2CO_3[2, 58], formic acid[95], and acetic acid[96] in bulk water. To study the decomposition of H_2CO_3 using metadynamics, we chose three suitable collective variables (CVs) which trace the course of the reaction: the C-O coordination number (CV_1), the O-H coordination number (CV_2), and the number of water hydrogens hydrogen-bonded to a hydroxyl oxygen (CV_3). More specifically, CV_1 and CV_3 involve the oxygen in the hydroxyl group pointing towards the carbonyl oxygen, and CV_2 involves the hydroxyl group pointing away from the carbonyl oxygen. The coordination numbers used as the collective variables (CVs) in our metadynamics simulations have the following basic form:

$$\frac{1-(\frac{\mathrm{d_{ij}}}{\mathrm{d_0}})^{\mathrm{p}}}{1-(\frac{\mathrm{d_{ij}}}{\mathrm{d_0}})^{\mathrm{p+q}}} \tag{4.1}$$

where d_{ij} is the instantaneous distance between atoms i and j, d_0 is the distance below which the atoms are considered bonded, and p and q are parameters chosen such that the coordination number tends to zero beyond d_0. The first collective variable is the C-O coordination number (CV_1), where d_{ij} is now the instantaneous distance between the C(1) and O(3) atoms (see Figure 4.1 for atomic labels). The second collective variable is the O-H coordination number (CV_2), where d_{ij} is now the instantaneous distance between the O(4) and H(5) atoms. The third collective variable is the number of water hydrogen atoms bonded to the O(3) atom (CV_3) and is given by

$$\mathrm{CV_3} = \sum_{\mathrm{j\epsilon H_w}} \frac{1-(\frac{\mathrm{d_{ij}}}{\mathrm{d_0}})^{\mathrm{p}}}{1-(\frac{\mathrm{d_{ij}}}{\mathrm{d_0}})^{\mathrm{p+q}}} \tag{4.2}$$

where H_w refers to set of hydrogen atoms in the water molecules and d_{ij} is now the instantaneous distance between the O(3) and a water hydrogen atom.

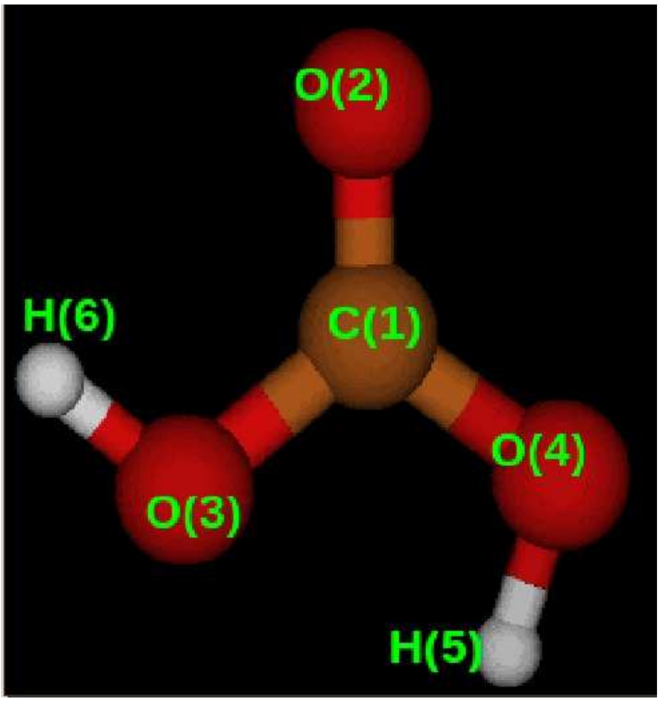

Figure 4.1: The atomic labels used for defining the collective variables used in the metadynamics simulations of the solvated H_2CO_3 molecule.

The parameters associated with the various CVs used in our metadynamics simulations are summarized below:

	CV_1	CV_2	CV_3
Harmonic spring constant, k (hartee)	1	1	5
Mass of the fictitious particle, μ (hartee (a.u.)^2)	50	50	100
Gaussian height, W (hartee)	0.0002	0.0002	0.0002
Gaussian width, $\Delta s'$	0.03	0.03	0.03
Metadynamics time step, Δt (a.u.)	200	200	200
p	8	6	6
q	24	14	14
d_0	1.80	1.40	1.40

Table 4.1: Metadynamics parameters for the 6- and 9-water cluster simulations.

	CV_1	CV_2	CV_3
Harmonic spring constant, k (hartee)	1	1	1
Mass of the fictitious particle, μ (hartee (a.u.)^2)	500	500	500
Gaussian height, W (hartee)	0.001	0.001	0.001
Gaussian width, $\Delta s'$	0.01	0.08	0.04
Metadynamics time step, Δt (a.u.)	400	400	400
p	8	6	6
q	24	14	14
d_0	1.90	1.40	1.40

Table 4.2: Metadynamics parameters for the 20- and 45-water cluster simulations.

We used the following procedure to prepare thermally stable clusters: A H_2CO_3 molecule and 45 H_2O molecules are placed in a cubic cell with an edge length of 22.3 Å and periodic boundary conditions. Since CPMD employs a plane wave basis set, which is intrinsically periodic, to expand the Kohn-Sham orbitals, the edge length is set to be (at least) twice as large as that used in bulk simulations to ensure that the cluster does not interact with its periodic images[46, 83]. The cluster is equilibrated for 40 ps, after which clusters with 6, 9, 20, and 45 water molecules were extracted from the final configuration of that trajectory. The 6-water cluster corresponds to the H_2CO_3 molecule surrounded by its first hydration shell (i.e., those waters which form hydrogen bonds with the oxygen and hydrogen atoms of H_2CO_3); the 9-water cluster contains additional water molecules which allow for the formation of a hydrogen bond wire with one of the hydroxyl groups in H_2CO_3; and the 20-water cluster corresponds to the H_2CO_3 molecule surrounded by its first and second hydration shells. These numbers of water molecules were chosen based on integration of the carbon-water oxygen radial distribution function as shown in Figure 4.2.

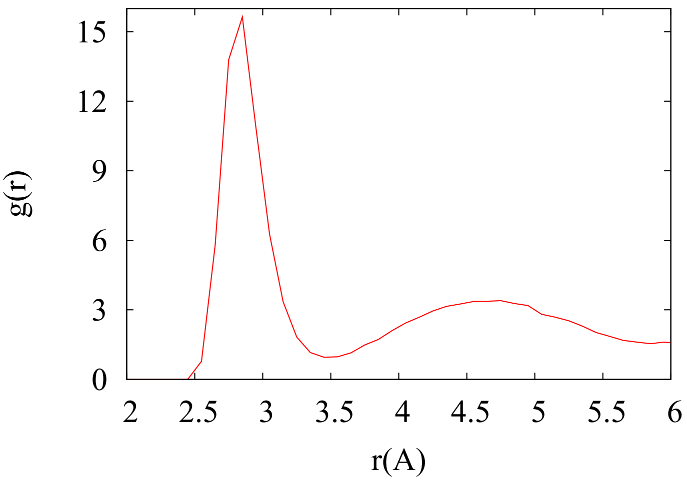

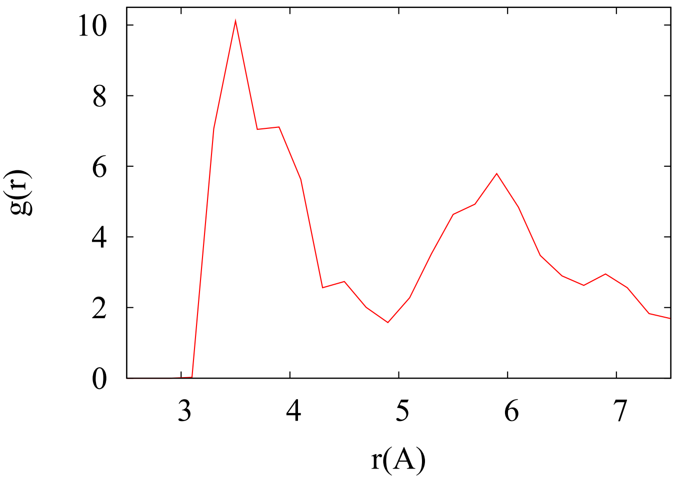

FIGURE 4.2: Radial distribution functions calculated from 15 ps CPMD trajectories of the 45−water cluster. Top: Oxygen-oxygen radial distribution function for water. Bottom: Carbon-water oxygen radial distribution function.

For each of these cluster configurations, the electronic wave function is re-optimized using the method of preconditioned conjugate gradients, followed by 40 ps equilibration runs. The resulting configurations are used as initial configurations for the metadynamics simulations. All simulations were carried out at a temperature of 150 K (with the aid of Nosé-Hoover thermostats), since at this temperature the clusters are still liquid-like and do not evaporate. It should be noted that we have only considered clusters in which H_2CO_3 is solvated in the core (thereby creating a bulk-like environment around it, given a sufficient number of water molecules), since one of our primary interests was to shed light on the decomposition mechanism in bulk water.

4.3 Results and discussions

4.3.1 Decomposition of H_2CO_3 in 6- and 9-water clusters

Figure 4.3 shows snapshots from a representative metadynamics trajectory (taken from an ensemble of 10 trajectories) for the decomposition of H_2CO_3 in a cluster of 6 water molecules. Initially, the hydrogen of one of the O-H groups in H_2CO_3 forms a hydrogen bond with an adjacent water molecule (see Figure 4.3 [top left]), which is followed by the formation of a Zundel-like structure, $HCO_3^{\delta-} \cdots H \cdots {}^{\delta+}OH_2$ (see Figure 4.3 [top right]). The O-H bond then breaks and the proton shuttles to the O of the other O-H group through a wire of two water molecules (see Figure 4.3 [bottom left]). As can be seen from Figure 4.3 [bottom left], the participation of two water molecules in the proton transport mechanism gives rise to an 8-membered transition state structure. After the proton shuttles to the O, the C-O bond breaks and a straight CO_2 molecule ultimately forms (see Figure 4.3 [bottom right]).

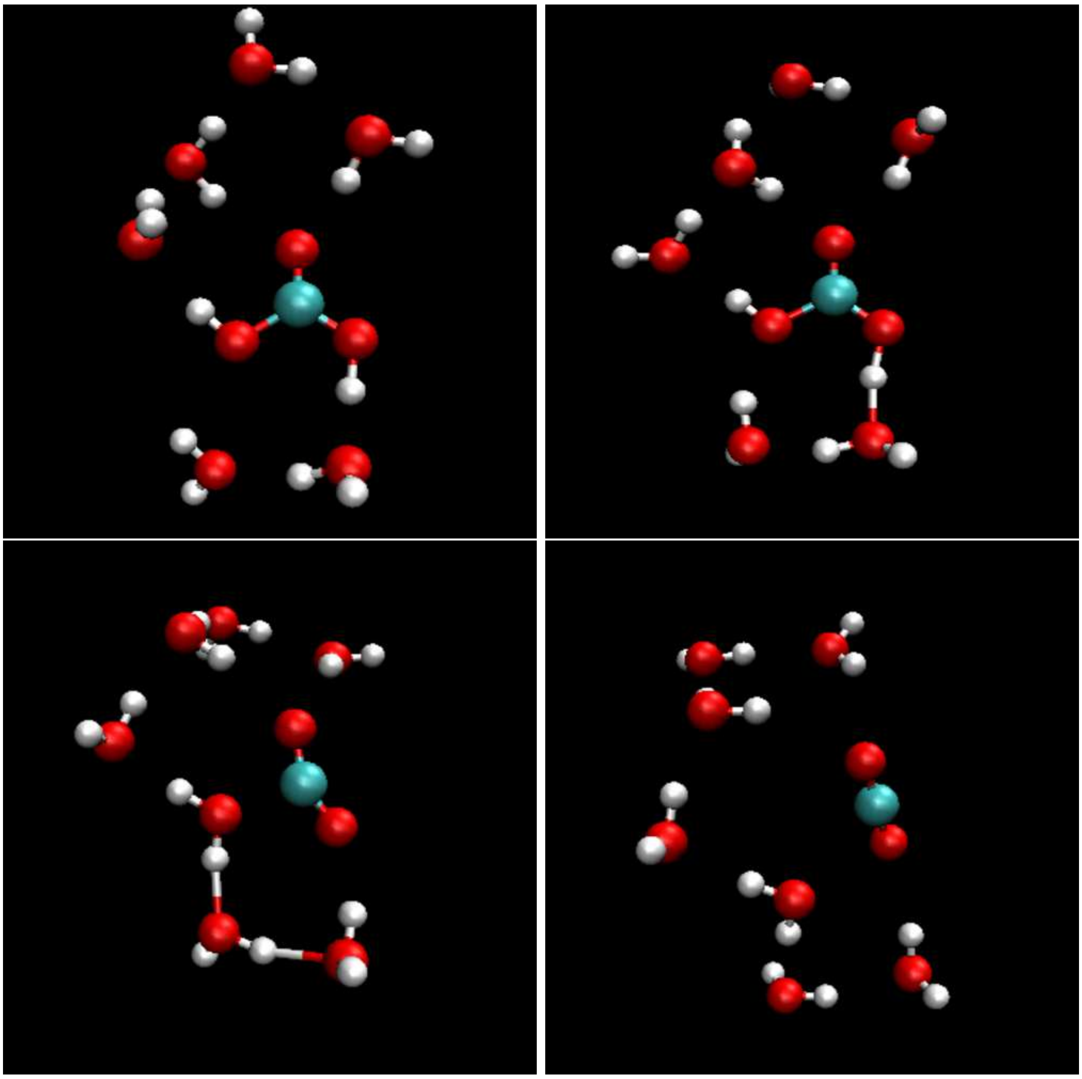

Figure 4.3: Snapshots of the decomposition of H_2CO_3 in a 6-water cluster from a representative metadynamics trajectory. Top left: H-bond formation between the donor O in H_2CO_3 and the acceptor O in an adjacent water molecule. Top right: Formation of a Zundel-like structure. Bottom left: Proton transport through two water molecules. Bottom right: C-O bond breaks, yielding CO_2.

As seen, this decomposition involves three proton transports (PTs): first, between the hydroxyl O in H_2CO_3 and the O in the adjacent H_2O molecule; second, between the O atoms of the two water molecules; and third, between the O in the second water molecule and the other hydroxyl O in H_2CO_3 (see Figure 4.4 for an illustration of these PT coordinates).

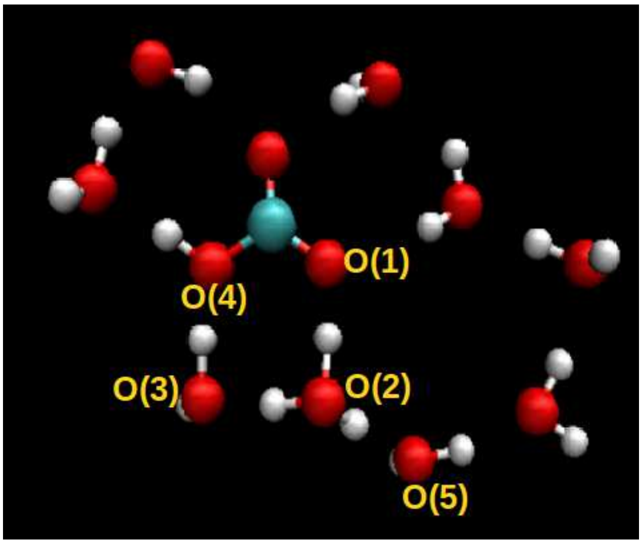

FIGURE 4.4: The atomic labels used for defining the proton transport coordinates. Q_{PT_1}, Q_{PT_2}, Q_{PT_3}, and Q_{PT_4} correspond to PT between O(1) and O(2), O(2) and O(3), O(3) and O(4), and O(2) and O(5), respectively.

Figure 4.5 shows the coordinates corresponding to these three proton transports as a function of the number of metadynamics hills added to the potential, which are defined by[115]

$$\mathrm{Q_{PT}} = \frac{(\mathrm{R_{O_dH}} - \mathrm{R'_{O_dH}}) - (\mathrm{R_{O_aH}} - \mathrm{R'_{O_aH}})}{(\mathrm{R_{O_dH}} - \mathrm{R'_{O_dH}}) + (\mathrm{R_{O_aH}} - \mathrm{R'_{O_aH}})}, \tag{4.3}$$

where R_{O_dH} is the distance between the donor O and the proton, R'_{O_dH} is the average distance between the donor O and the proton in an undissociated molecule, R_{O_aH} is the distance between the acceptor O and the proton, and R'_{O_aH} is the average distance between the acceptor O and the proton in a completely dissociated molecule. We see that after the addition of 39635 hills, all three proton transports occur simultaneously. This concurrent nature of the proton transports is also evident from the evolution of the CVs as a function of the number of metadynamics steps as shown in Figure 4.6. After 39635 steps, the system escapes from the reactant well to the product well, as seen by the change in all three CV values, viz., CV_2

changes from ~ 0.9 to 0 (i.e., the O-H bond breaks), CV_3 changes from 0 to ~ 0.9 (i.e., the proton shuttles to the O of the other O-H group), and CV_1 changes from ~ 0.9 to 0 (i.e., the C-O bond breaks).

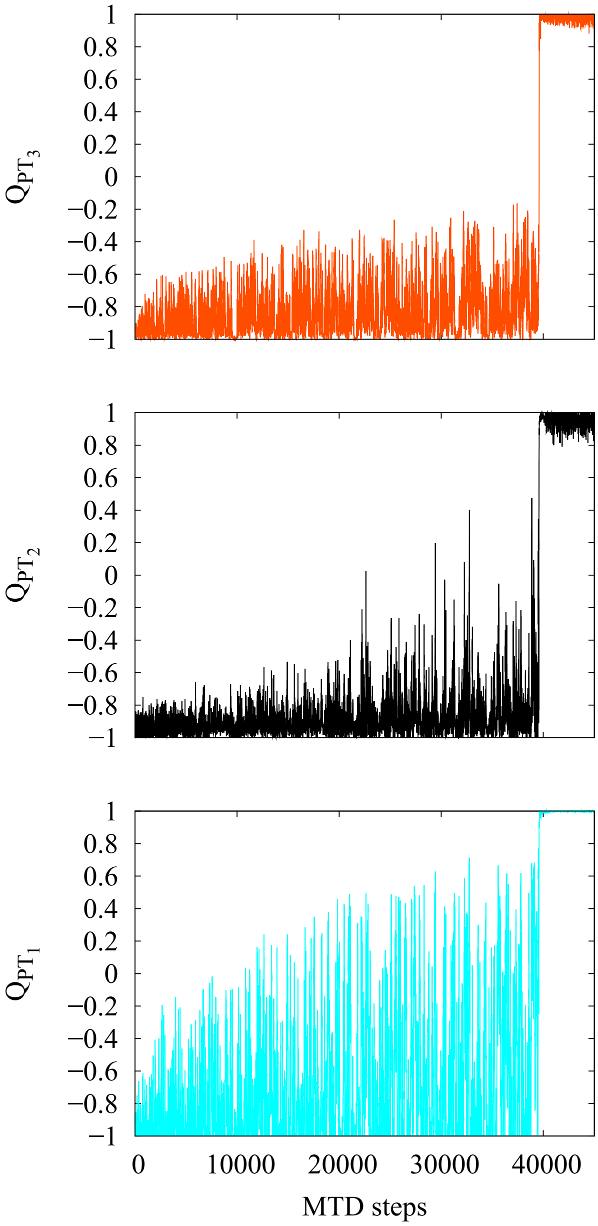

FIGURE 4.5: Representative metadynamics trajectories of the proton transport (PT) coordinates for the decomposition of H_2CO_3 in a 6-water cluster. Bottom: Coordinate corresponding to PT between the hydroxyl O in H_2CO_3 and O in the adjacent H_2O molecule, Q_{PT_1}. Middle: Coordinate corresponding to PT between the O atoms of the two water molecules, Q_{PT_2}. Top: Coordinate corresponding to PT between O in the second water molecule and the other hydroxyl O of H_2CO_3, Q_{PT_3}. Each metadynamics (MTD) step = 50 CPMD steps.

The simultaneous changes in the PT coordinates and CV values clearly indicate that the decomposition takes place in a concerted fashion. Therefore, in the case of the 6-water cluster, we see that H_2CO_3 undergoes decomposition into CO_2 and

H_2O according to a concerted mechanism like in the gas phase, involving the direct participation of two water molecules.

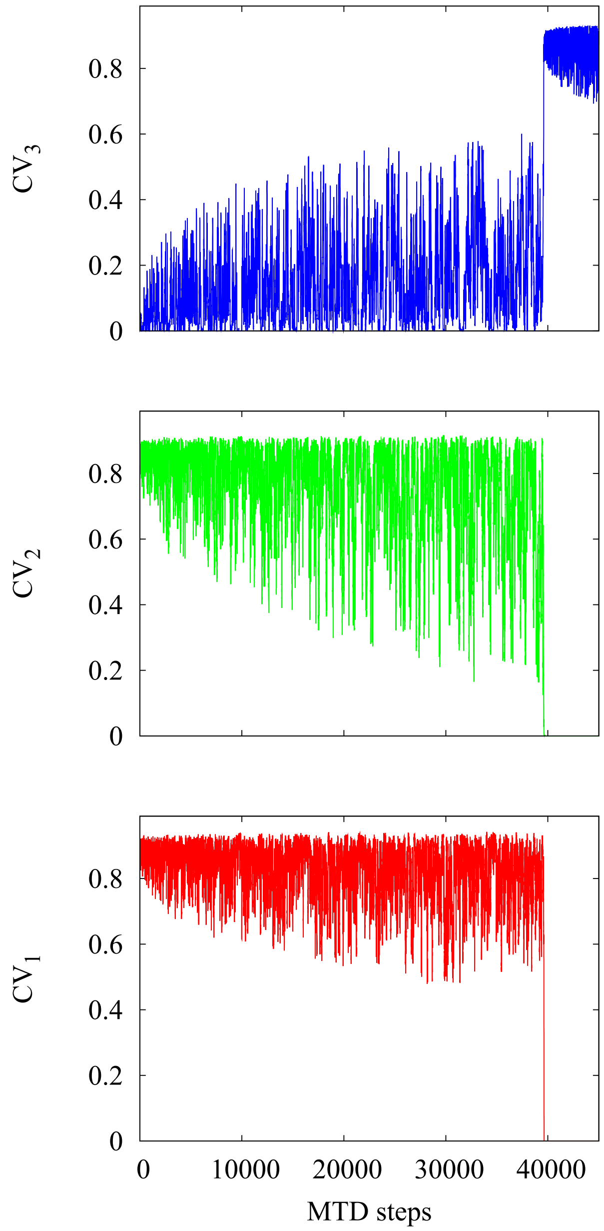

FIGURE 4.6: Representative metadynamics trajectories of the CVs for the decomposition of H_2CO_3 in a 6-water cluster. Each metadynamics (MTD) step = 50 CPMD steps.

Next, we investigated the effect of changing the nature of the initial configuration on the decomposition mechanism in the 6-water cluster. In Ref. 34, a 6-membered transition state was proposed for the decomposition of a H_2CO_3 molecule surrounded by 3 water molecules based on electronic structure calculations. It was found that the pathway going through a 6-membered transition state has a lower energy barrier (by 1.8 kcal/mol) and a faster decomposition rate (by a factor of ~ 20) than the pathway going through an 8-membered transition state. However, in another electronic structure study of the reverse reaction (i.e., the formation of H_2CO_3 via the hydration of CO_2), a pathway going through an 8-membered transition state was found to be more favourable based on a calculation involving 4 water molecules [116]. The difference between the 6- and 8-membered transition state pathways is the number of water molecules actively taking part in the proton shuttle from one hydroxyl O to the other hydroxyl O of H_2CO_3, viz., one and two water molecules for the 6- and 8-membered transition state pathways, respectively. In light of these different mechanisms, we decided to investigate the feasibility of a 6-membered transition state pathway within our approach. We carried out metadynamics simulations starting from another initial configuration with only one water molecule available to form the proton wire. We found that H_2CO_3 undergoes a decomposition via a 6-membered transition state when there is only one water molecule in the vicinity of the hydroxyl group for the proton shuttle. Thus, the presence of an additional water molecule in close proximity to the water molecule hydrogen-bonded to the hydroxyl group of H_2CO_3 facilitates the formation of an 8-membered transition state (as opposed to a 6-membered transition state). We ran 50 ps CPMD simulations starting from both configurations (i.e., one with one water molecule and the other with two water molecules potentially available for the proton transfer in the vicinity of the hydroxyl group) and found that the number of water molecules available to take part in the proton transfer remains unchanged for both starting configurations. These results suggest that both initial configurations can undergo reactions, i.e., both the 6- and 8-membered transition states are possible and depend on the proximity of the water molecules to the hydroxyl groups.

The free energy profile projected on to the two fictitious coordinates associated with CV_1 and CV_2 is shown in Figure 4.7 for the decomposition of H_2CO_3 in the 6-water cluster. The reactant well (located at $\{S_1 \sim 0.9,\ S_2 \sim 0.9\}$) corresponds to the intact H_2CO_3 hydrogen-bonded to neighbouring water molecules and the product well (located at $\{S_1 \sim 0.0, S_2 \sim 0.0\}$) corresponds to CO_2 and H_2O.

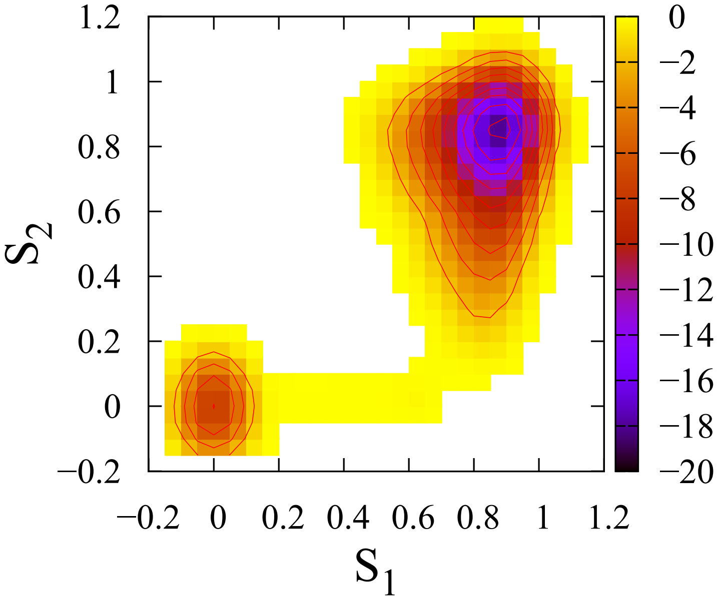

FIGURE 4.7: Free energy (in kcal/mol) projected on to the two auxiliary variables corresponding to CV_1 and CV_2 (S_1 and S_2, respectively) for the decomposition of H_2CO_3 in a 6-water cluster.

From the figure, we find that the free energy barrier for the decomposition is 18.5 kcal/mol. Currently, there are no experimental free energy barriers reported for the decomposition of H_2CO_3 in water clusters to compare with our calculated value. However, it should be noted that our calculated barrier for the 6-water cluster is 4.2 kcal/mol lower than that calculated for a 3-water cluster in Ref. 34. This suggests that increasing the size of the cluster lowers the energy barrier, since additional water molecules stabilize the transition state.

We also studied the decomposition mechanism in a 9-water cluster. Like in the 6-water cluster, we observed that H_2CO_3 undergoes decomposition via a concerted mechanism involving either a 6-membered or 8-membered transition state, depending on the nature of the initial configuration of water molecules surrounding the H_2CO_3. Figures 4.8 and 4.9 show the evolution of the CVs and proton transport coordinates, respectively, as a function of the number of metadynamics steps.

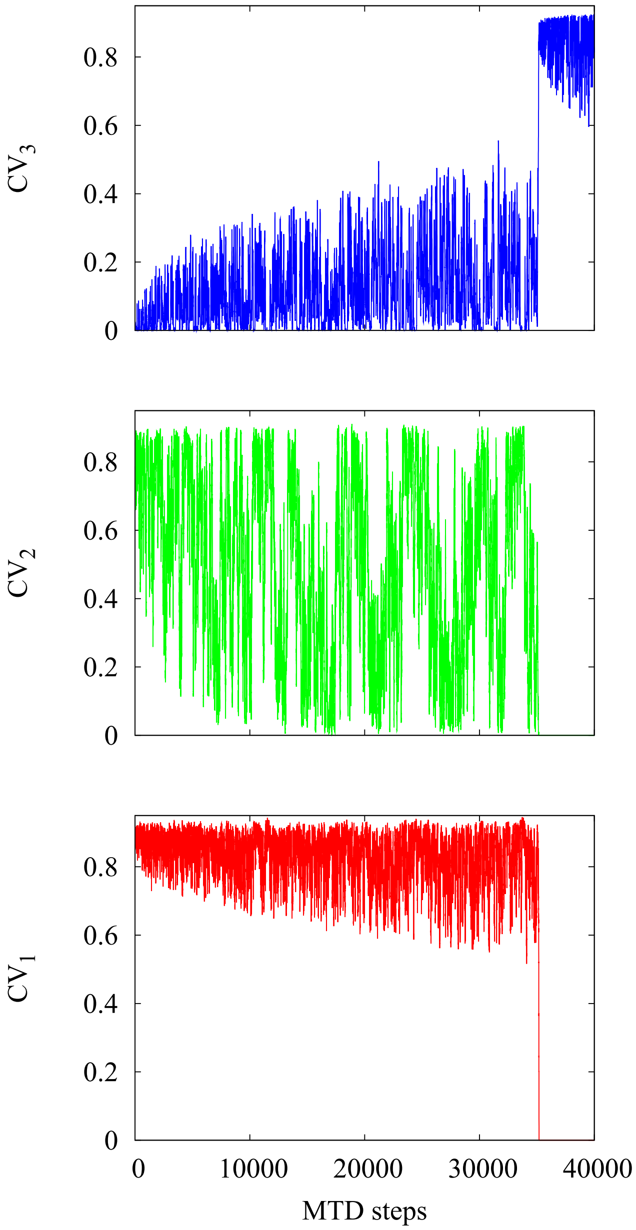

Figure 4.8: Representative metadynamics trajectories of the CVs for the decomposition of H_2CO_3 in a 9-water cluster. Each metadynamics (MTD) step = 50 CPMD steps.

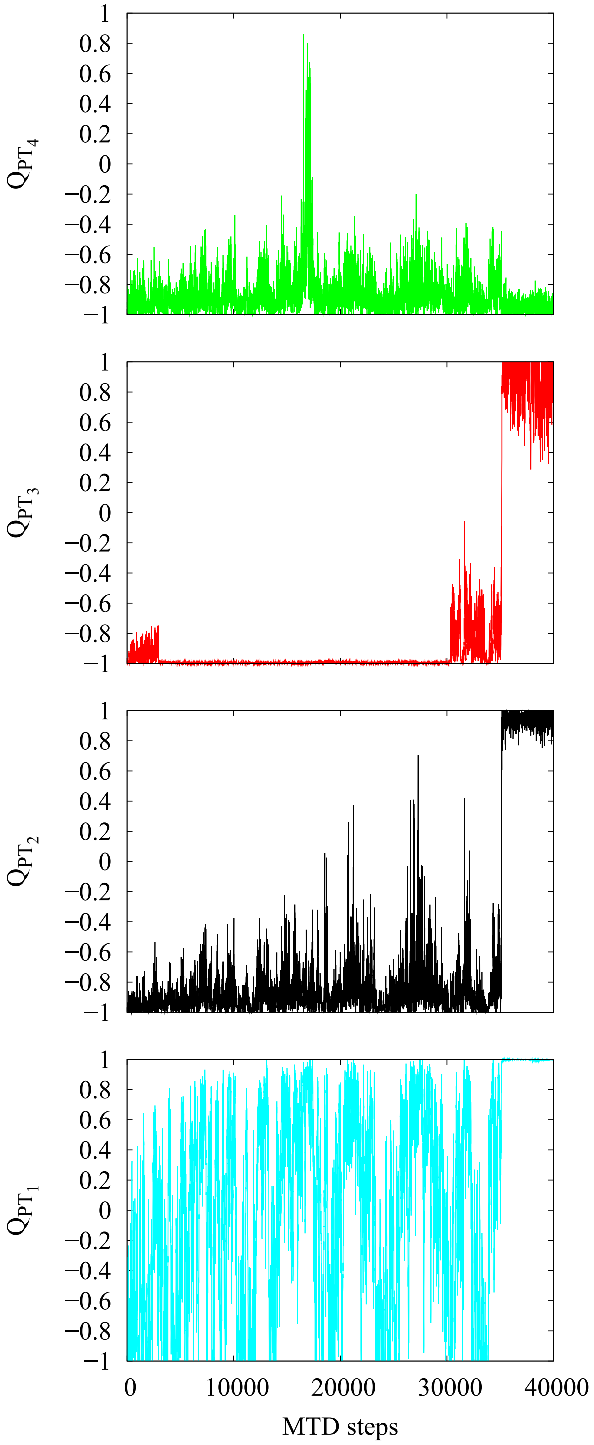
Q_{PT_4}
Q_{PT_3}
Q_{PT_2}
Q_{PT_1}
1
0.8
0.6
0.4
0.2
0
−0.2
−0.4
−0.6
−0.8
−1
0
10000
20000
30000
40000
MTD steps

Figure 4.9: Representative metadynamics trajectories of the proton transport (PT) coordinates for the decomposition of H_2CO_3 in a 9-water cluster. Bottom: Coordinate corresponding to PT between the hydroxyl O in H_2CO_3 and O in the adjacent H_2O molecule, Q_{PT_1}. Lower Middle: Coordinate corresponding to PT between the O atom of the hydronium ion in the contact ion pair and the O atom of the nearest water molecule adjacent to the other hydroxyl O, Q_{PT_2}. Upper Middle: Coordinate corresponding to PT between O in the second water molecule and the other hydroxyl O of H_2CO_3, Q_{PT_3}. Top: Coordinate corresponding to PT between the O atom of the hydronium ion in the contact ion pair and the O atom of the nearest water molecule non-adjacent to the other hydroxyl O, Q_{PT_4}. Each metadynamics (MTD) step = 50 CPMD steps.

We see in Figure 4.8 that after the addition of 35135 hills, all three CVs change their values simultaneously, as in the case of the 6-water cluster. However, unlike in the 6-water cluster, a metastable contact ion pair forms in the 9-water cluster. This becomes apparent upon examination of the CV_2 and Q_{PT_1} trajectories for the two cluster sizes. First, by comparing the CV_2 trajectories (see middle panels of Figures 4.6 and 4.8), we see that in case of the 6-water cluster, CV_2 never reaches a value of ~ 0 until the decomposition is complete; however, in the case of the 9-water cluster, it starts fluctuating between ~ 0.9 and ~ 0.0 after ~ 6000 metadynamics steps. Second, by comparing the Q_{PT_1} trajectories (see lower panels of Figures 4.5 and 4.9), we see that Q_{PT_1} fluctuates rapidly between ~ -1 and ~ 0.5 for the 6-water cluster and between ~ -1 and ~ 1 after ~ 6000 metadynamics steps for the 9-water cluster. Values of 1 for Q_{PT_1} and 0 for CV_2 correspond to a complete transfer of the proton from the H_2CO_3 to the adjacent water molecule to form a contact ion pair. In the case of the 9-water cluster, the proton is seen to reside on the adjacent water molecule for hundreds of metadynamics steps before it transfers back to the H_2CO_3. The formation of this metastable contact ion pair is facilitated by the stabilizing effect of the additional water molecules in its vicinity. The third proton transport coordinate, Q_{PT_3} remains constant around -1 until $\sim$ 30000 metadynamics steps, then begins to fluctuate between ~ -1.0 and ~ -0.2 before it finally becomes ~ 1.0 after $\sim$ 35000 metadynamics steps (see Figure 4.9). This is in contrast to what is observed in the 6-water cluster, where we that Q_{PT_3} fluctuates between ~ -1.0 and ~ -0.4 until it finally changes to ~ 1.0 after $\sim$ 35000 metadynamics steps (see Figure 4.5). The formation of the contact ion pair in the 9-water cluster pulls the nearest water molecule adjacent to the other hydroxyl group in H_2CO_3 away from that hydroxyl O giving rise to a value of ~ -1 for Q_{PT_3} until the decomposition takes place. However, no proton transport occurs between the contact ion pair and the surrounding water molecules to form a solvent-separated ion pair. This is revealed by a fourth proton transport coordinate, Q_{PT_4}, which monitors the proton transfer between the hydronium O in the contact ion pair and the O of the nearest water molecule nonadjacent to the hydroxyl group (see upper panel of Figure 4.9). We see that between 16400 to 17400 metadynamics steps, the proton attempts to transfer to a nearby water molecule, but ultimately cannot. Rather, the proton transfers to the other hydroxyl O in H_2CO_3 via a water molecule (see Q_{PT_2} and Q_{PT_3} in Figure 4.9), which then leads to the production of CO_2 and H_2O in a concerted fashion (involving the formation of a metastable contact ion pair), as mentioned above.

Figure 4.10 shows the free energy surface for the decomposition in the 9-water cluster. In contrast to the 6-water cluster, the reactant well (located at $\{S_1 \sim 0.9, S_2 \sim 0.9\}$) is much broader due to the formation of the metastable contact ion pair. Our calculated free energy barrier for the decomposition is 14.7 kcal/mol, which is lower (by 3.8 kcal/mol) than our calculated value for the 6-water cluster, as expected for a larger water cluster.

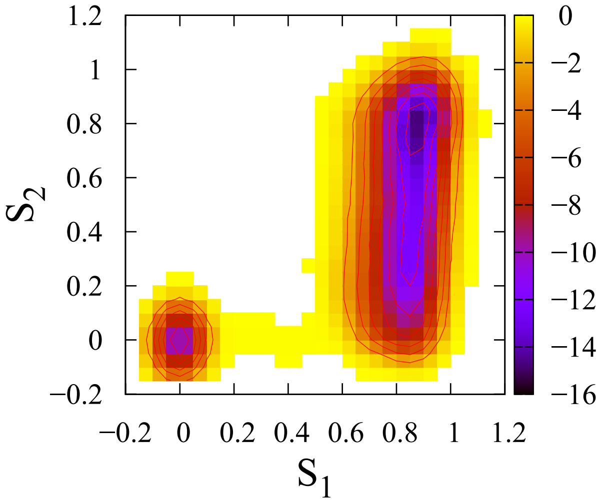

FIGURE 4.10: Free energy (in kcal/mol) projected on to the two auxiliary variables corresponding to CV_1 and CV_2 (S_1 and S_2, respectively) for the decomposition of H_2CO_3 in a 9-water cluster.

4.3.2 Decomposition of H_2CO_3 in 20- and 45-water clusters

After studying the decomposition mechanism in the 6- and 9-water clusters, we studied larger water clusters in order to see if and how the mechanism changes as the system becomes more bulk-like, and thereby shed light on how the mechanism in the bulk phase differs from that in the cluster and gas phases. To accomplish this, we considered 20- and 45-water clusters with one H_2CO_3 molecule located in their centers and observed the decomposition mechanisms with the aid of metadynamics.

Figure 4.11 contains snapshots from a representative metadynamics trajectory of H_2CO_3 in a cluster of 20 water molecules.

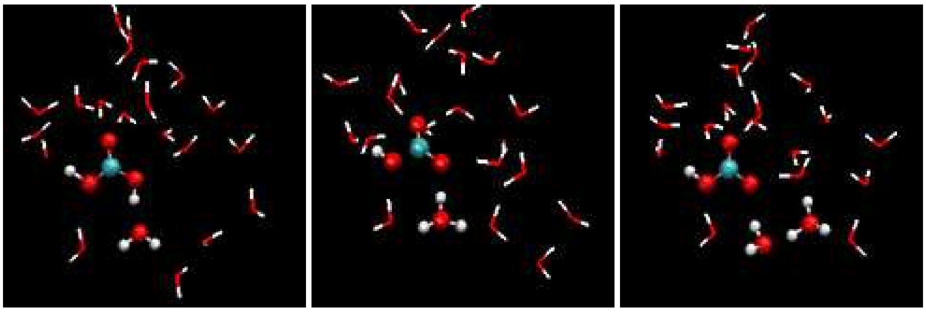

Figure 4.11: Snapshots of the dissociation of H_2CO_3 in a 20-water cluster along a representative metadynamics trajectory. Left: H-bond formation between the donor O in H_2CO_3 and the acceptor O in an adjacent water molecule. Center: Formation of a metastable contact ion pair. Right: Formation of a solvent-separated ion pair.

We see that H_2CO_3 first forms a hydrogen bond with an adjacent water molecule (see left panel Figure 4.11), followed by the formation of a meta-stable HCO_3^-/H_3O^+ contact ion pair (see middle panel of Figure 4.11). Then, the proton shuttles to the O of a neighbouring water molecule, yielding a stable solvent-separated ion pair (see right panel Figure 4.11). At this point, the trajectories were continued using the same set of CVs, but in order to suppress the recombination of HCO_3^- and H_3O^+ to form H_2CO_3 and observe the decomposition of HCO_3^- into CO_2 and H_2O, we restricted the value of CV_2 (i.e., the O-H coordination number) to the range of 0 to 0.02 using a restraining potential. Figure 4.12 shows snapshots of the decomposition of $HCO_3{}^-$ into CO_2 and H_2O from a representative trajectory. We see that the decomposition first involves a proton transfer through a water wire connecting the hydronium to the hydroxyl O in $HCO_3{}^-$ (see top panels of Figure 4.12), followed by the association of a proton to that O and the formation of a coordinated water (see bottom left of Figure 4.12), which is then followed by the separation of the coordinated water from the CO_2 moiety, yielding CO_2 and H_2O (see bottom right of

Figure 4.12). This sequential mechanism (i.e., dissociation followed decomposition) is the same as that observed previously in bulk water[2, 58].

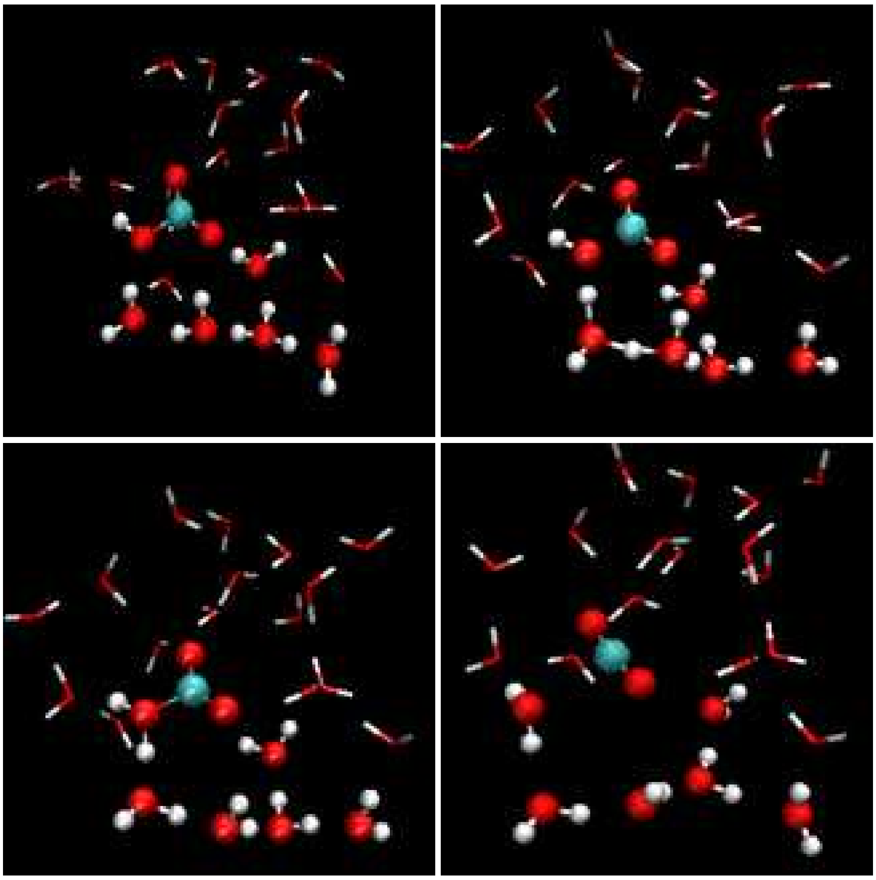

FIGURE 4.12: Snapshots of the decomposition of H_2CO_3 in a 20-water cluster along a representative metadynamics trajectory. Top left: Solvent-separated ion pair. Top right: Proton transport to the hydroxyl O of HCO_3^-. Bottom left: Formation of a water−bent CO_2 complex. Bottom right: Water has split off from bent CO_2 moiety and a straight CO_2 molecule forms.

Figure 4.13 shows the metadynamics trajectories of Q_{PT_1}, Q_{PT_2}, and Q_{PT_3} during the dissociation step. We see that Q_{PT_1} first undergoes large fluctuations between ~ -1 and ~ 0.5 up to 3600 steps, and then fluctuates between ~ 0.2 and ~ 0.8, revealing that the proton first transfers back and forth between H_2CO_3 and the adjacent water molecule before a contact ion pair forms. Unlike in the 9-water clusters, Q_{PT_2} remains relatively constant around ~ -1, i.e., no proton transfer occurs between the contact ion pair and the hydroxyl O of HCO_3^-.

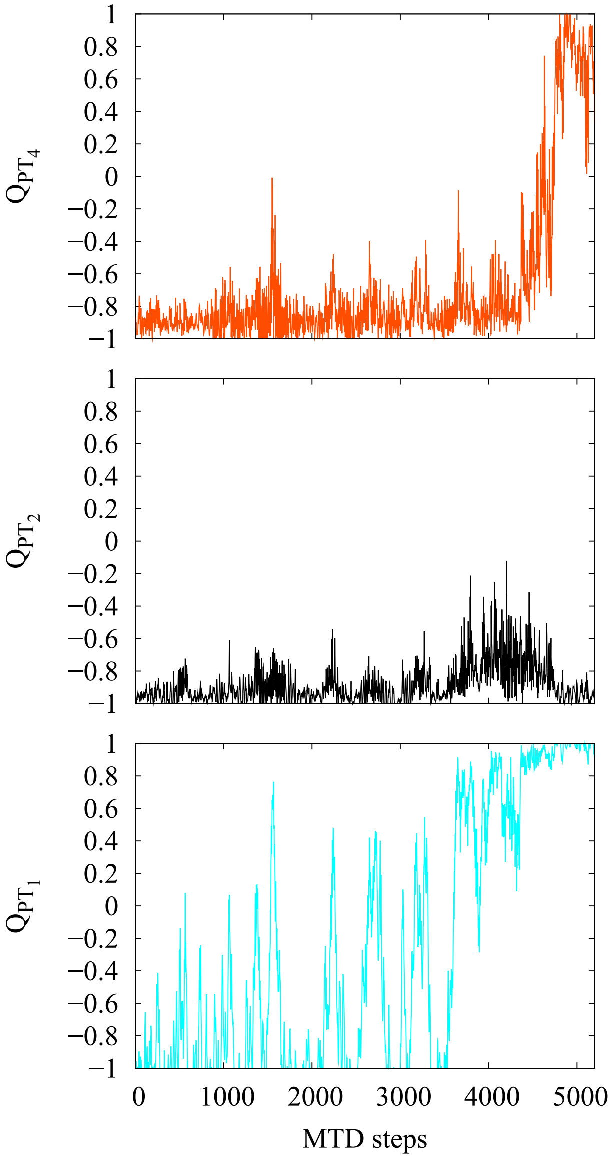

FIGURE 4.13: Representative metadynamics trajectories of the proton transport (PT) coordinates for the dissociation of H_2CO_3 in a 20-water cluster. Bottom: Coordinate corresponding to PT between the hydroxyl O of H_2CO_3 and the O of an adjacent H_2O molecule, Q_{PT_1}. Center: Coordinate corresponding to PT between the O of the hydronium ion in the contact ion pair and the O of the nearest water molecule adjacent to the other hydroxyl O, Q_{PT_2} Top: Coordinate corresponding to PT between the O of the hydronium ion in the contact ion pair and the O of the nearest water molecule non-adjacent to the other hydroxyl O, Q_{PT_4}. Each metadynamics (MTD) step = 50 CPMD steps.

Instead, Q_{PT_3} changes from ~ -1 to ~ 1 after 4769 steps, i.e., the proton transfers from the contact ion pair to a neighbouring water oxygen, yielding a solvent-separated ion pair. The formation of this reaction intermediate was also observed in previous metadynamics studies of H_2CO_3 decomposition in bulk water via the water route[2] and hydroxide route[58].

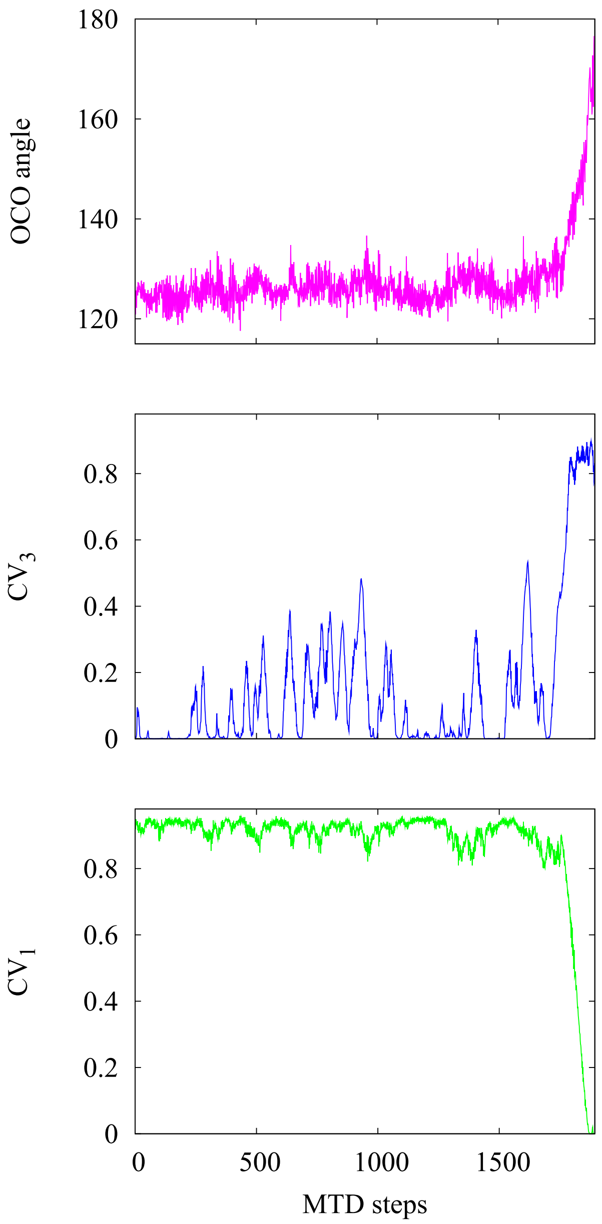

FIGURE 4.14: Representative metadynamics trajectories of CV_1, CV_3, and the OCO angle for the decomposition of H_2CO_3 in a 20-water cluster. Each metadynamics (MTD) step = 100 CPMD steps.

Figure 4.14 illustrates the decomposition of HCO_3^- in terms of the evolutions of CV_1, CV_3, and the O-C-O angle in the CO_2 moiety. We see that after the addition of 1793 metadynamics hills, CV_3 changes from ~ 0 to ~ 0.9 (i.e., the coordinated water forms), followed by a change in CV_1 from ~ 0.9 to ~ 0 after the addition of 78 more hills (i.e., the coordinated water separates from the CO_2 moiety), and the O-C-O angle simultaneously becomes $\sim 180^o$ (i.e, a straight CO_2 molecule forms).

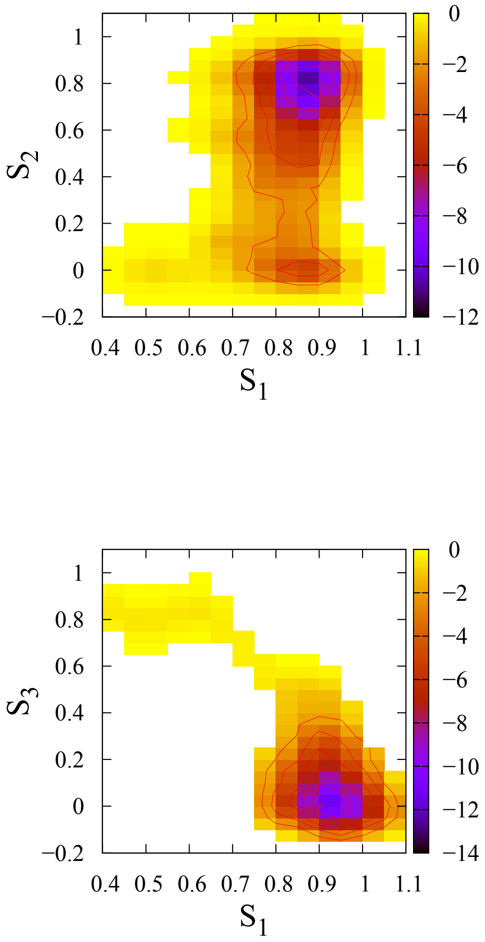

FIGURE 4.15: Top: Free energy (in kcal/mol) projected on to the two auxiliary variables corresponding to CV_1 and CV_2 (S_1 and S_2, respectively) for the dissociation of H_2CO_3 in a 20-water cluster. Bottom: Free energy (in kcal/mol) projected on to the two auxiliary variables corresponding to CV_1 and CV_3 (S_1 and S_3, respectively) for the decomposition of HCO_3^- in a 20-water cluster.

The free energy profiles for the dissociation and decomposition in the 20-water cluster are shown in Figure 4.15. From this figure, we found that the calculated free energy barriers for the dissociation and decomposition are 10.4 kcal/mol and 12.2 kcal/mol, respectively.

We also studied the decomposition mechanism in a 45-water cluster in order to determine whether or not increasing the size of the cluster affects the energetics, as compared to the 20-water cluster. Our metadynamics results show that, like in the 20-water cluster, H_2CO_3 undergoes a step-wise decomposition and the calculated free energy barriers for the dissociation and decomposition are 9.6 kcal/mol and 10.7 kcal/mol, respectively (which are comparable to those of the 20-water cluster considering the size of the error bars). The corresponding snapshots from the metadynamics simulations and free energy profiles are shown in Figures 4.16, 4.17, and 4.18.

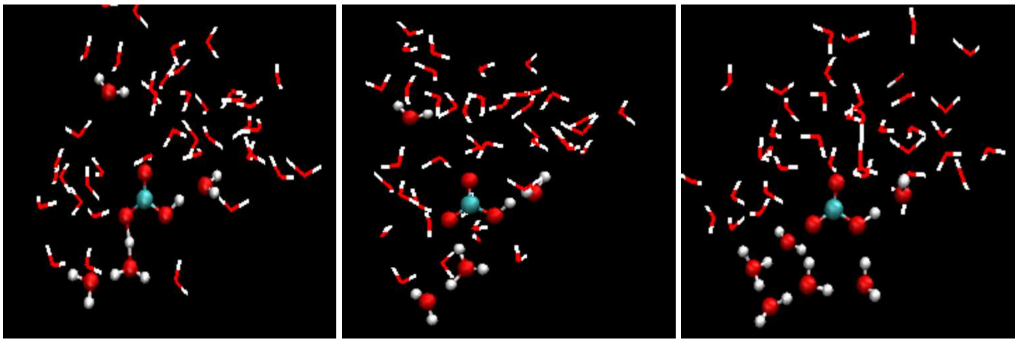

FIGURE 4.16: Snapshots of the dissociation of H_2CO_3 in a 45−water cluster along a representative metadynamics trajectory. Left: Hydrogen bond formation between the donor oxygen in H_2CO_3 and the acceptor oxygen in an adjacent water molecule. Center: Formation of a metastable contact ion pair. Right: Formation of a solvent-separated ion pair.

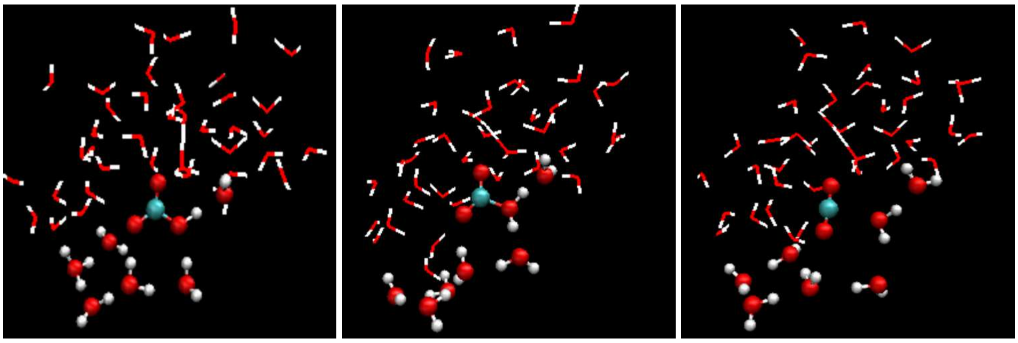

FIGURE 4.17: Snapshots of the decomposition of H_2CO_3 in a 45−water cluster along a representative metadynamics trajectory. Left: Solvent-separated ion pair. Middle: Formation of a water−bent CO_2 complex. Right: Water has split off from bent CO_2 moiety and a straight CO_2 molecule forms.

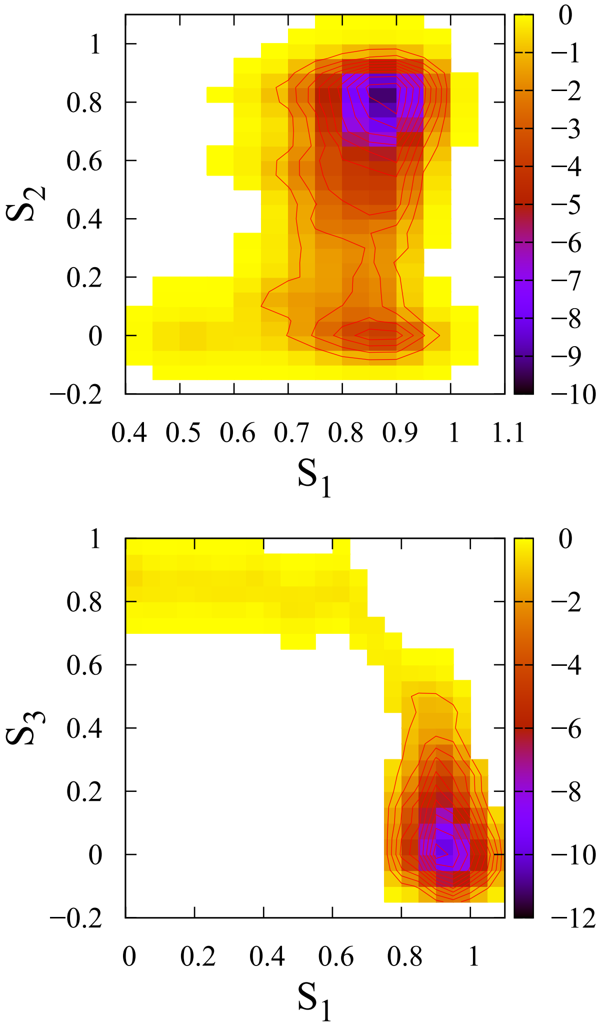

FIGURE 4.18: Top: Free energy (in kcal/mol) projected on to the two auxiliary variables corresponding to CV_1 and CV_2 (S_1 and S_2, respectively) for the dissociation of H_2CO_3 in a 45−water cluster. Bottom: Free energy (in kcal/mol) projected on to the two auxiliary variables corresponding to CV_1 and CV_3 (S_1 and S_3, respectively) for the decomposition of HCO_3^- in a 45−water cluster.

4.3.3 Role of hydrogen bonding in determining the reaction mechanism

To gain deeper insight into what dictates whether the decomposition proceeds via the formation of the stable solvent-separated ion pair (as observed in the larger clusters) or via the concerted route (as observed in the smaller clusters), we analyzed the solvation environments encountered in an ensemble of 10 metadynamics trajectories giving rise to the sequential decomposition and in an ensemble of 15 trajectories giving rise to the concerted decomposition. In the trajectories that proceed via the sequential mechanism, we always saw that H_3O^+ forms three hydrogen bonds with neighbouring water molecules. In contrast, in the trajectories that proceed via the concerted mechanism, we found that either there were not enough water molecules to form three hydrogen bonds with the *transient* H_3O^+ ion or the water molecules were arranged in such a way that three hydrogen bonds could not form with H_3O^+. Figure 4.19 contains snapshots from representative metadynamics trajectories, showing the contact ion pair formation in the 9-water cluster and the solvent-separated ion pair formation in the 20-water cluster.

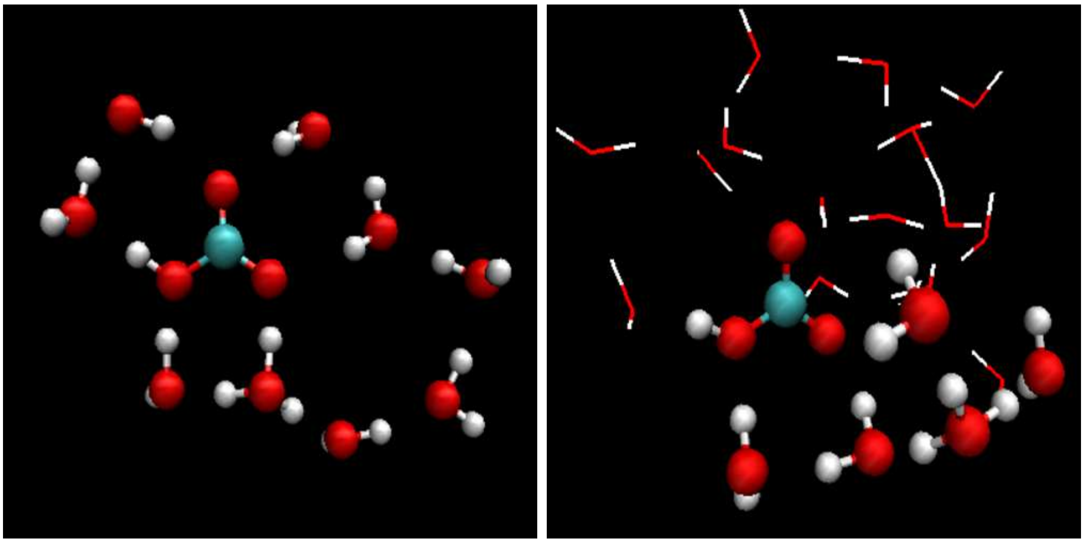

Figure 4.19: Snapshots of the dissociation/decomposition of H_2CO_3 in 9- and 20-water clusters from representative metadynamics trajectories. Left: No proton transfer occurs between the contact ion pair and the O of the nearest water molecule nonadjacent to the hydroxyl O in the 9-water cluster. Right: Solvent-separated ion pair forms since the proton transfers from the contact ion pair to the O of the nearest water molecule nonadjacent to the hydroxyl O in the 20-water cluster.

In case of the 9-water cluster, the solvent-separated ion pair does not form from the contact ion pair since there is an insufficient number of water molecules available to form the three hydrogen bonds which would result in the proton transport to the adjacent water O. However, in the case of 20-water cluster, the proton transports from the contact ion pair to the nearest water O nonadjacent to the hydroxyl O and the H_3O^+ forms three hydrogen bonds with neighbouring water molecules (with O$-$O distances of ~ 2.7 Å). When H_3O^+ is solvated by three water molecules in its first hydration shell, the solvent-separated ion pair remains stable for tens of picoseconds, as observed in 10 unbiased CPMD trajectories. To determine if the solvation environment of HCO_3^- has an effect on the reaction pathway, we generated an ensemble of 10 metadynamics trajectories for the 20-water cluster, five in which the carbonyl oxygens of H_2CO_3 were hydrogen-bonded to at least one water molecule and five in which they were not. We found that in all 10 trajectories H_2CO_3 undergoes decomposition via the sequential mechanism, suggesting that the solvation environment of HCO_3^- does not affect which pathway the reaction takes. This is supported by a recent electronic structure study using the cluster-continuum model, in which a step-wise decomposition was proposed based on a configuration which did not contain any water molecules in the vicinity of the carbonyl oxygen of H_2CO_3 or HCO_3^-[114].

4.3.4 Concerted vs. step-wise decomposition

In this study, we investigated the decomposition of H_2CO_3 in water clusters of various sizes to understand how the nature of the solvation environment around a H_2CO_3 molecule affects its decomposition mechanism. In small clusters (containing 6 and 9 water molecules), we found that the decomposition occurs via a concerted proton shuttle mechanism, which involves (a) the formation of a Zundel-like structure, $HCO_3^{\delta-} \cdots \ H \ \cdots {}^{\delta+}OH_2$, (b) a proton transfer along a chain of one or two water molecules to the hydroxyl O in $HCO_3{}^-$, and (c) the simultaneous breakage of the C-O bond in $HCO_3{}^-$ to form CO_2 and H_2O. However, in larger clusters (containing 20 and 45 water molecules), the decomposition occurs via a two-step route, which involves (a) the formation of a Zundel-like structure, (b) the formation of a contact ion pair, $HCO_3^- \cdots H_3O^+$, (c) the formation of a stable solvent-separated ion pair, $HCO_3^- \cdots H_2O_n \cdots H_3O^+$ (step 1), (d) the formation of a hydrogen bond between a H_3O^+ ion and the hydroxyl O of HCO_3^-, giving rise to the formation of a coordinated water, and (e) the separation of the coordinated water molecule from the CO_2 moiety through the breaking of the C-O bond (step 2). In the presence of a sufficient number of water molecules, the dissociation of H_2CO_3 into stable HCO_3^- and H_3O^+ species is energetically favourable, which precludes the concerted decomposition via the cyclic transition state from occurring.

Our results show that the transition from the concerted decomposition pathway to the step-wise pathway hinges upon the solvation structure surrounding the H_3O^+ intermediate, which in turn depends on the size of the cluster. More specifically, we found that if the H_3O^+ forms three hydrogen bonds with neighbouring water molecules, then the solvent-separated ion pair is sufficiently stabilized and the decomposition commits to the step-wise pathway. However, it should be noted that although the formation of these hydrogen bonds is a necessary condition for the stabilization of the solvent-separated ion pair, their formation might not be a sufficient condition. As discussed in Ref. 94, the fluctuating electric field of the surrounding water molecules also plays an important role in stabilizing the ion pair in solution, viz., the presence of a large number of solvating water molecules can prevent the recombination of the ions since destabilizing fluctuations of the electric field become rare. In the small clusters, there is a low probability that the H_3O^+ intermediate will be solvated by three water molecules and so the decomposition proceeds via an alternate pathway. However, in the larger clusters, after the formation of the Zundel-like structure, the probability of the HCO_3^- and H_3O^+ ions becoming separated by at least one water molecule is very high. Therefore, H_3O^+ can readily form hydrogen bonds with three water molecules in its vicinity and the solvent-separated ion pair can be stabilized. We also found that H_2CO_3 decomposes via the step-wise mechanism in the larger clusters irrespective of the solvation structure surrounding the HCO_3^- intermediate, i.e., the solvent-separated state formed in all trajectories whether or not the carbonyl oxygen of HCO_3^- was hydrogen-bonded to other water molecules.

Since large clusters mimic a bulk-like state, the decomposition of H_2CO_3 most likely occurs via the step-wise mechanism in bulk water. The facts that both the concerted and step-wise mechanisms were captured using the same set of CVs and that a similar set of CVs has previously yielded free energy changes/barriers in bulk water that are in decent agreement with experiment[2], lend credence to both the change in mechanism with increasing cluster size and the mechanisms themselves. Thus, this study, not only sheds light on the stability of H_2CO_3 in water clusters, but also gives a strong argument for why the step-wise decomposition mechanism predominates in bulk water over the concerted mechanism based on considerations of the solvation structure surrounding the reaction intermediates in going from the small to large water clusters.

4.3.5 Error estimation in the metadynamics simulations

We estimated the errors in the metadynamics simulations of all clusters studied using the procedure given in Refs. [82] and [90]. Their values are given in the second column of Table 4.3. It should be noted that the magnitude of the error may be reduced by decreasing the height of the Gaussian hills and the frequency at which they are added, at the cost of increasing the simulation time. We also calculated the standard deviations (SD) of the dissociation and decomposition free energy barriers based on the ensembles of trajectories generated for each cluster size. The numbers of trajectories in each ensemble and the standard deviations are given in the third and fourth columns of Table 4.3, respectively.

Cluster size	Metadynamics error (kcal/mol)	Number of trajectories	SD (kcal/mol)
6-water	1.2	10	1.0
9-water	1.2	10	1.0
20-water	1.8	5	1.2
45-water	1.8	5	1.2

Table 4.3: Estimates of the error in the metadynamics simulations and standard deviations of the decomposition free energy barriers for each cluster size.

4.4 Conclusions

The mechanisms and energetics of the decomposition of H_2CO_3 in four different sized water clusters were investigated using CPMD and metadynamics. Using a common set of CVs in our metadynamics simulations, we observed that in the two small clusters (i.e., 6- and 9-water clusters) the decomposition occurs via a concerted mechanism and in the two larger clusters (i.e., 20- and 45-water clusters) the decomposition occurs via a step-wise mechanism. The concerted mechanism involves the transfer of one of the hydroxyl hydrogens to the other hydroxyl O in H_2CO_3 through a chain of one or two water molecules, which is accompanied by a concurrent breakage of the C-O bond yielding CO_2 and H_2O. In contrast, the sequential mechanism initially involves the formation of HCO_3^- and H_3O^+ intermediates, followed by the breakage of the C-OH bond to yield CO_2. Our results show that this change in mechanism with increasing cluster size occurs due to the presence of a sufficient number of water molecules which renders the dissociation of H_2CO_3 and the subsequent formation of the HCO_3^-/H_3O^+ ion pair to be energetically favourable. In particular, we found that the nature of the hydrogen bonding environment around the H_3O^+ ion determines whether or not the decomposition proceeds via the step-wise mechanism. Since larger clusters can mimic a bulk-like state, the 20- and 45-water clusters are expected to provide bulk-like environments for the reaction and, therefore, we propose that the decomposition of H_2CO_3 in bulk water follows the step-wise route.

Previous attempts at calculating the H_2CO_3 decomposition rate constant in bulk water were based on the concerted mechanism and yielded unsatisfactory agreement with experiment[34]. In light of our findings, one may be able to more accurately calculate the rate constant based on the step-wise mechanism and using the minimum number of water molecules to mimic a bulk-like environment. Such calculations for the decomposition of H_2CO_3 via both the water and hydroxide routes are currently underway in our group and will be reported in a future publication. Moreover, our study sheds light on the role of the water environment in the mechanisms of H_2CO_3 decomposition. This will have implications on H_2CO_3 reactivity in different environments such as those encountered in atmospheric and geochemistry. For example, the decomposition mechanism is likely different at the air/water interface than that in the bulk due to the inhomogeneous environment surrounding an H_2CO_3 molecule. Thus, the insights gained in this study set the stage for further studies of H_2CO_3 reactivity in a wide range of aqueous environments with different morphologies and compositions.

Chapter 5

Mechanistic insights into the dissociation of H_2CO_3 at the air/water interface

5.1 Introduction

Reactions of acid gases (e.g., SO_2, NO_2, CO_2, etc.) and their associated acids with aqueous aerosols and water droplets are ubiquitous in the atmosphere.[53–56] Mechanistic insight into these reactions is important for understanding the composition and reactivity of other gases in aerosols and water droplets and the role played by such particles in atmospheric pollution and the greenhouse effect.[54, 56] Since the first point of contact with a water droplet or aerosol is its surface, a detailed understanding of the reactivity of acid gases and their associated acids at the air-water interface is crucial. In particular, the kinetics and energetics of acid dissociation at the air-water interface are expected to be significantly different than those in bulk water since the intermolecular forces experienced are fundamentally different in interfacial environments than in bulk environments.[43, 117, 118] For example, both experimental and computational studies have shown that the dissociation energetics and kinetics of HNO_3 change significantly at the water surface.[42, 43, 115] More specifically, X-ray photoelectron spectroscopy has shown that the degree of dissociation of HNO_3 decreases by $\sim 20\%$ at the water surface relative to in bulk water.[43] This study was accompanied by ab initio molecular dynamics simulations which found that the solvation environment around HNO_3 at the water surface is more structured than in bulk water, and could thereby stabilize the undissociated HNO_3. Another ab initio molecular dynamics study has shown that HNO_3 remains undissociated at the water surface during a 20 ps long simulation, suggestive of a more stable HNO_3 at the surface and a higher dissociation energy barrier than in the bulk (cf. in bulk, HNO_3 was found to dissociate within 0.5 ps).[42] A classical molecular dynamics study of the hydration structure of NO_3^- has revealed that the hydrogen bond distances between an oxygen of NO_3^- and adjacent water hydrogens increase at the surface compared to in the bulk (1.95 Å vs. 1.87 Å), suggesting that NO_3^- is preferentially stabilized in the bulk than at the surface.[57] Although these results can explain the shift in the equilibrium at the surface favouring HNO_3 over NO_3^-, it is not clear why the dissociation barrier increases at the surface. Hence, further computational studies of the dissociation of atmospherically relevant acids on the surface of water are needed to elucidate the underlying reasons for these changes in dissociation behaviour.

In this chapter, we focus on carbonic acid (H_2CO_3), one of the prevalent acids in the atmosphere, since its reactivity at the air-water interface has been previously studied neither experimentally nor theoretically. In the presence of water, H_2CO_3 can dissociate to form HCO_3^- and H_3O^+ and thereby increase the acidity of its environment. Its pK_a was previously thought to be ∼6.4, based on electromotive force and conductance measurements.[14–16] However, it was later discovered that this is not the true pK_a, since the earlier experiments had taken into account the equilibrium with CO_2 and H_2O in addition to the dissociation, i.e., $CO_2 + 2H_2O \rightleftharpoons H_2CO_3 + H_2O \rightleftharpoons HCO_3^- + H_3O^+$. The actual pK_a lies in the range of $3.4 - 3.8$,[2, 17, 18, 58, 119] indicating that H_2CO_3 is a stronger acid than originally believed and is comparable in acidity to, for example, formic acid (pK_a ∼3.8). Therefore, the impact of H_2CO_3 on the acidity of atmospheric aerosols and water droplets should not be neglected in view of its presence in the upper troposphere (it is formed by the reaction of gaseous CO_2 with water clusters[5] or by the sublimation of solid

H_2CO_3[5, 44]), especially in light of the increasing CO_2 levels in the atmosphere.

The decomposition of H_2CO_3 into CO_2 in the gas phase and in bulk water has been studied extensively both experimentally[5, 18–20, 30, 92, 93] and theoretically. [1–3, 21, 31–38, 58] In the gas phase, H_2CO_3 has a high decomposition energy barrier of $\sim$ 43.5 kcal/mol,[33] but in the presence of water, the barrier decreases substantially to $\sim$15 kcal/mol.[17, 26, 30] As a result, the lifetime of H_2CO_3 in water is short ($\sim$300 ns[18]), which has made it difficult for experiments to identify the exact elementary steps of the decomposition mechanism. However, recent theoretical studies have revealed that the decomposition of H_2CO_3 in bulk water (i.e., $H_2CO_3 \rightleftharpoons CO_2 + H_2O$) occurs predominantly via a step-wise mechanism (i.e., dissociation into $HCO_3{}^-$ and H_3O^+ first, followed by decomposition of $HCO_3{}^-$ into CO_2 and H_2O), as opposed to both step-wise and concerted mechanisms.[2, 102] This is in contrast to the gas phase decomposition, which solely takes place in a concerted fashion via a cyclic transition state.[1] In a recent ab initio metadynamics study of H_2CO_3 decomposition in water clusters,[102] it was found that a mechanistic shift from the concerted to the step-wise pathway takes place when there is a sufficient number of water molecules solvating the H_3O^+. These water molecules stabilize the H_3O^+, which prevents a rapid recombination of the $HCO_3{}^-$ and H_3O^+ ions and thereby leads to the formation of a stable solvent-separated $HCO_3{}^-/H_3O^+$ ion pair, a pre-requisite for the step-wise decomposition to occur.

To gain a microscopic understanding of the reactivity of H_2CO_3 at the surface of a water droplet, we investigated the dissociation of H_2CO_3 at the air-water interface and the solvation environments experienced by the acid and its conjugate base using Car-Parrinello molecular dynamics (CPMD)[76] and metadynamics.[77] The mechanisms and timescales of the dissociation are elucidated and a free energy surface along collective variables appropriate for the dissociation at the water surface is constructed. From this, an upper limit on the dissociation free energy barrier is extracted and insight into the differences between reactions at the water surface and in the bulk is gained. Based on our findings, we also propose a reason for why HNO_3 has a higher dissociation barrier at the water surface than in the bulk.

5.2 Computational details

The dissociation of H_2CO_3 at the air-water interface was investigated using CPMD. To construct the water surface, we first added 49 pre-equilibrated water molecules to an 11.4 X 11.4 X 11.4 Å^3 box with periodic boundary conditions in the x and y directions, but not in the z direction (giving rise to ∼5 molecular layers). We note that 5 water layers were also used in a CPMD study of the dissociation of HNO_3 on top of and within a water slab.[115] Then, the box was elongated by 8.5 Å in both the $+z$ and $-z$ directions to create vacuums above and below the water cube, and equilibrated for 10 ps. This approach was previously used to study the interfacial reactivities of HNO_3[42, 43, 115] and H_2SO_4.[110] Different initial configurations were generated by introducing a cis-trans H_2CO_3 molecule at different positions above the water cube and with different orientations with respect to the water surface. More specifically, we considered two orientations: (i) *Orientation A*− the OH group cis to the carbonyl oxygen pointing toward the surface, and (ii)

Orientation B− the OH group trans to the carbonyl oxygen pointing toward the surface. The two positions we considered are (i) *Position 1*− H_2CO_3 physisorbed to the water surface (the distance between the hydroxyl hydrogen of H_2CO_3 and the nearest water oxygen is ∼3.5 Å), and (ii) *Position 2*− H_2CO_3 above the water surface (the distance between the hydroxyl hydrogen of H_2CO_3 and the nearest water oxygen is ∼5.0 Å). Therefore, we generated four types of initial configurations corresponding to all combinations of orientations and positions (denoted by A1, A2, B1, and B2), as depicted in Figure 5.1.

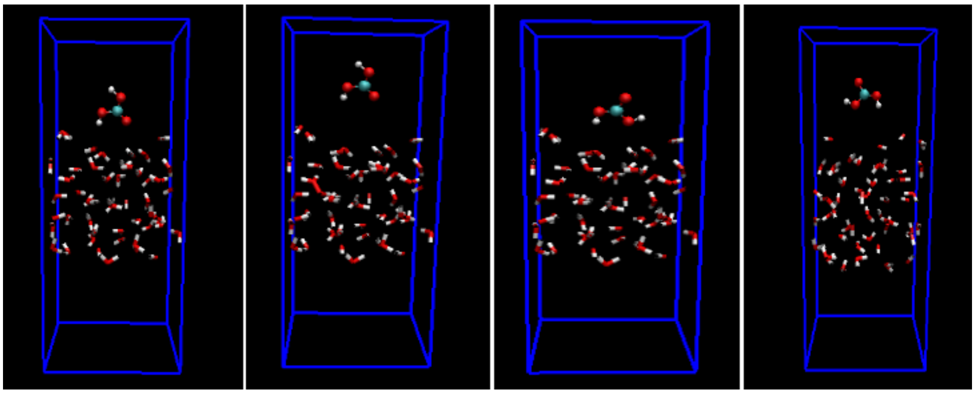

FIGURE 5.1: Snapshots of the various initial configurations used in our simulations, each containing one H_2CO_3 on the surface of a water slab. From left to right: 1. H_2CO_3 near the surface, with the carbonyl oxygen pointing toward the surface (configuration A1). 2. H_2CO_3 at a height of 5.0 Å from the surface, with the carbonyl oxygen pointing toward the surface (configuration A2). 3. H_2CO_3 near the surface, with the carbonyl oxygen pointing toward the vacuum (configuration B1). 4. H_2CO_3 at a height of 5.0 Å from the surface, with the carbonyl oxygen pointing toward the vacuum (configuration B2).

Using CPMD, each configuration was equilibrated for another picosecond, followed by a 15 ps production run. This procedure was followed to generate an ensemble of three different trajectories for each type of initial configuration, in order to validate the reproducibility of our observations. All simulations were carried out at a temperature of 300 K (with the aid of Nosé-Hoover thermostats), in order to compare our results to previous results for H_2CO_3 in bulk water at this temperature. The valence electrons were treated within the DFT formalism using the BLYP functional[86, 87] and the interaction between the core and valence electrons was treated using ultrasoft pseudopotentials[88]. This functional and these pseudopotentials have yielded sensible results in earlier studies of H_2CO_3 in bulk water and water clusters[2, 37, 58, 102]. A plane wave basis set with a cutoff of 40 Ry was used to expand the Kohn-Sham orbitals. The fictitious electron mass and the time step were 600 a.u. and 4 a.u., respectively. Dissociation free energy barriers were calculated using the metadynamics technique.

We used two collective variables (CVs) in our metadynamics simulations. CV_1 is the O(4)-H(5) coordination number in H_2CO_3 and CV_2 is the distance between that O(4) and the H_3O^+ ion in the system (see Figure 5.2 for the atom labels). CV_1 has the following form:

$$\mathrm{CV_1} = \frac{1-(\frac{\mathrm{d}}{\mathrm{d_0}})^{\mathrm{p}}}{1-(\frac{\mathrm{d}}{\mathrm{d_0}})^{\mathrm{p+q}}}, \tag{5.1}$$

where d is the instantaneous distance between O(4) and H(5), d_0 is the distance below which the atoms are considered bonded, and p/q are parameters chosen such that the coordination number tends to zero beyond d_0. CV_2 has the following form:

$$\mathrm{CV_2} = \mathrm{G_{H_2CO_3}R_{H_3O^+}}. \tag{5.2}$$

In the above equation, $\mathrm{R}_{H_3O^+}$ is defined as

$$\mathrm{R_{H_3O^+}} = \frac{\sum_{\mathrm{j}\in \mathrm{O_w}} \mathrm{d_j} \exp(\lambda \mathrm{n_j^H})}{\sum_{\mathrm{j}\in \mathrm{O_w}} \exp(\lambda \mathrm{n_j^H})}, \tag{5.3}$$

where d_j is the instantaneous distance between O(4) in H_2CO_3 and a particular water oxygen, λ is a constant, and n_j^H is the number of hydrogen atoms bonded to that oxygen atom, defined by

$$n_j^H = \sum_{i \in H_w} \frac{1 - (\frac{d_i}{d_0})^p}{1 - (\frac{d_i}{d_0})^{p+q}}, \tag{5.4}$$

where d_i is the instantaneous distance between the water oxygen atom and a water hydrogen atom, and p/q are parameters chosen such that n_j^H tends to zero beyond d_0. $G_{H_2CO_3}$ is a cutoff function, which becomes approximately zero when the H_2CO_3 is undissociated and there is no H_3O^+ ion present in the system and becomes approximately 1 when the dissociation takes place. It is defined as

$$G_{H_2CO_3} = 1 - \frac{1 - (\frac{CV_1}{0.1})^p}{1 - (\frac{CV_1}{0.1})^{p+q}} \tag{5.5}$$

where p and q are parameters chosen such that $G_{H_2CO_3}$ tends to zero when CV_1 is greater than 0.1.

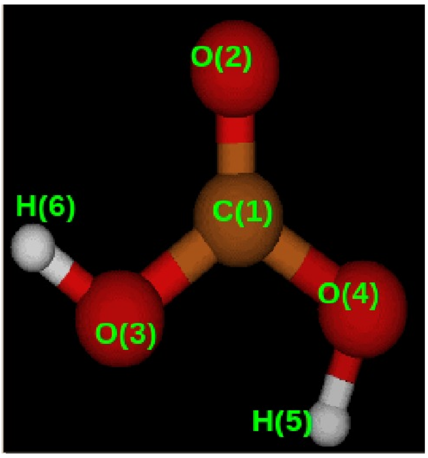

FIGURE 5.2: The atomic labels used in defining the metadynamics collective variables.

The parameters associated with the various CVs used in our metadynamics simulations are summarized in the following table:

	CV_1	CV_2
Gaussian height, W (hartee)	0.0002	0.0002
Gaussian width, $\Delta s'$	0.02	0.05
Metadynamics time step, Δt (a.u.)	200	200
p	6	8
q	24	24
d_0 (Å)	1.60	1.20
λ	-	20

TABLE 5.1: Metadynamics parameters for the dissociation of H_2CO_3.

Based on these parameters, we estimated an error of 1.5 kcal/mol in our metadynamics simulations using the procedure given in Refs. [82] and [90].

5.3 Results and discussions

The dissociation mechanism for configuration A1 is illustrated in Figure 5.3, which shows snapshots from key points along a representative CPMD trajectory. As shown in Figure 5.3, H_2CO_3 first chemisorbs to the surface through two hydrogen bonds, one between a surface water oxygen and a hydroxyl oxygen of H_2CO_3 (i.e., hydrogen bond donor) and the other between a surface water oxygen (i.e., hydrogen bond donor) and the carbonyl oxygen of H_2CO_3.

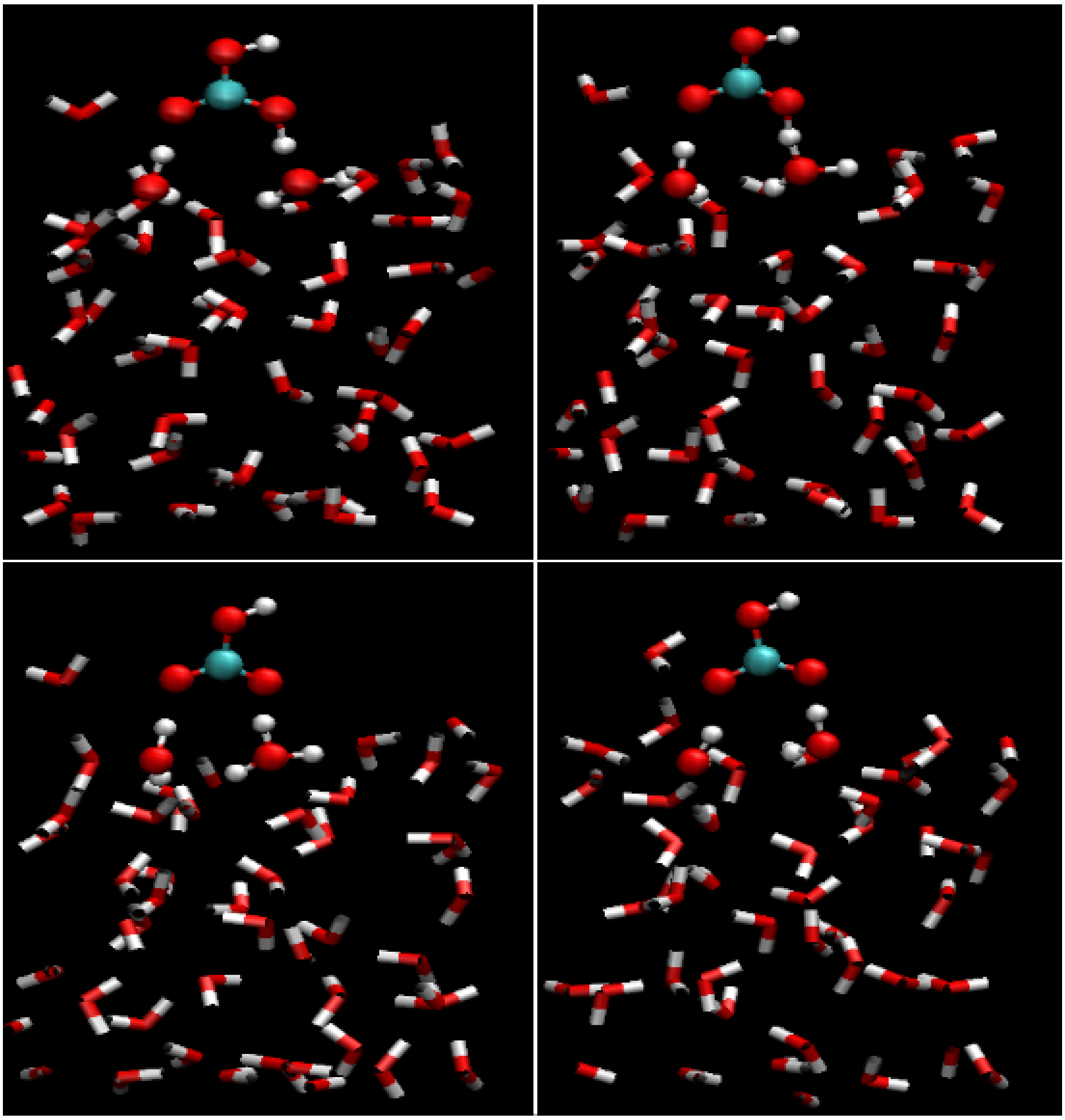

FIGURE 5.3: Snapshots of the dissociation of H_2CO_3 from a representative CPMD trajectory starting in configuration A1. Top left: Hydrogen bond formation between H_2CO_3 and two adjacent water molecules ($t \approx 0.5$ ps). Top right: Formation of a Zundel-like structure ($t \approx 0.8$ ps). Bottom left: Formation of a contact ion pair ($t \approx 1.0$ ps). Bottom right: Complete dissociation takes place yielding solvent-separated ion pair ($t \approx 1.1$ ps).

An examination of the trajectories of the O-H distances (between the H_2CO_3 hydroxyl hydrogen and the nearest water oxygen, and between the H_2CO_3 carbonyl oxygen and the nearest water hydrogen) indeed shows that H_2CO_3 is not hydrogen bonded at the beginning of the simulation, but then forms a hydrogen bond after ~0.6 ps as shown in the Figure 5.4.

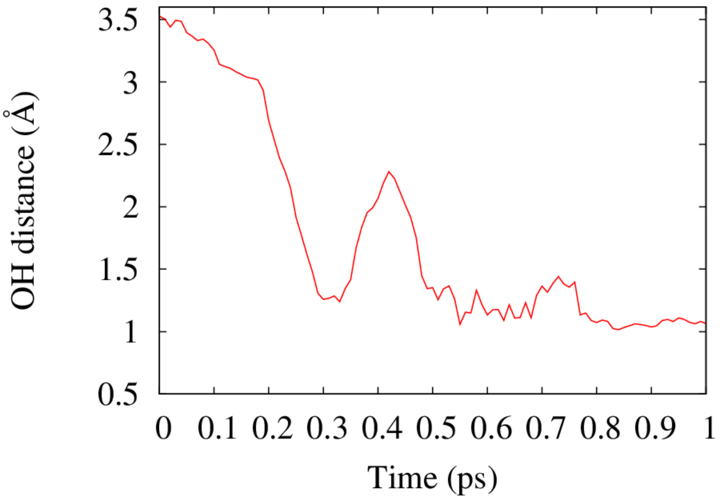

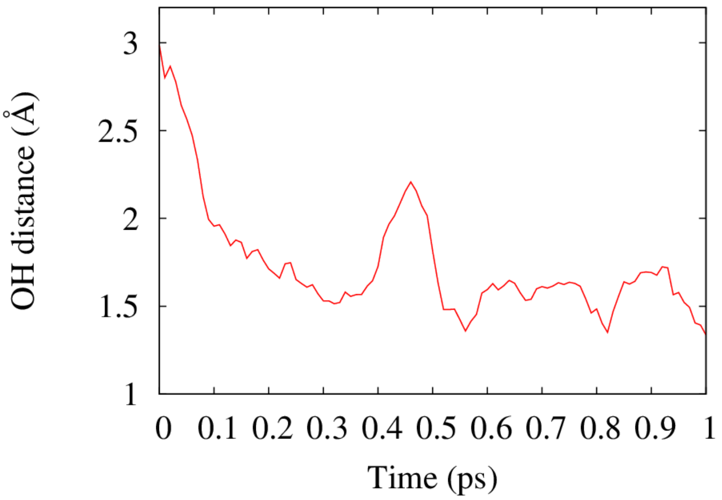

FIGURE 5.4: Trajectory of the OH distances along a representative CPMD trajectory for configuration A1. Top: The distance between H(6) in H_2CO_3 and the nearest water oxygen. Bottom: The distance between O(2) in H_2CO_3 and the nearest water hydrogen. At the begining of the simulation H_2CO_3 is not hydrogen bonded to the surface waters. At t ≈ 0.6 ps H_2CO_3 get adsrobed by two hydrogen bonds.

After 1 ps, H_2CO_3 undergoes dissociation into HCO_3^- and H_3O^+ according to the same steps as in the bulk: (i) the formation a Zundel-like structure (as manifested by a decrease in the distance between the hydroxyl oxygen and the water oxygen), (ii) the breakage of the O-H bond, (iii) the formation of a contact ion pair ($HCO_3^- \cdots H_3O^+$), and (iv) hopping of the excess proton of H_3O^+ to neighbouring water molecules via the Grotthuss mechanism resulting in a solvent-separated ion pair ($HCO_3^- \cdots (H_2O)_n \cdots H_3O^+$). For the remainder of the 15 ps trajectory, a recombination of the ions does not occur, i.e., the system has settled into the stable product well. The above observations are common to the other two trajectories generated for this initial configuration type.

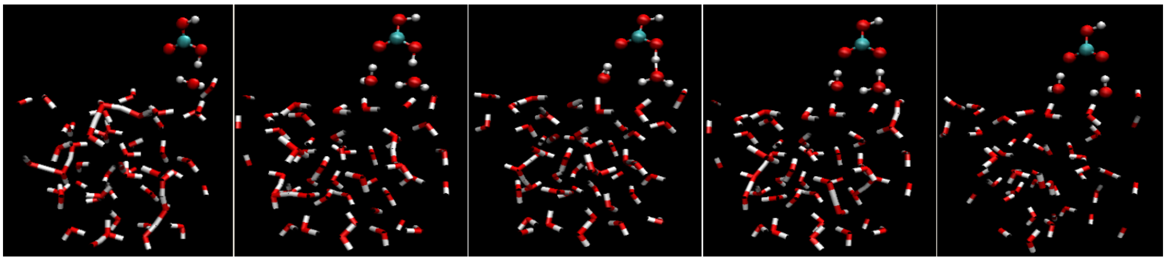

FIGURE 5.5: Snapshots of the dissociation of H_2CO_3 from a representative CPMD trajectory starting in configuration A2. From left to right: 1. Hydrogen bond formation between the hydroxyl oxygen of H_2CO_3 and an adjacent water molecule ($t \approx 2.0$ ps) 2. Hydrogen bond formation between the carbonyl oxygen and an adjacent water molecule ($t \approx 3.0$ ps) 3. Formation of a Zundel-like structure ($t \approx 3.3$ ps) 4. Formation of a contact ion pair ($t \approx 3.5$ ps) 5. Complete dissociation takes place, yielding solvent-separated ion pair ($t \approx 3.6$ ps).

In the case of initial configuration A2, we see in Figure 5.5 that the H_2CO_3 approaches the surface and, at $t \approx 2$ ps, donates the proton from its hydroxyl group to form a hydrogen bond with a surface water oxygen. At $t \approx 3$ ps, the carbonyl oxygen accepts a proton from another surface water oxygen to form another hydrogen bond. Once this hydrogen-bonded complex forms with the surface waters, the dissociation takes place via the same steps and in a similar amount of time as in the case of A1. However, in contrast to the case of A1, the hydrogen-bonded complex forms with two water molecules that are displaced from the surface (see panel 2 in Figure 5.5). This happens due to the fact that, in the case of A2, H_2CO_3 is further from the surface and, as a result, there are fewer waters in its vicinity to solvate it.

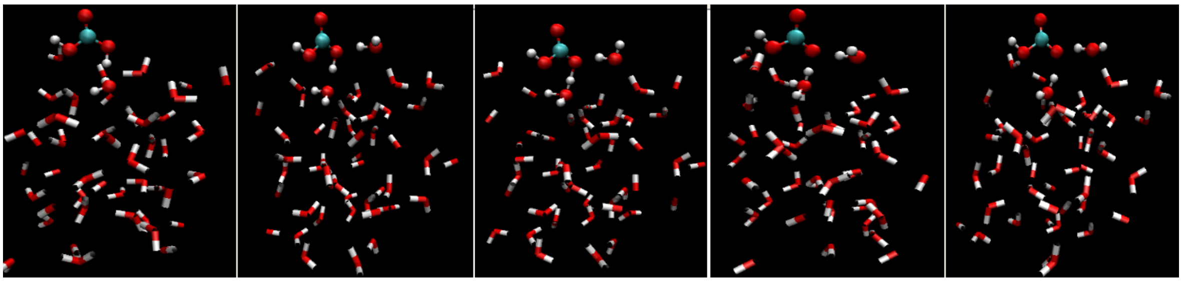

FIGURE 5.6: Snapshots of the dissociation of H_2CO_3 from a representative CPMD trajectory starting in configuration B1. From left to right: 1. Hydrogen bond formation between the hydroxyl oxygen in H_2CO_3 and an adjacent water molecule ($t \approx 0.5$ ps) 2. Second hydrogen bond formation between the same hydroxyl oxygen and another adjacent water molecule ($t \approx 2.0$ ps) 3. Formation of a Zundel-like structure ($t \approx 3.5$ ps) 4. Formation of a contact ion pair ($t \approx 4.0$ ps) 5. Complete dissociation takes place, yielding solvent-separated ion pair ($t \approx 4.1$ ps).

In contrast to initial configuration A1, one hydroxyl group and the carbonyl oxygen of initial configuration B1 point toward the vacuum and, in turn, are not available for hydrogen bonding with the water surface (see Figure 5.1). Therefore, only the remaining hydroxyl group is available for hydrogen bond formation with the surface. In Figure 5.6, we see that H_2CO_3 first forms a hydrogen bond by donating the proton from this hydroxyl group to a neighbouring water oxygen and, after 2 ps, a second hydrogen bond with the same hydroxyl oxygen by accepting a proton from a neighbouring water (see panel 2 of Figure 5.6). We have verified that the other hydroxyl oxygen does not hydrogen bond with the surface water molecules via integration of the radial distribution function (RDF) between that hydroxyl oxygen and the water hydrogens up to 2.5 Å (see top panel of Figure 5.7), which yields only 0.20.

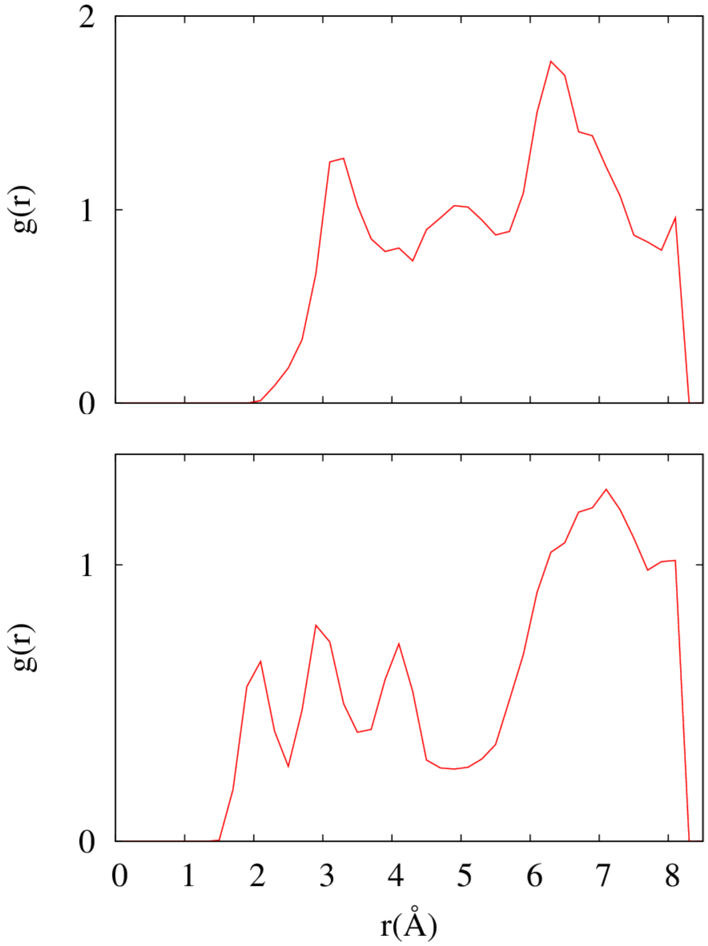

FIGURE 5.7: H_2CO_3 oxygen [O(3)]−water hydrogen radial distribution functions for configurations B1 (top) and B2 (bottom). They were calculated by averaging data from the start of the production run until the dissociation takes place.

Over the next 2 ps, the dissociation takes place via the same mechanism as in the case of A1 (see panels 2, 3, and 4 in Figure 5.6), but more slowly than in the case of A1 (4 ps vs. 1 ps). In the case of initial configuration B2, we see that H_2CO_3 first forms a hydrogen bond by donating the proton from the hydroxyl group to a neighbouring water oxygen in 1 ps and, one picosecond later, a *weak* hydrogen bond by accepting a proton from a nearby water through the other hydroxyl oxygen (see Figure 5.8).

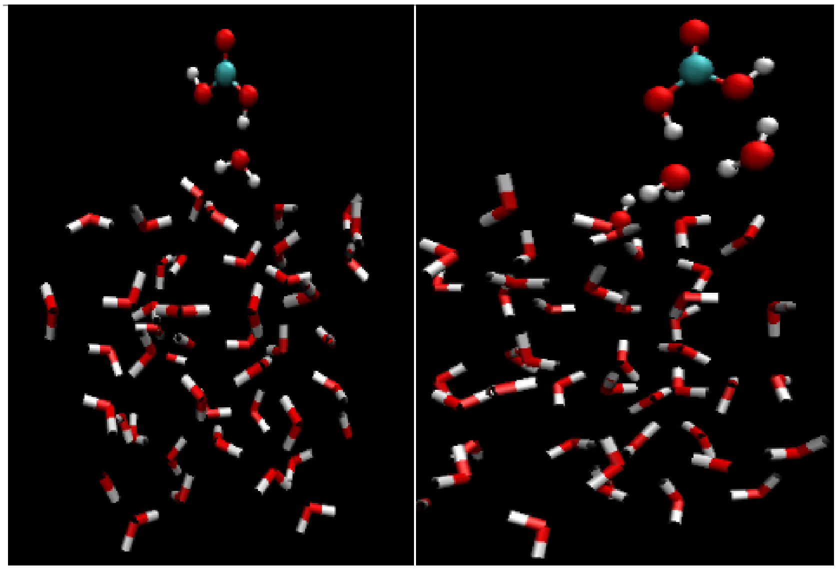

FIGURE 5.8: Snapshots of the hydrogen bond formation of H_2CO_3 from a representative CPMD trajectory starting in configuration B2. Left: Hydrogen bond formation between the hydroxyl oxygen in H_2CO_3 and an adjacent water molecule ($t \approx 1.0$ ps) Right: Formation of a weak hydrogen bond between the other hydroxyl oxygen in H_2CO_3 and another water molecule ($t \approx 2.0$ ps).

This hydrogen bond was deemed to be weak based on a distance of ~2.0 Å between that hydroxyl oxygen and the nearest water hydrogen (determined from the position of the first peak in the RDF between that hydroxyl oxygen and the water hydrogens in the lower panel of Figure 5.7) and integration of this RDF up to the first minimum which yields 0.6. In contrast to initial configuration B1, the hydroxyl oxygen that donates a hydrogen bond to a neighbouring water does not accept another hydrogen bond from another water due to the scarcity of waters in its vicinity at this greater distance from the surface (compare panel 2 of Figure 5.6 to left panel of Figure 5.8). For the remainder of the 15 ps trajectory, B2 remains undissociated, unlike the other initial configurations which undergo rapid dissociations. This was also observed in the other two trajectories generated for this initial configuration type.

The above results reveal that the differences in dissociation times for the various relative orientations and distances of H_2CO_3 to the surface is due to the differences in the hydrogen bonding environments experienced by H_2CO_3, which arise due to the anisotropic nature of the water surface. When H_2CO_3 is in the A orientation, hydrogen bonding between the carbonyl oxygen and the surface speeds up the dissociation compared to H_2CO_3 in the B orientation (where the carbonyl oxygen points toward the vacuum and, hence, cannot form a hydrogen bond with the surface). This suggests that hydrogen bond formation between the carbonyl oxygen and water stabilizes (1) the transition state more than the undissociated acid, thereby decreasing the barrier, and (2) the HCO_3^-, thereby facilitating the rapid departure of the H_3O^+ from the HCO_3^- moiety In the case of configuration B2, H_2CO_3 is not seen to undergo dissociation during the 15 ps trajectories since it forms only one strong hydrogen bond with a nearby water, which does not reduce the energy barrier sufficiently to observe dissociation on the timescale of the simulations.

The formation of the stable solvent-separated ion pair (i.e., the dissociation of H_2CO_3 into HCO_3^- and H_3O^+) observed for the A1, A2, and B1 configurations in our short CPMD runs is significant in several respects. First, our results strongly suggest that the dissociation of H_2CO_3 at the water surface has a substantially lower energy barrier than in bulk water. Previous theoretical studies have found an energy barrier of ~ 9.5 kcal/mol for the dissociation of H_2CO_3 in bulk water[2, 58]. Since the bulk barrier is high relative to k_bT ($\sim$16 k_bT at 300 K), the dissociation could not be observed in unbiased CPMD runs which were tens of picoseconds long and, therefore, metadynamics was used to compute it. Similarly, since configuration

B2 did not dissociate within a 15 ps CPMD trajectory, we used metadynamics to calculate a dissociation barrier. Figure 5.9 shows snapshots of the dissociation of H_2CO_3 along a representative metadynamics trajectory. Our calculated energy barrier (see figure 5.10 for the free energy profile) is 5.0 kcal/mol ±1.1 kcal/mol (~8.5 $k_b T$), which constitutes the upper bound of the dissociation barriers encountered in this study.

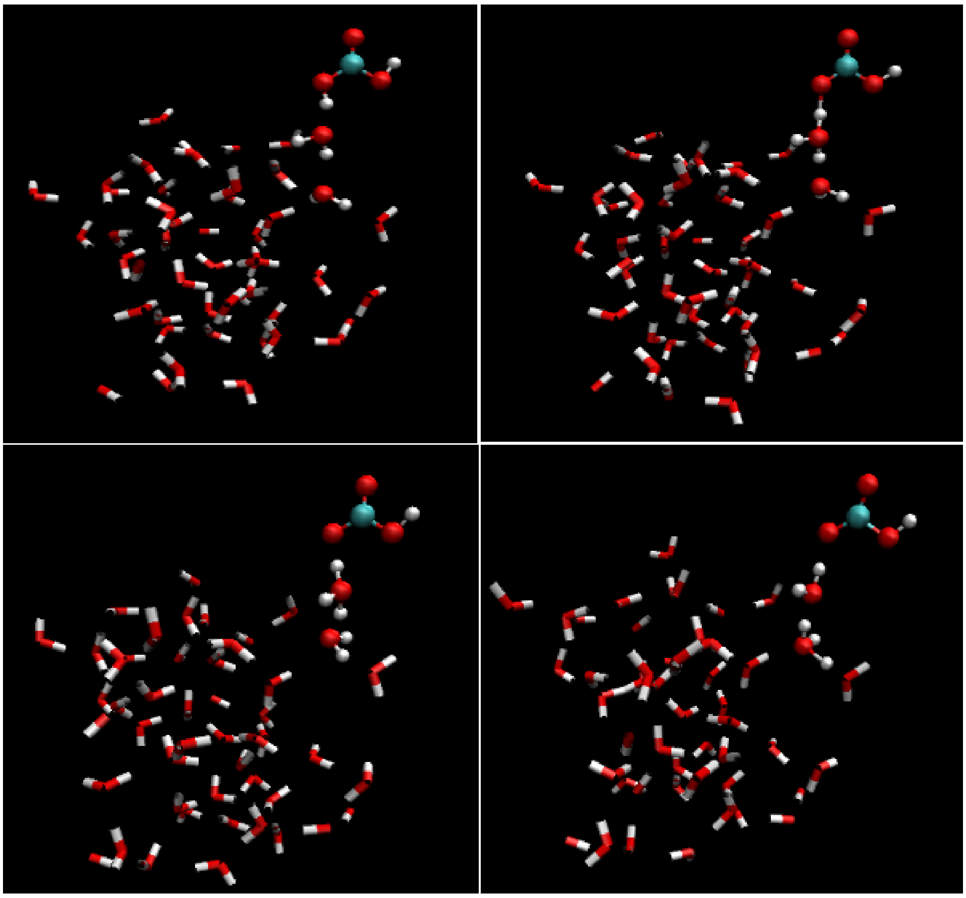

FIGURE 5.9: Snapshots of the dissociation of H_2CO_3 along a representative metadynamics trajectory for configuration B2. Top Left: Hydrogen bond formation between the donor oxygen in H_2CO_3 and the acceptor oxygen in an adjacent water molecule. Top right: Formation of a Zundel-like structure. Bottom left: Formation of a metastable contact ion pair. Bottom right: Complete dissociation takes place, yielding a solvent-separated ion pair.

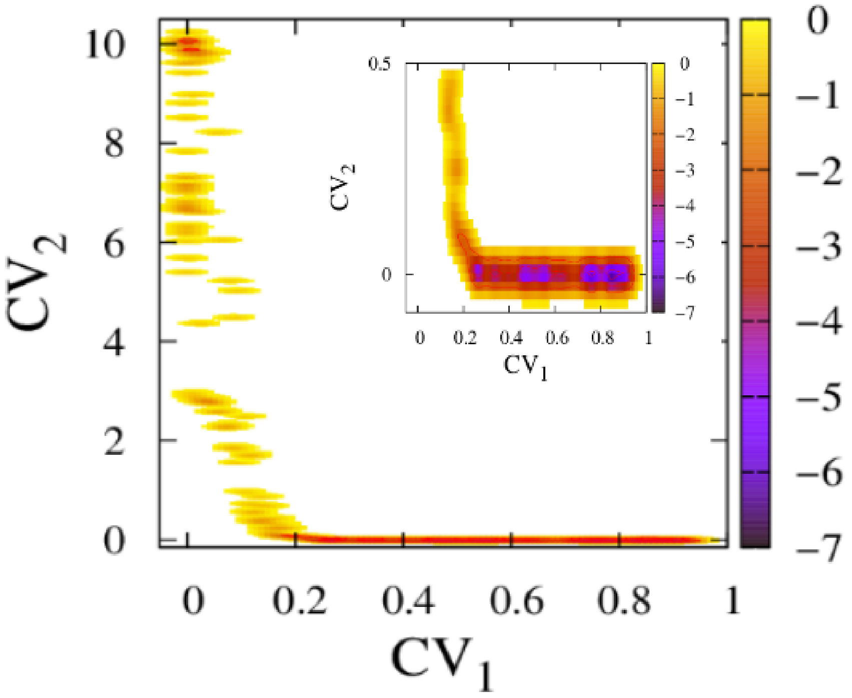

FIGURE 5.10: Free energy (in kcal/mol) profile as a function of CV$_1$ and CV$_2$ for the dissociation of H_2CO_3 in configuration B2. The inset zooms in on the reactant well.

Therefore, the dissociation of H_2CO_3 at the surface of an aqueous particle is expected to be orders of magnitude faster than in the bulk. Second, our results suggest that the concerted decomposition pathway is highly unlikely at the water surface. After the H_3O^+ ion forms at the surface, it diffuses into the bulk and becomes fully solvated there. This allows for the formation of a stable solvent-separated ion pair (see product well at $\{CV_1 \approx 0, CV_2 \approx 10\}$ in the free energy surface in Figure 5.10), despite the fact that the HCO_3^- residing at the surface is not fully solvated. This is consistent with our recent finding that hydrogen bond formation with the carbonyl oxygen is not a pre-requisite for a step-wise decomposition to occur in bulk water, but rather the full solvation of the H_3O^+ ion, which inhibits the recombination of the ion pair and thereby precludes the concerted pathway[102]. Therefore, we expect H_2CO_3 to decompose via a step-wise pathway at the water surface, but this remains to be confirmed.

The (at least) 4.5 kcal/mol decrease in the dissociation energy barrier in going from the bulk to the surface may happen for one or both of the following reasons: (1) the reactant destabilizes relative to the transition state, and/or (2) the transition state stabilizes relative to the reactant. To gain insight into exactly what causes the accelerated dissociation at the water surface, we must first consider the solvation environment around H_2CO_3. Unlike in bulk water, all of the oxygens and hydrogens in H_2CO_3 cannot be implicated in hydrogen bonds at the surface. However, H_2CO_3 can form hydrogen-bonded complexes with at least two water molecules, as shown earlier. Figure 5.11 shows the H_2CO_3 carbon−water oxygen RDFs for configurations A2, B1, and B2. These RDFs were calculated based on trajectory data from the start of the production run until the time of dissociation[120].

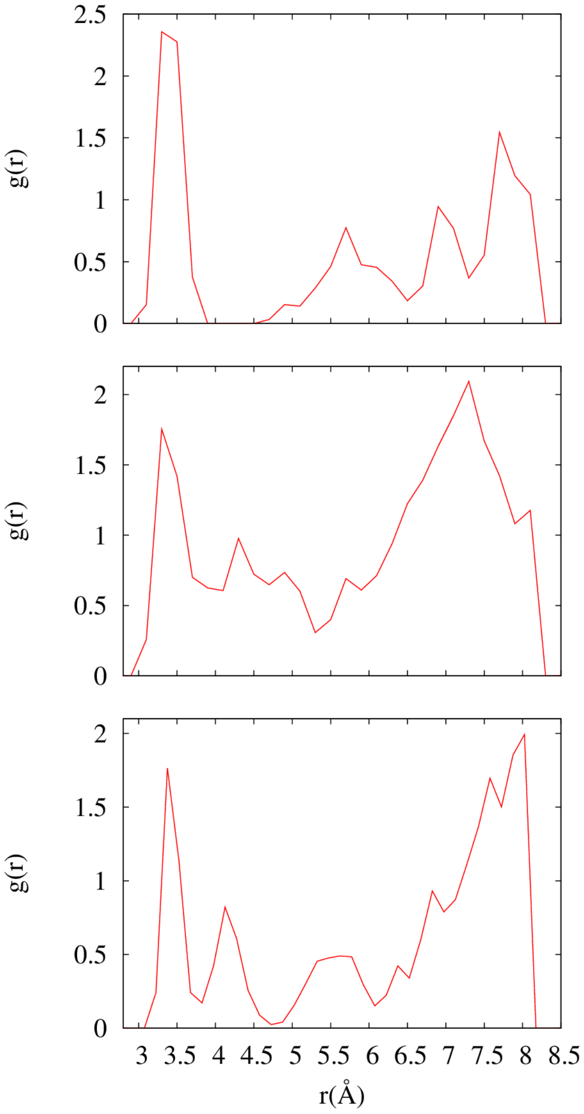

FIGURE 5.11: H_2CO_3 carbon−water oxygen radial distribution functions for configurations A2 (top), B1 (middle), and B2 (bottom).

Overall, they show that the water molecules are well-structured around the H_2CO_3 molecule, even up to the third solvation shell. This should be contrasted with the bulk, where second and third hydration shells cannot be resolved (i.e., the water molecules beyond the first hydration shell are randomly arranged)[37]. As mentioned earlier, a structured solvation environment around HNO_3 at the water surface was observed in the ab initio molecular dynamics study of Lewis et al.[43], but based only on a more structured first peak in the HNO_3 oxygen to water oxygen RDF (as compared to the bulk). In the case of A2, the first peak is centred at ∼3.4 Å, which when integrated gives ~ 2, indicating that H_2CO_3 forms a hydrogen-bonded complex with two water molecules. Beyond this first hydration shell, the RDF becomes zero between $\sim 4-4.5$ Å due to the fact that, since H_2CO_3 is further from the surface, two water molecules migrate away from the surface to form a hydrogen-bonded complex with the H_2CO_3, leaving a gap between them and the remaining water molecules. Integration of the second and third hydration shells reveals that they each contain three water molecules. In the case of B1, the first peak is centred at ∼3.4 Å, which when integrated out to 4 Å reveals that two water molecules are found in this range. However, unlike in the case of A2, there is a shoulder at ~ 3.6 Å since the two hydrogen bonds accepted and donated by the hydroxyl oxygens in H_2CO_3 are not of equal length. In addition, the RDF never becomes zero since, in this case, H_2CO_3 forms a hydrogen-bonded complex with two water molecules closer to the surface than in the case of A2. The second and third hydration shells contain two and one water molecules, respectively. In the case of B2, the first peak is centred at ∼3.4 Å, which when integrated reveals that one water molecule is found in this range. Therefore, unlike A2 and B1, H_2CO_3 is hydrogen-bonded primarily to one water molecule. Like B1, integration of the second and third hydration shells reveals that they contain two and one water molecules, respectively. We also examined the H_2CO_3 oxygen$-$water oxygen and H_2CO_3 hydrogen$-$water oxygen distances to gain insight into the hydrogen bond forming and breaking dynamics for configuration B2 (see Figure 5.12). For the duration of the 15 ps simulation, these distances do not exceed 2.8 and 1.5 Å, respectively, indicating that the hydrogen bond remains intact. In contrast, in the bulk, the hydrogen bond breaks a few times during the course of a 14 ps simulation (yielding an average hydrogen bond lifetime of several picoseconds)[37]. This suggests that the average lifetime at the water surface is longer than in the bulk.

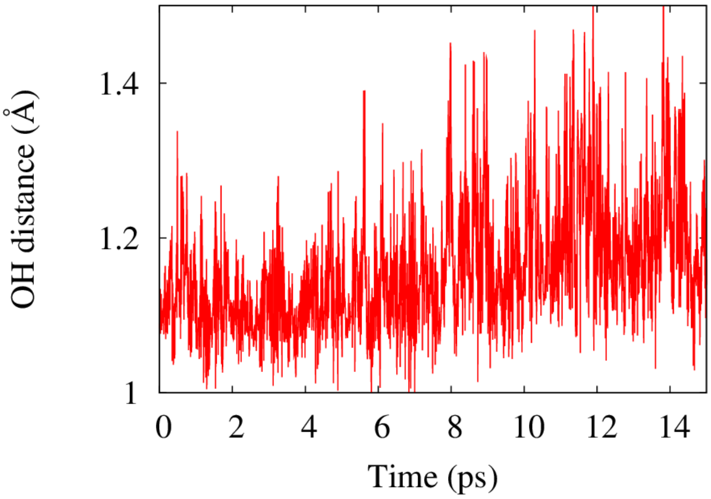

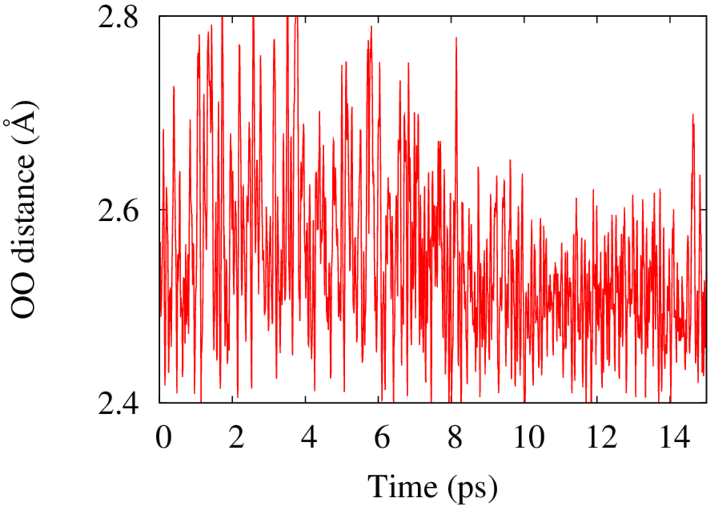

Figure 5.12: Trajectory of the distances along a representative CPMD trajectory for configuration B2 during the 15 ps production run. Top: The distance between H(5) in H_2CO_3 and the nearest water oxygen. Bottom: The distance between O(4) in H_2CO_3 and the nearest water oxygen. During the entire simulation time, the OH and OO distances remain within the typical cutoff for a hydrogen bond.

Based on the information in these RDFs and the assumption that the reactant and transition state experience similar solvation environments, we propose that the second reason (mentioned above) is responsible for the decrease in the dissociation energy barrier. Although we did not directly probe the solvation structure of the transition state, the transition state is also expected to experience a structured solvation environment based on the argument that both H_2CO_3 and HCO_3^- experience such an environment (see Figure 5.13 for the HCO_3^- oxygen−water hydrogen RDFs of configurations A1, A2, and B1).

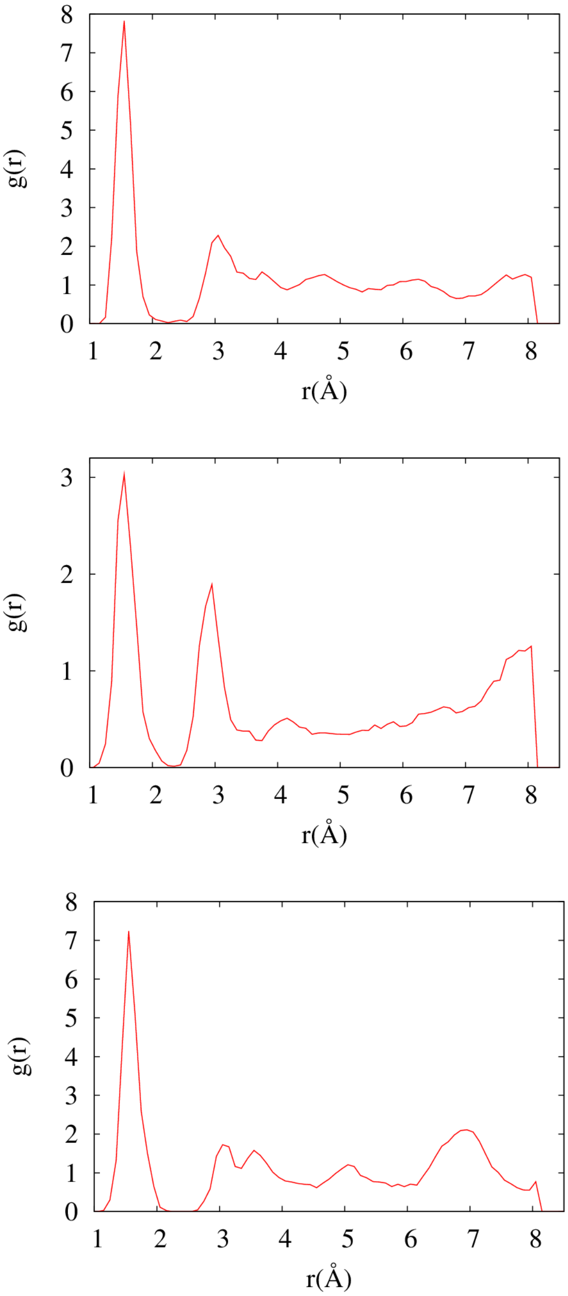

FIGURE 5.13: HCO_3^- oxygen[O(2) for A, and O(4) for B]−water hydrogen radial distribution functions for configurations A1 (top), A2 (middle), and B1 (bottom).

Now, since the transition state is more polar than the reactant, it is expected to be substantially more stabilized than the reactant in this structured solvation environment (due to more favourable electrostatic interactions), and thereby give rise to the decrease in the dissociation barrier. The question is then why does this not happen in the case of HNO_3 at the water surface? As mentioned earlier, the propensity of HNO_3 to dissociate dramatically decreases at the water surface compared to in bulk water[42, 43, 115]. Although the solvation environment of HNO_3 is more structured at the water surface compared to in bulk[43], it is not as well-structured as that of H_2CO_3 and HCO_3^-. Hence, the contribution to the relative stabilization of the transition state is not as large in the case of the HNO_3 dissociation as in the case of H_2CO_3 dissociation. This combined with the fact that there is a strong electrostatic interaction between NO_3^- and H_3O^+ at the water surface compared to in the bulk, means that more energy has to be put in to separate these ions. Therefore, it is reasonable to expect that the transition state of the HNO_3 dissociation will be significantly higher in energy than in the bulk. It should be noted that in the case of HCO_3^-, this interaction is not as strong due to its smaller charge density.

5.4 Concluding Remarks

In summary, we have found that the dissociation energy barrier of H_2CO_3 is substantially reduced at the air/water interface compared to that in bulk water (a few to $\sim 8.5\ k_bT$ at the surface compared to $\sim 16\ k_bT$ in the bulk), based on ab initio molecular dynamics and metadynamics simulations of H_2CO_3 on and near the surface of a slab of water molecules. This could mean that the role played by H_2CO_3 in the acidification of atmospheric aerosols and water droplets may be more important than originally thought. Based on our findings, we proposed that this reduction is due to an enhanced solvation of the transition state (relative to the undissociated acid), owing to the higher structure of interfacial water molecules than bulk ones. This is in stark contrast to HNO_3, whose propensity to dissociate is substantially weaker at the surface of water relative to in the bulk. Our results suggest that the solvation environment of H_2CO_3 is more structured than that of HNO_3 at the water surface, which leads to a higher relative stabilization of the transition state in the case of the H_2CO_3 dissociation. In addition, there is a weaker electrostatic interaction between HCO_3^- and H_3O^+ than between NO_3^- and H_3O^+ at the water surface compared to in the bulk, which means that more energy has to be put in to separate the NO_3^- and H_3O^+ ions. These reasons combined imply that HNO_3 is kinetically more stable at the water surface compared to in the bulk. Overall, these findings give general insight into the kinetic stability of protic acids at the air-water interface.

Chapter 6

Mechanistic insights into the hydration of CO_2 at the air/water interface

6.1 Introduction

The hydration and hydroxylation of CO_2 are fundamental processes which occur in many environmental and biological settings. For example, the hydration of CO_2 to form H_2CO_3 which then dissociates into HCO_3^- and H_3O^+ in the presence of water, plays an important role in the acidification of water bodies [121–128] and atmospheric aerosols[53–56]. The hydroxylation of CO_2 under high pH conditions to form HCO_3^- is involved in physiological pH balance[129–131]. In light of increasing CO_2 levels in the atmosphere, an in-depth understanding of these reactions in a variety of aqueous environments is of paramount importance. Gaseous CO_2 can react with H_2O to form H_2CO_3, which can then dissociate in the presence of water into HCO_3^- and H_3O^+, thereby increasing the acidity of an aqueous medium[91, 128]:

$$\mathrm{CO_2(g) + 2H_2O \rightleftharpoons H_2CO_3 + H_2O \rightleftharpoons HCO_3^- + H_3O^+} \tag{6.1}$$

In bulk water, recent ab initio metadynamics[2] and quantum chemical[114] studies have proposed that the formation of H_2CO_3 takes place via a step-wise pathway involving the formation of the $HCO_3{}^-$ and H_3O^+ ion pair as a stable intermediate.

$$\mathrm{CO_2(aq) + 2H_2O \rightleftharpoons HCO_3^- + H_3O^+ \rightleftharpoons H_2CO_3 + H_2O} \tag{6.2}$$

The reactivity of CO_2 with H_2O in the gas phase and in bulk water has been investigated both theoretically[1–3, 21, 31–38, 58], and experimentally[17, 23–30]. However, little is known about the absorption of CO_2 and its reactions at the air/water interface. Acid-base chemistry at the air/water interface is expected to be different than in bulk water, since a heterogeneous interface provides a different solvation environment than bulk water does[43, 117, 118]. Therefore, a detailed investigation of CO_2 hydration at the air/water interface, its first point-of-contact with an aerosol or water droplet, is crucial for understanding its affect on the acidity of such particles.

The CO_2/H_2O interface has been previously studied by X-ray diffraction[132] and vibrational sum frequency generation (SFG) spectroscopy[54]. The focus of the X-ray diffraction study was mainly on the gas hydrate formation mechanisms at the surface. In the SFG study, the authors examined the adsorption and reaction of CO_2 at the water surface and found that no surface-bound H_2O/CO_2 complex forms. However, there was a slight increase in the intensity of the sum-frequency spectrum at $\sim$3200 cm^{-1}, which was attributed to the presence of the reaction products, i.e., HCO_3^-, CO_3^-, and H_3O^+. Therefore, this study successfully confirmed the presence of hydration products of CO_2 at the air/water interface, but the mechanisms of the formation of these hydration products were beyond the scope of this study. The CO_2/H_2O interface has also been studied by classical and ab initio molecular dynamics under low CO_2 pressure conditions[59–61], clathrate hydrate-forming conditions[62–65], and supercritical and subcritical CO_2 conditions[66–68]. However, no theoretical attention has previously been given to the mechanisms, energetics, and kinetics of the hydration reactions of CO_2 at the CO_2/H_2O interface. In this chapter, we study the mechanism and energetics of the hydration of CO_2 at the air/water interface in the limit of low CO_2 pressure. More specifically, we investigate the solvation environment around CO_2, the identity of the reaction products, the mechanism of the reaction, and the free energy barrier of the reaction.

6.2 Computational details

To gain microscopic insight into the reactivity of CO_2 at the surface of a water droplet, we have studied a CO_2 molecule on a water slab using Car-Parrinello molecular dynamics (CPMD)[76] and metadynamics[77]. In our simulations, the water surface was set up in the following way: We first added 49 pre-equilibrated water molecules to an 11.4 X 11.4 X 11.4 Å^3 box with periodic boundary conditions in the x and y directions, but not in the z direction (giving rise to ∼5 molecular layers). The box was elongated by 8.5 Å in both the $+z$ and $-z$ directions to create vacuums above and below the water cube, and then equilibrated for 10 ps. It should be noted that this approach was previously used to study the interfacial reactivities of HNO_3[42, 43, 115] and H_2SO_4[110]. We generated two different initial configurations by introducing a CO_2 molecule with two different orientations with respect to the water surface at a distance of ∼4 Å above the water cube (i.e., distance between the carbon of CO_2 and the nearest water oxygen). The two (extreme) orientations considered were: (i) *Orientation A*− CO_2 parallel to the water surface, and (ii) *Orientation B*− CO_2 perpendicular to the water surface (see Figure 6.1 for a depiction of the initial configurations).

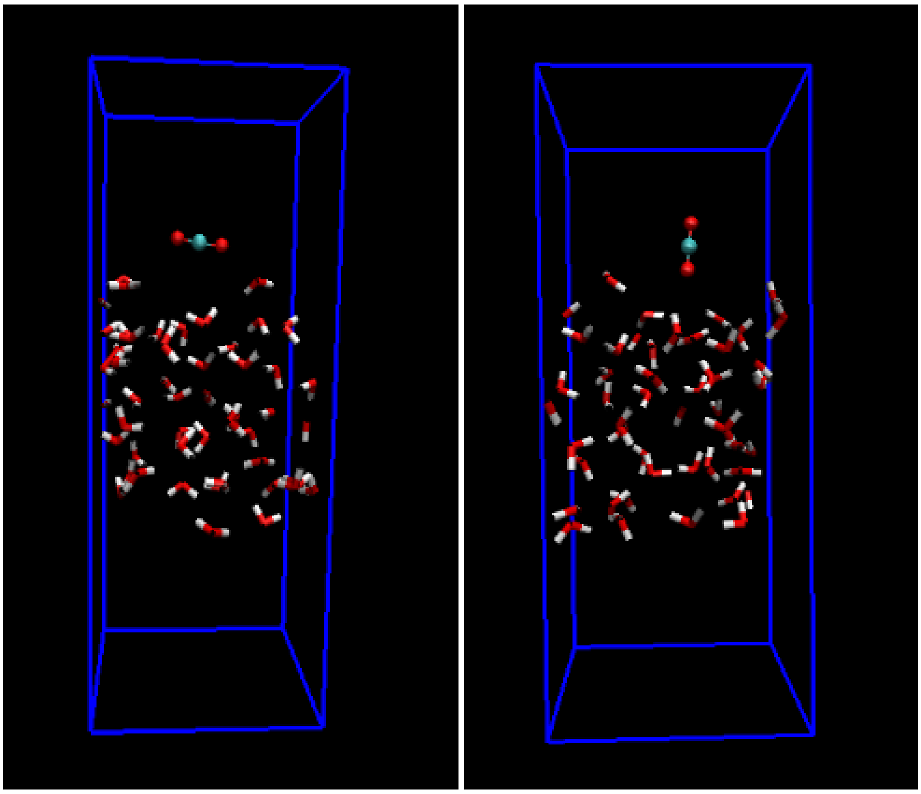

Figure 6.1: Snapshots of the two initial configurations used in our simulations, each containing one CO_2 on the surface of a water slab at a distance of ∼4 Å from the nearest surface water molecule. Left: CO_2 parallel to the surface (configuration 1). Right: CO_2 perpendicular to the surface (configuration 2).

Using CPMD, each configuration was equilibrated for 10 ps, followed by a 15 ps production run. This procedure was followed to generate an ensemble of three different trajectories for each type of initial configuration, in order to validate the reproducibility of our observations. All simulations were carried out at a temperature of 300 K (with the aid of Nosé-Hoover thermostats), in order to compare our results to previous results for CO_2 in bulk water at this temperature. The valence electrons were treated using the BLYP functional[86, 87] and the interaction between the core and valence electrons was treated using ultrasoft pseudopotentials[88]. This functional and these pseudopotentials have yielded sensible results in earlier studies of CO_2 in bulk water[2, 35, 37]. A plane wave basis set with a cutoff of 40 Ry was employed to expand the Kohn-Sham orbitals. A fictitious electron mass of 600 a.u. and a time step of 4 a.u. (or 0.1 fs) were used. The reaction free energy barriers were calculated using the extended Lagrangian form of metadynamics[80], in which a fictitious particle of mass 100 hartee(a.u.)^2 was coupled to the collective variable via a spring constant of 0.03 hartee. We used the coordination number between the carbon in CO_2 and all the water oxygens present in the system as the collective variable (CV), defined by

$$\mathrm{CV} = \sum_{\mathrm{j} \in \mathrm{O_w}} \frac{1 - (\frac{\mathrm{d_j}}{\mathrm{d_0}})^{\mathrm{p}}}{1 - (\frac{\mathrm{d_j}}{\mathrm{d_0}})^{\mathrm{p+q}}}, \tag{6.3}$$

where d_j is the instantaneous distance between the carbon and a water oxygen, d_0 is the distance below which the atoms are considered bonded, and p/q are parameters chosen such that the coordination number tends to zero beyond d_0. We have set $p = 2$, $q = 10$, and $d_0 = 2.50$ Å. This single CV was used previously to explore the hydration reaction in bulk water[2]. Gaussian hills (each with a height 0.31375 kcal/mol) were added every 100 CPMD steps throughout the metadynamics simulations. When all of the potential wells were filled with these Gaussian hills, the free energy as a function of the fictitious particle coordinate was calculated by summing these biasing potentials (see Eq. A.4 in Appendix A).

6.3 Results and discussion

Figure 6.2 shows the atom-atom radial distribution functions (RDFs) between the CO_2 carbon (C) and all water oxygens (O_W) based on CPMD trajectories starting from both types of initial configurations[120].

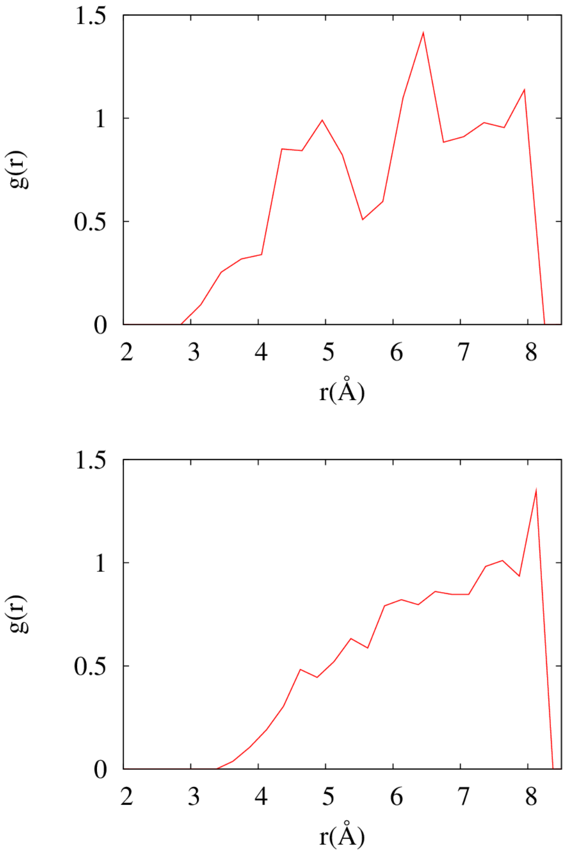

FIGURE 6.2: CO_2 carbon–water oxygen radial distribution functions for configurations 1 (top) and 2 (bottom).

The RDF for configuration 1 has a small shoulder at ∼3.8 Å, a first solvation shell ranging from $\sim 4-6$ Å, and a second solvation shell ranging from $\sim 6-7$ Å. This should be contrasted with the bulk RDF, in which the shoulder is found at ∼2.75 Å and the first peak ranges between $\sim 3-5$ Å[37]. Therefore, in contrast to in the bulk, CO_2 is more weakly associated to water at the water surface, i.e., CO_2 does not form a stable CO_2-H_2O complex. Integration of the shoulder (up to ∼4.0 Å) yields a value of 0.60, suggesting that a water molecule is not always present within this distance. This is consistent with the fact that no spectral signature of a CO_2-H_2O surface complex was observed in the vibrational sum-frequency spectrum of CO_2 at the water surface[54]. Integration of the first hydration shell (up to 6.0 Å) yields a value of 6.0 (cf. fewer waters in the case of H_2CO_3 at the water surface, due to the formation of hydrogen-bonded surface complexes). In contrast to configuration 1, the corresponding RDF for configuration 2 is unstructured. There is no shoulder at shorter distances and no clear minima are observed. This is due to the fact that, in the perpendicular position, the carbon remains further away from the surface and, therefore, does not interact as strongly with the surface (compared to configuration 1). This is also confirmed by integrating the RDF up to ∼4.0 Å, which yields a value of only 0.09 (cf. 0.60 for configuration 1). It should be noted that the RDF for configuration 1 is more similar to that of the bulk than the RDF for configuration 2.

Figure 6.3 shows the RDFs between the CO_2 oxygen(s) (O) and all of the water hydrogens (H_W) for both types of initial configurations. The RDFs are fairly similar and show little intensity at distances below 2.5 Å. Since 2.5 Å is a typical cutoff distance for defining hydrogen bonds[37]. we integrated the RDFs up to this distance, yielding values of 0.08 in configuration 1 (corresponds to both oxygen atoms) and 0.09 in configuration 2 (corresponds to the oxygen atom that approaches the surface). These values should be contrasted with the value of 0.3 coordinated water molecules per CO_2 oxygen in the bulk, determined from an ab initio molecular dynamics calculation of CO_2 in bulk water[35]. Therefore, like the C-O_w RDFs, the O-H_w RDFs also reveal that CO_2 experiences a weaker solvation environment at the water surface compared to in the bulk.

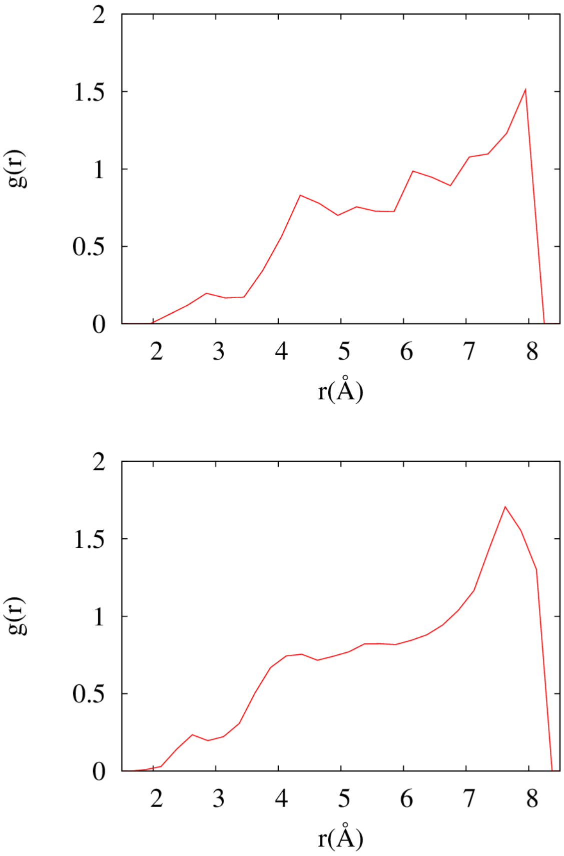

FIGURE 6.3: CO_2 oxygen–water hydrogen radial distribution functions for configurations 1 (top) and 2 (bottom).

Since we did not observe any reactions of CO_2 with the surface H_2O molecules in any of the CPMD simulations, it is likely that the formation of products is a rare event at this temperature. We therefore employed metadynamics to investigate the formation of products. Figure 6.4 shows snapshots from a representative metadynamics trajectory, illustrating the reaction mechanism for configuration 1.

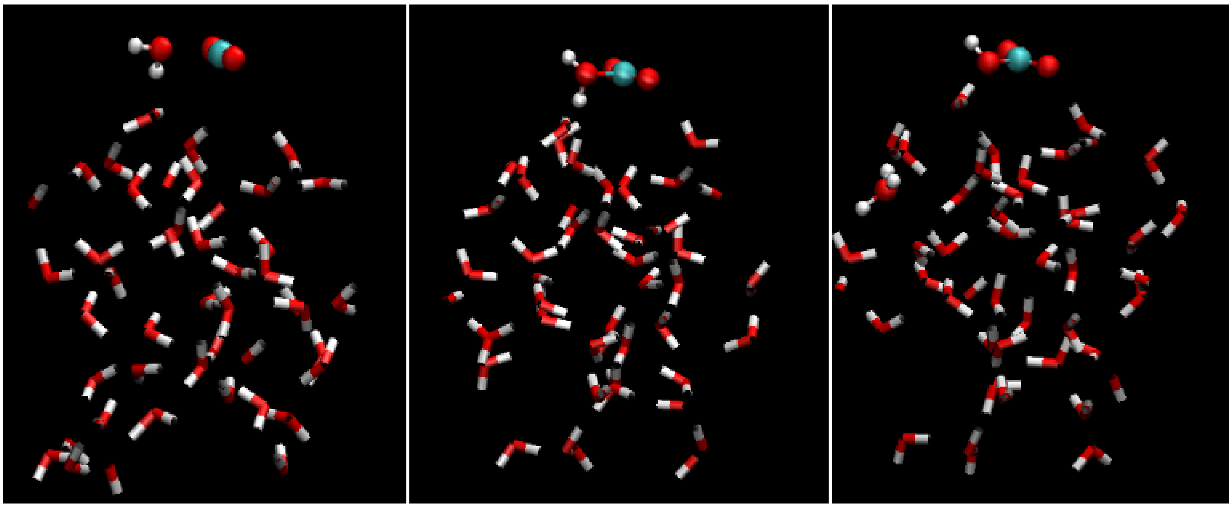

FIGURE 6.4: Snapshots of HCO_3^- formation from a representative metadynamics trajectory. Left: Approach of an H_2O to CO_2 (at ∼650 MTD steps). Middle: Formation of the $H_2O^+CO_2^-$ zwitterion (at ∼720 MTD steps). Right: Formation of the stable solvent-separated HCO_3^-/H_3O^+ ion pair (at ∼760 MTD steps). Each MTD step = 100 CPMD steps.

As shown, after ∼650 metadynamics (MTD) steps, a H_2O molecule becomes displaced from the surface and approaches the CO_2 to form a $CO_2{-}H_2O$ complex. Then, the C-O_W distance becomes shorter and, after ∼720 MTD steps, a $H_2O^+CO_2^-$ zwitterion forms. This is followed by a proton transfer to an adjacent water molecule after ∼760 MTD steps to yield solvent-separated HCO_3^- and H_3O^+ ions. Afterwards, H_3O^+ diffuses into the bulk and becomes fully solvated there (not shown in Figure 6.4). Figure 6.5 shows representative metadynamics trajectories of the distance between the CO_2 carbon atom and the attacking water oxygen atom, the O-C-O angle in CO_2, and the distance between the attacking water oxygen atom and the hydrogen atom which leaves that water during the formation of HCO_3^-.

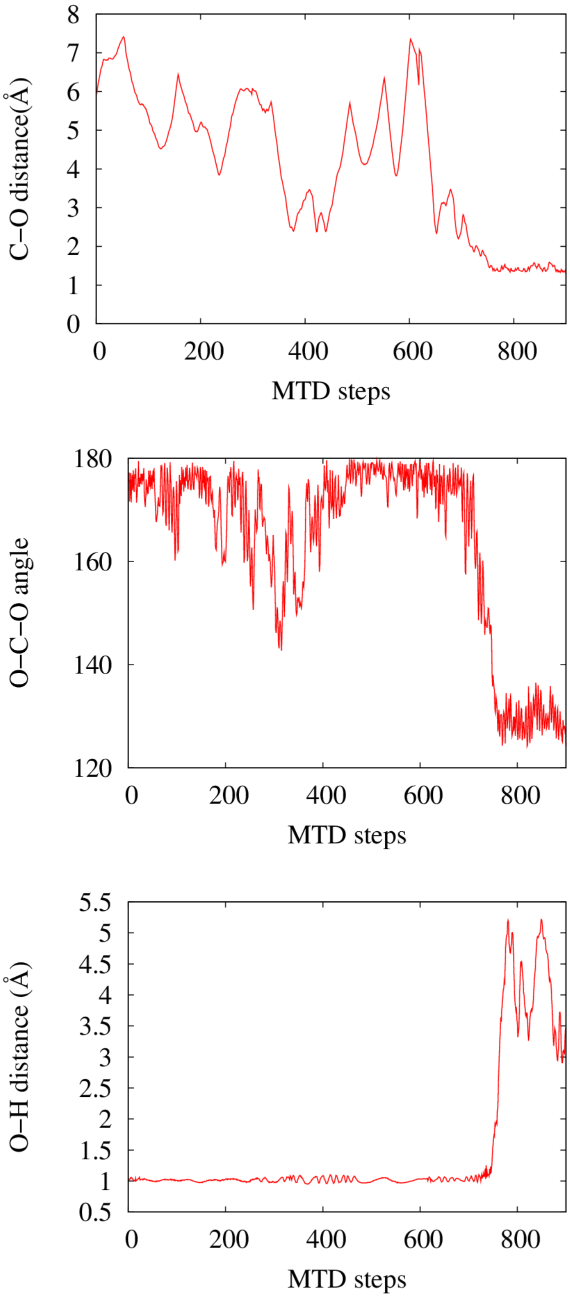

Figure 6.5: Representative trajectories of the distance between the CO_2 carbon and water oxygen (top), the O-C-O angle of CO_2 (middle), and the distance between the attacking water oxygen and its leaving hydrogen (bottom) for configurations 1. Each MTD step = 100 CPMD steps.

We see that when the C-O_W bond length in the CO_2-H_2O complex becomes less than 2.1 Å, the O-C-O angle changes from ~177° to ~150°, forming the $H_2O^+CO_2^-$ zwitterion after 720 MTD steps. This is followed by further bending of the CO_2

moiety to ~130° and the simultaneous proton transfer from the attacking water to the adjacent water molecule (at ~ 760 MTD steps). It should be noted that this mechanism for the formation of HCO_3^- is similar to that observed previously in bulk water[2]. Figure 6.6 shows the free energy surface calculated from our metadynamics simulations.

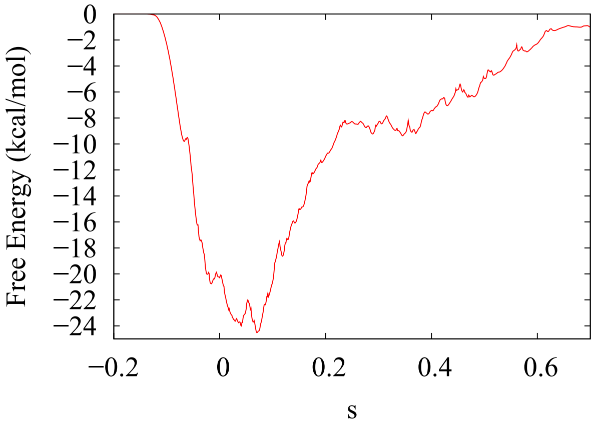

FIGURE 6.6: Free energy (in kcal/mol) profile as a function of the fictitious particle coordinate coupled to the CV for the HCO_3^- formation starting from configuration 1.

The reactant well is located at s ~0.1 and the product well at s ~0.9. Based on this surface, the energy barrier for the reaction $CO_2 + 2H_2O \rightarrow HCO_3^- + H_3O^+$ is 22.6 kcal/mol±1.3kcal/mol (based on an ensemble of three trajectories), which is similar to the experimental bulk energy barrier of 21.1 kcal/mol [115].

The reaction mechanism for configuration 2 is illustrated in Figure 6.7, which shows snapshots at key points along a representative metadynamics trajectory.

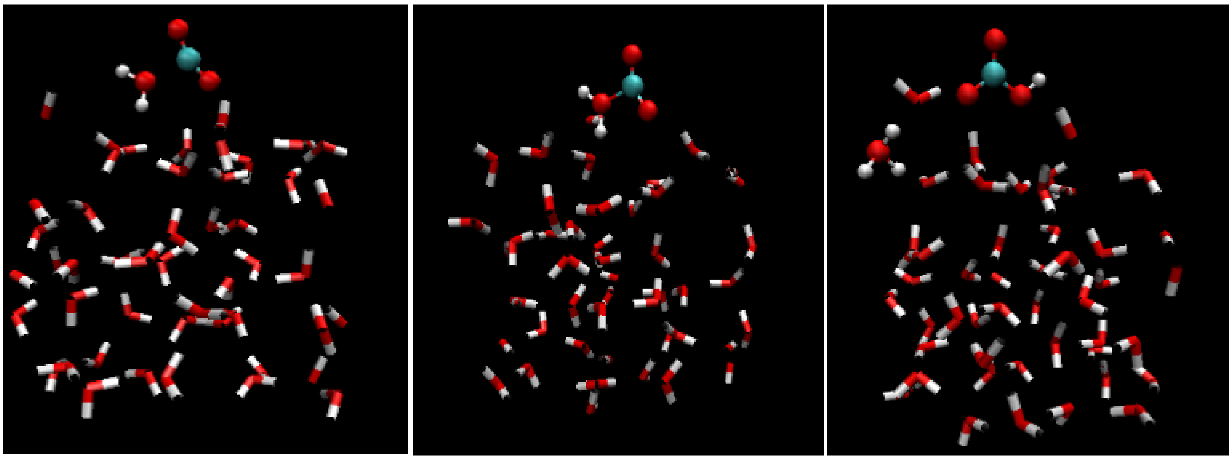

Figure 6.7: Snapshots of HCO_3^- formation from a representative metadynamics trajectory. Left: Approach of an H_2O to CO_2 (at ~440 MTD steps) Middle: Formation of the $H_2O^+CO_2^-$ zwitterion (at ~570 MTD steps) Right: Formation of stable solvent-separated HCO_3^-/H_3O^+ ion pair (at ~ 660 MTD steps). Each MTD step = 100 CPMD steps.

As seen, the reaction mechanism is the same as that observed in the case of configuration 1. Examination of the trajectories of the distance between the CO_2 carbon atom and the attacking water oxygen atom, the O-C-O angle in CO_2, and the distance between the attacking water oxygen atom and the hydrogen atom which leaves that water during the formation of HCO_3^- shows that, like for configuration 1, the C-O bond formation is coupled to the bending of the CO_2 moiety and the simultaneous proton transfer from the attacking water molecule to a nearby water molecule (see Figure 6.8). We also calculated a free energy barrier of 20.9 kcal/mol±1.2 kcal/mol (based on an ensemble of three trajectories) for the formation of HCO_3^-, which is lower than that for configuration 1, but still within error bars (see Figure 6.9).

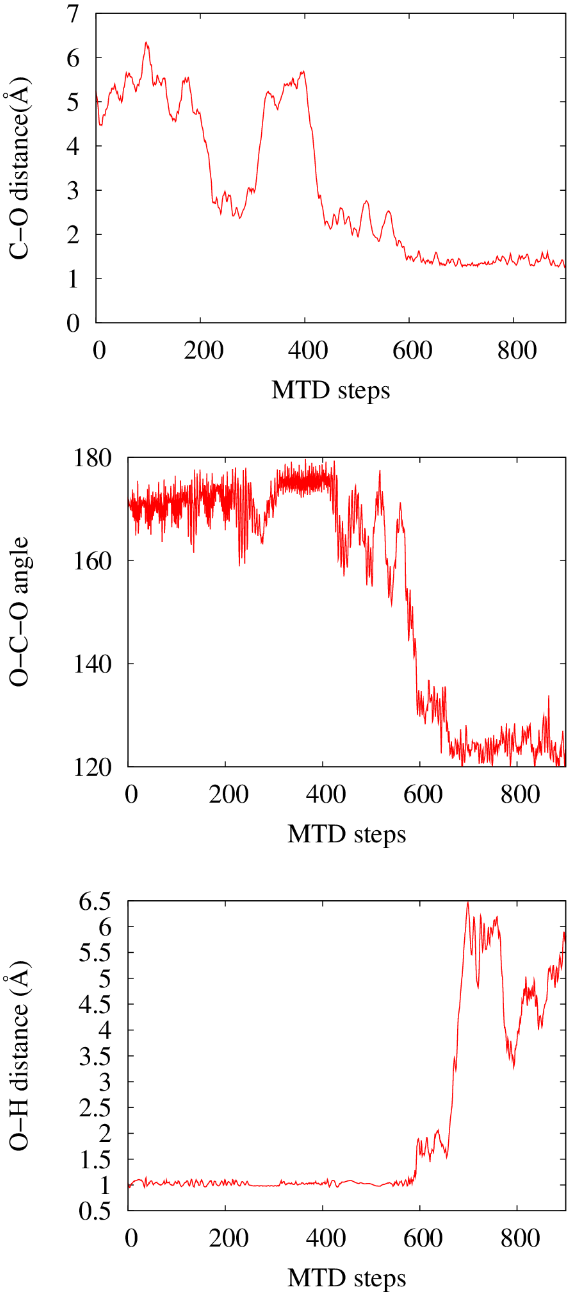

FIGURE 6.8: Representative trajectories of the distance between the CO_2 carbon and water oxygen (top), the O-C-O angle of CO_2 (middle), and the distance between the attacking water oxygen and its leaving hydrogen (bottom) for configurations 2. Each MTD step = 100 CPMD steps.

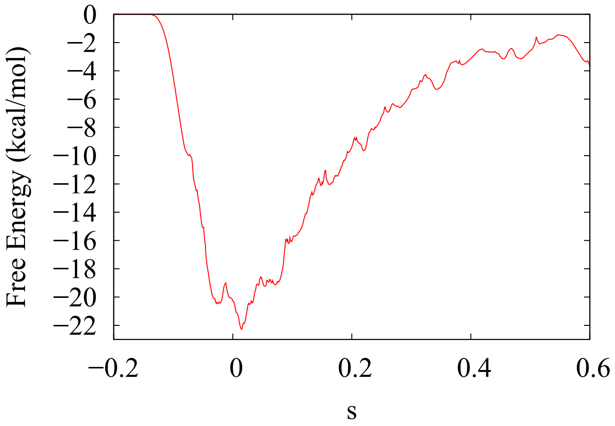

Figure 6.9: Free energy (in kcal/mol) profile as a function of the fictitious particle coordinate coupled to the CV for the HCO_3^- formation starting from configuration 2.

Unlike in the case of the dissociation of H_2CO_3 at the water surface studied in chapter 5, we did not find a significant difference between the energy barrier for the hydration of CO_2 at the water surface and that in bulk water. This is likely due to the differences in the changes of hydration structures encountered by H_2CO_3 and CO_2 in going from the bulk to the water surface. Namely, we found that the solvation structure around H_2CO_3 becomes more structured at the surface compared to in the bulk, which leads to a decrease in the dissociation energy barrier at the water surface. On the other hand, CO_2 forms two very weak hydrogen bonds in bulk water, which becomes slightly weaker at the surface, but does not affect the formation energy barrier.

6.4 Conclusions

In this chapter, we have investigated the solvation environment of CO_2 at the surface of water by CPMD and explored the reaction mechanisms and energetics of its hydration to form HCO_3^- and H_3O^+ with the aid of metadynamics. Our study revealed that CO_2 becomes even more weakly hydrogen bonded at the water surface than it is in bulk water. Unlike in the gas phase, the hydration reaction involves the formation of a solvent-separated HCO_3^-/H_3O^+ pair intermediate, which was also previously observed for this reaction in bulk water[2]. The energy barrier for the formation of HCO_3^- was found to be similar to that in the bulk. The weak solvation of CO_2 along with the formation of stable hydration products is consistent with the findings of the SFG study by Tarbuck et al.[54], in which the authors found evidence of HCO_3^-, H_3O^+, and CO_3^{2-} reaction products, but no $CO_2{-}H_2O$ surface complex was detected. The results of our study constitute another piece of the scheme of reactions involving CO_2 and H_2CO_3 at the water surface. To gain a complete picture of this reaction scheme, the decomposition ($HCO_3^- + H_3O^+ \rightarrow CO_2{+}2H_2O$) and the protonation ($HCO_3^- + H_3O^+ \rightarrow H_2CO_3 + H_2O$) reactions should be studied, which will shed light on the acidification of atmospheric aerosols and water droplets.

Chapter 7

Conclusions and future work

In this work, the mechanisms and energetics of a variety of processes involving H_2CO_3, HCO_3^-, and CO_2 were investigated computationally using CPMD, a popular type of ab initio molecular dynamics. For those processes whose barriers were large relative to k_BT, metadynamics was used in conjunction with CPMD to accelerate the dynamics along a proposed reaction coordinate, albeit in a biased fashion. Specifically, we studied the conformational changes of H_2CO_3 in bulk water, the hydroxide route decomposition of H_2CO_3 in bulk water, the water route decomposition of H_2CO_3 in different-sized water clusters, and the dissociation of H_2CO_3 and the hydration of CO_2 to form HCO_3^- at the water surface.

The relative stabilities of the three conformers (CC, CT, and TT) of H_2CO_3 in water were studied first. We found that TT and CC conformers were the most and least stable conformers, respectively, like in the gas phase. However, the CC conformer was found to be more stable when it is solvated by water as compared to the gas phase. The free energy change for the conformational change CC $\rightarrow$ CT was found to be 3.9 kcal/mol lower in water than in the gas phase, which indicates that CC becomes more stable than CT in water. Two different mechanisms for the interconversions between the conformers were observed, viz., one involving a change in the O-C-O-H dihedral angle and the other involving a proton transfer through a hydrogen bond wire. This is unlike the gas phase, where the interconversion occurs only via a change in the dihedral angle since the energy barrier to the proton transfer is too high in the absence of water molecules. Thus, it is the hydrogen bond formation between H_2CO_3 and the adjacent water molecules which renders this route energetically favourable in water. The energy barriers for the various conformational changes via the dihedral angle change were calculated and compared to those in the gas phase. We found that the barrier for CC → CT increases by ∼1.9 kcal/mol in water compared to that in the gas phase, whereas the barrier for CT → CC decreases by ∼2 kcal/mol. The increase in stability of the CC conformer due to hydrogen bond formation with adjacent water molecules causes the increase in the energy barrier. However, in the case of CT, hydrogen bonding with adjacent water molecules reduces the strength of intramolecular hydrogen bond, which thereby decreases the energy barrier. The energy barriers for the CT → TT and TT → CT were not found to change significantly in water compared to the gas phase, indicating that the dihedral angle changes in these conformers are primarily dominated by the intramolecular hydrogen bond dynamics.

We then investigated the dissociation and decomposition mechanisms of the hydroxide route for all three conformers of H_2CO_3 in water. Interestingly, the CC conformer did not directly decompose, but first converted to either the CT or TT conformer prior to decomposition. Unlike in the gas phase, we found that for CT and TT, H_2CO_3 undergoes a step-wise decomposition in water. First, H_2CO_3 dissociates into HCO_3^- and H_3O^+, which is followed by the decomposition of HCO_3^- into CO_2 and OH^-. The dissociation equilibrium was seen to involve the formation and subsequent breakage of a hydrogen bond wire with a neighbouring water molecule. During this process, two intermediates were observed: (1) a proton-shared Zundel-like structure ($HCO_3^{\delta-}\cdots H\cdots{}^{\delta+}OH_2$), and (2) a contact ion pair ($HCO_3^-{\cdot}H_3O^+$). The decomposition of HCO_3^- involves the breaking of the C-OH bond, yielding OH^- and a bent CO_2 moiety, which straightens to form CO_2 as the OH^- diffuses away into the bulk. The OH^- eventually acquires a proton from an adjacent water molecule, which leads to the diffusion of OH^- via the Grotthuss mechanism. Unlike in the case of the water route dehydration, H_3O^+ does not take part in the decomposition via the hydroxide route. Our metadynamics simulations yielded dissociation free energy barriers of 9.7, 9.3, and 8.4 kcal/mol and free energy changes of 3.8, 5.5 and 4.4 kcal/mol for the CT_1, CT_2, and TT, respectively. (CT_1 and CT_2 correspond to the dissociation of the hydroxyl group cis and trans to the carbonyl oxygen of H_2CO_3, respectively). Based on these free energy changes, the corresponding pK_a values were calculated to 2.6, 3.8, and 3.0, respectively. This trend in the pK_a's is in agreement with the results of a constrained ab-initio MD calculation[3], but is different from what was found in an ab-initio electronic structure study[21] with an implicit solvent (which found the TT conformer to be less acidic than CT_2). This strongly suggested that a dynamical treatment with an explicit solvent is required to properly describe the reactive dynamics of such aqueous systems. Our values were also in good agreement with the experimental pK_a value of 3.45[18], and thereby suggested that the overall pK_a has significant contributions from all three conformers in water. The decomposition free energy barrier was found to be 25.2 kcal/mol for the CT conformer and 26.2 kcal/mol for the TT conformer, which are in decent agreement with the experimentally measured value of 22.24 kcal/mol at 298 K [30].

In an effort to pin down the water route decomposition mechanism, we studied the reaction dynamics of H_2CO_3 (CT conformer) in four different-sized water clusters. We found that in the six- and nine-water clusters, the decomposition occurs via a concerted mechanism and in the 20- and 45- water clusters, the decomposition occurs via the step-wise mechanism. The concerted mechanism involves the transfer of one of the hydroxyl hydrogens to the other hydroxyl oxygen in H_2CO_3 through a chain of one or two water molecules, which is accompanied by the simultaneous breakage of the C-O bond yielding CO_2 and H_2O. In contrast, the sequential mechanism initially involves the formation of HCO_3^- and H_3O^+ intermediates, followed by the breakage of the C-OH bond to yield CO_2. The change in mechanism with increasing cluster size was found to occur when there is a sufficient number of water molecules to prevent the recombination of the ions. In this case, destabilizing fluctuations of the local electric field become rare, thereby stabilizing the ion pair in the product well. More importantly, if H_3O^+ forms three hydrogen bonds with neighbouring water molecules, then the solvent-separated ion pair is sufficiently stabilized and the decomposition commits to the step-wise pathway. Therefore, our results showed that the transition from the concerted decomposition pathway to the step-wise pathway hinges upon the solvation structure surrounding the H_3O^+ intermediate, which in turn depends on the size and shape of the cluster. Since, larger clusters can mimic a bulk-like environment, we concluded that the decomposition of H_2CO_3 in bulk water predominantly follows the step-wise route.

Our next study focused on the dissociation of H_2CO_3 (CT conformer) at the air/water interface. Our CPMD simulations showed that the dissociation of H_2CO_3 is accelerated at the surface compared to in bulk water. H_2CO_3 was found to dissociate into HCO_3^- and H_3O^+ with an energy barrier of 5.0 kcal/mol, which is 4.5 kcal/mol lower than that in bulk water. We find that the water surface allows for a more structured solvation environment around H_2CO_3 than in bulk water, which contributes to a decrease in the dissociation energy barrier via a stabilization of the transition state relative to the undissociated acid. This is in contrast to the recent experiments[43] and simulations[42, 43, 115] which have shown that HNO_3 has a lower propensity to dissociate at the water surface than in bulk water due to a stronger electrostatic interaction between NO_3^- and H_3O^+ at the water surface compared to in the bulk (i.e., more energy is required to separate these ions at the water surface than in the bulk).

We also studied the solvation environment of CO_2 and the mechanism and energetics of its hydration at the air/water interface in the limit of low CO_2 pressure. Our study revealed that CO_2 becomes more even weakly hydrogen bonded at the water surface than it is in bulk water. Unlike in the gas phase, the hydration reaction involves the formation of a solvent-separated HCO_3^-/H_3O^+ pair, as in the case of bulk water. The energy barrier for the formation of HCO_3^- was found to be similar to that in the bulk.

The insights gained from this work have set the stage for numerous future studies. Previous attempts at calculating the H_2CO_3 decomposition rate constant in bulk water were based on the concerted mechanism and yielded unsatisfactory agreement with experiment[34]. In light of our findings, one may be able to more accurately calculate the rate constant based on the step-wise mechanism, using the minimum number of water molecules needed to mimic a bulk-like environment. The altered dissociation behaviour of H_2CO_3 at the water surface suggests that its pK_a may also change significantly, which would have important consequences on the ability of atmospheric aerosols and water droplets to take up gases. Therefore, further studies are needed to investigate how the acidity of H_2CO_3 varies at the surface and how the presence of HCO_3^- and excess protons might affect the uptake and the reactions of atmospheric gases like SO_2 and other organic compounds on the surface of aerosols. The energetics and kinetics of the whole reaction scheme of the hydration of CO_2 and dehydration of H_2CO_3 at the air/water interface remains to be investigated. An NMR study of the uptake of atmospheric pressure CO_2 by water pools encapsulated in reverse micelles has shown that the pH drops significantly upon introduction of the CO_2[41]. However, it was not clear from the experiment how this comes about and, thus, studies of the dissociation of H_2CO_3 in nanoconfined water pools are worthwhile. There is also great interest in investigating the effects of temperature, pressure, and composition on the stability of H_2CO_3 and its derivatives in water for the purpose of assessing the viability sequestering CO_2 in an aqueous medium.

Appendix A

Metadynamics

Metadynamics is a technique used to enhance the sampling of phase space for systems with high energy barriers and thereby calculate free energy profiles as a function of suitable collective variables. When metadynamics is combined with ab initio molecular dynamics (MD), one can efficiently study rare chemically reactive events. Metadynamics can readily generate free energy surfaces as a function of a small set of collective variables, making it a better choice than methods that are either restricted to a single reaction coordinate (e.g. umbrella sampling) or are expensive for multidimensional systems (e.g. constrained MD).

In metadynamics, history-dependent biasing potentials are added periodically to the potential of the system to discourage it from revisiting points in the configurational space, thereby driving it over an energy barrier. When the biasing potentials accumulate in a potential well, the system escapes from that well via the lowest free energy saddle point. Therefore, the reaction pathway observed in a metadynamics simulation is the most probable reaction pathway provided that a suitable set of collective variables is made. The free energy as a function of the collective variables may be obtained by simply summing up the total potential added without any unbiasing. A comparison of the calculated free energy barriers with the experimental barriers provides a good check of the suitability of the chosen collective variables for monitoring the underlying reaction mechanisms.

In this thesis, we used both the direct[77] and the extended Lagrangian[80] versions of metadynamics. In the direct approach, the Lagrangian, L_{MTD}, has the following form:

$$\mathrm{L_{MTD}} = \mathrm{L_{CP}} - \mathrm{V(t,s)}, \tag{A.1}$$

where L_{CP} is the CPMD Lagrangian, and $V(t,s)$ is the history-dependent biasing potential acting on the collective variables (CVs), which is given by

$$\mathrm{V(t,s)} = \mathrm{W}\sum_{\mathrm{i}} \exp\{-\frac{(\mathrm{s}-\mathrm{s^i})^2}{2(\Delta \mathrm{s}')^2}\}, \tag{A.2}$$

where W is the Gaussian height, $s = \{s_1, s_2, \ldots\}$ is a vector of CVs, s^i is a vector of the values of the CV at metadynamics step i, and $\Delta s'$ is the Gaussian width. In the extended approach, each collective variable is coupled to a fictitious particle via a harmonic confining potential. The extended Lagrangian, L_{MTD}, has the following form:

$$\mathrm{L_{MTD}} = \mathrm{L_{CP}} + \frac{\mu}{2}\sum_{\alpha} \dot{\mathrm{s}}_{\alpha}^2 - \frac{\mathrm{k}}{2}\sum_{\alpha}[\mathrm{S}_{\alpha}(\mathrm{r}) - \mathrm{s}_{\alpha}]^2 - \mathrm{V(t,s)}, \tag{A.3}$$

where $S_{\alpha}(r)$ is the coordinate of collective variable α, s_{α} is the coordinate of the fictitious particle that couples to collective variable α, μ is the mass of the fictitious particle, and k is the harmonic spring constant. $V(t, s)$ is the history-dependent biasing potential acting on the fictitious particles, which is given by

$$\mathrm{V(t,s) = W\sum_{i} \exp\{-\frac{(s-s^i)^2}{2(\Delta s')^2}\} \exp\{-\frac{[(s^{i+1}-s^i)\cdot(s-s^i)]^2}{2(\Delta s'')^4}\}}, \tag{A.4}$$

where W is the Gaussian height, $s = \{s_1, s_2, \ldots\}$ is a vector of variables corresponding to the fictitious particle coordinates, s^i is a vector of the values of the fictitious particle coordinates at metadynamics step i, and $\Delta s'$ and $\Delta s''$ are Gaussian widths. In both approaches, when all of the potential wells have been filled with the Gaussians, the total biasing potential added gives an estimate of the free energy as a function of the fictitious particle coordinates, i.e.,

$$\mathrm{F(s) = -\lim_{t\to\infty} V(t,s)}. \tag{A.5}$$

The accuracy and efficiency of a metadynamics simulation mainly depend on three parameters: (i) the Gaussian height, W; (ii) the Gaussian width, Δs; and (iii) the deposition frequency of the Gaussian hills. In general, if the Gaussians are small (i.e. having smaller heights and widths) and the deposition time is large, the simulation will be longer but the free energy profile will be more accurate. Thus, these parameters are chosen in such a way that the intrinsic metadynamics error is minimized within a given simulation time. A procedure for estimating the error as a function of these parameters is given in Refs. [82] and [90]. A detailed discussion of the selection of these parameters can also be found in Ref. [79].

Appendix B

Tutorial for setting up a CPMD-metadynamics simulation

B.1 Steps of simulation set-up

In order to set up a CPMD-metadynamics simulation, we followed the following steps:

1. System wavefunction optimization for an initial geometry, using the following keywords in the CPMD section of the input file:

   ```
   & CPMD
   OPTIMIZE WAVEFUNCTION XYZ
   PCG MINIMIZE
   TIMESTEP
   20
   ```

```
CONVERGENCE ORBITALS
1.0d-6
CONVERGENCE GEOMETRY
1.0d-5
STORE
1000
PRINT
1000
CENTER MOLECULE
& END
```

2. Equilibration of the system to the desired temperature. The wavefunction and the coordinates stored from the previous step are taken from the RESTART file. The corresponding keywords are as follows:

```
& CPMD
MOLECULAR DYNAMICS CP
RESTART WAVEFUNCTION COORDINATES LATEST
TRAJECTORY XYZ SAMPLE
100
SUBTRACT COMVEL ROTVEL
100
STORE
100
```

```
PRINT
1000
EMASS
400
TIMESTEP
3
MAXSTEP
200000
TEMPCONTROL IONS
150  100
REAL SPACE WFN KEEP
& END
```

3. Application of Nosé-Hoover chain thermostat for CPMD simulation.

```
& CPMD
MOLECULAR DYNAMICS CP
RESTART WAVEFUNCTION COORDINATES LATEST
RESTART VELOCITIES NOSEP NOSEE
TRAJECTORY XYZ SAMPLE
100
SUBTRACT COMVEL ROTVEL
100
STORE
```

```
100
PRINT
1000
EMASS
400
TIMESTEP
3
MAXSTEP
200000
NOSE IONS
150  1000
NOSE ELECTRONS
0.004  20000
REAL SPACE WFN KEEP
& END
```

4. Selection of appropriate collective variables and set-up of metadynamics simulation.

   ```
   METADYNAMICS COLLECTIVE VARIABLES
   DEFINE VARIABLES
   3
   BNSWT 1  3  8  24  2.80  SCF  1.0  KCV  10.0  MCV  500
   COOR_RF  INDAT  4  91  6  14  1.40  SCF  8.0  KCV  1.0  MCV  500
   ```

```
COOR_RF  INDAT  3  91  6  14  1.60  SCF  6.0  KCV  5.0  MCV  500
END DEFINE
METASTEPNUM
16000
HILLS  SHIFT  RCUT  2.0  1.0  =  0.03  0.001
LAGRANGE  TEMPERATURE
150
LAGRANGE  TEMPCONT
150  150
MAXSTEPNUM  INTERMETA
500
MINSTEPNUM  INTERMETA
400
METASTORE  [NO TRAJECTORY]
10  5  10000
MOVEMENT  CHECK
0.00015D0
MONITOR
400
END METADYNAMICS
```

B.2 Units used in simulations

The units used in the simulations are Hartree atomic units (a.u.). The conversion factors are given below:

time step	1 a.u. = 0.02418884326505 fs
coordinates	1 Bohr = 1 a_0 = 0.52917720859 Å
velocity	1 a.u. = 1 Bohr / 1 a.t.u. = 2187691.2541 m/s
energy	1 Eh = 27.21138386 eV = 627.5094706 kcal/mol = 2625.4996251 kJ/mol
plane wave cutoff	1 Ry = 1/2 Eh = 13.60569193 eV
atomic mass	1 a.u. = 0.00054857990943 a.m.u

B.3 A typical input file for a CPMD-metadynamics simulation

```
& INFO
H2C03 in water cluster
& END


& CPMD
MOLECULAR DYNAMICS CP
RESTART WAVEFUNCTION COORDINATES LATEST
RESTART VELOCITIES NOSEP NOSEE
```

```
TRAJECTORY XYZ SAMPLE
100
SUBTRACT COMVEL ROTVEL
100
STORE
100
PRINT
1000
EMASS
400
TIMESTEP
3
MAXSTEP
200000
NOSE IONS
150  1000
NOSE ELECTRONS
0.004  20000
REAL SPACE WFN KEEP
& END

& SYSTEM
ANGSTROM
```

```
SYMMETRY
SIMPLE CUBIC
CELL
22.30  1.0  1.0  0.0  0.0  0.0
CUTOFF
40
& END

& DFT
FUNCTIONAL PBE
GC-CUTOFF
1.0d-06
& END

& ATOMS
*006-C-gpbe–bm.uspp BINARY
LMAX=P
1
3.525976  -3.183641  0.504111
*008-O-gpbe–bm.uspp BINARY
LMAX=P
48
3.424595  -2.475697  -0.509552
```

2.585503	-4.200516	0.668265
4.507026	-3.076688	1.352900
0.616238	0.147605	-3.434991
-0.496915	6.550549	2.751616
-0.153408	-0.476686	-10.063225
0.012199	-6.789680	6.284837
2.920927	6.934166	8.214478
2.617829	4.657156	-4.607347
-2.039975	-4.424065	0.582934
2.224890	-2.067091	-3.941100
-0.987638	2.383119	-6.364376
6.047002	3.056142	5.527150
8.150495	-1.612761	-0.228334
-5.714688	-5.017524	2.584329
-4.074562	6.820924	7.925370
-2.300093	-6.746960	-3.669716
-2.929185	-1.583437	2.500692
0.340387	-7.590524	-1.138539
-4.210803	0.566881	4.513699
-0.208932	7.103738	-4.653260
-5.952782	-5.412258	-1.914112
-5.915092	1.691734	-1.193541
-7.707898	2.183290	0.888287

-4.069000 -1.816345 -3.795119

7.923852 4.823745 4.223852

4.809969 3.316370 8.060708

2.011423 2.171393 -2.555829

-3.236843 2.314637 -1.982998

2.204303 -1.144798 -8.416456

-5.238101 -2.082307 -6.137401

0.861825 -4.657317 -1.195112

-3.894335 2.754674 2.028618

0.785627 0.499099 -6.248340

4.310859 -0.409033 6.745824

-1.526746 1.509738 0.979549

3.853319 -5.463512 4.563797

3.579383 1.876177 5.224322

0.929317 -1.339029 -0.975579

-4.313369 5.388969 0.491037

-1.923551 -0.462191 -2.862311

-1.378421 -3.843501 -2.208698

-2.056942 -3.585265 -6.748618

-0.057812 3.889045 1.479541

1.941382 -3.187723 4.763466

5.840007 -1.059052 -1.248089

4.581233 0.487101 2.964873

2.577428 4.539930 2.379128

*001-H-gpbe–bm.uspp BINARY

LMAX=P

92

1.881104 -4.108086 -0.005214

4.695941 -3.980172 1.968674

1.257330 0.824951 -3.043042

1.195146 -0.668680 -3.573426

0.356686 6.848515 2.922379

-1.047312 7.014864 3.437491

-0.895459 -1.057681 -9.876685

0.261516 -0.838567 -10.904806

0.922922 -7.047976 6.462434

-0.387118 -7.383295 5.579062

3.824353 6.587784 8.557184

2.224159 6.888735 9.019289

2.593809 5.524770 -4.069633

3.141654 4.035192 -4.053247

-1.375944 -4.386563 1.315655

-2.137177 -3.735318 -0.059816

2.938985 -1.459781 -4.292738

2.716568 -2.857431 -3.498549

-1.311063 2.340253 -7.277057

-0.353540	1.645070	-6.285769
6.355230	2.146623	5.153803
5.237219	3.216848	5.091749
7.915476	-1.641424	0.722287
7.260976	-1.265326	-0.656616
-5.227549	-5.653307	2.062115
-5.916642	-5.385131	3.489142
-3.888112	7.760775	7.688479
-3.349661	6.333656	7.522963
-1.445604	-7.098473	-4.014917
-2.675612	-7.384572	-2.940401
-2.591812	-2.207055	3.276023
-3.528549	-0.949611	2.984731
-0.533515	-7.917787	-1.368620
0.378266	-7.564679	-0.156572
-3.514324	0.712966	5.156426
-4.719173	-0.242814	4.855607
0.662747	7.508722	-4.850801
-0.198132	6.089590	-4.708079
-5.580934	-5.515918	-1.021452
-5.198839	-4.995738	-2.551234
-6.156990	2.218061	-2.014671
-6.516882	2.050566	-0.475824

-7.817086	3.065356	1.342100
-7.410881	1.596482	1.649838
-3.284031	-1.250568	-3.871620
-4.500962	-1.597851	-2.957798
8.006165	4.312957	3.371736
7.463097	4.354367	4.960558
5.262981	4.083299	8.506506
5.351370	3.097381	7.264183
1.368179	2.696439	-2.015946
2.878879	2.267330	-2.085452
-3.046682	1.396912	-2.299266
-4.108100	2.168169	-1.536966
1.380536	-0.971494	-8.970916
1.922087	-1.798169	-7.738620
-5.496965	-2.818320	-6.710280
-4.550019	-2.371487	-5.518817
0.028667	-4.131111	-1.361783
0.574689	-5.595480	-1.381195
-4.717886	2.279226	2.155503
-3.245433	2.092962	1.657109
1.654251	0.769998	-6.629664
0.903221	0.484579	-5.261997
4.652921	-0.329111	7.649447

5.042795	-0.939097	6.311321
-1.966195	1.502516	0.060712
-0.908163	0.708937	1.149307
3.219448	-5.884500	3.969437
3.569234	-5.841175	5.437427
3.814655	1.091820	5.759165
3.313532	2.622587	5.774203
0.882718	-0.801383	-1.792510
1.840919	-1.748682	-1.033274
-3.987132	4.484816	0.440418
-3.547909	6.060735	0.349300
-1.044043	-0.000483	-3.110634
-1.717320	-0.790901	-1.952429
-2.087775	-3.183482	-2.084964
-0.993470	-3.814664	-3.111973
-2.674253	-4.369790	-6.667000
-1.361445	-3.810138	-6.048031
-0.532608	4.721178	1.538666
-0.580494	3.094884	1.483403
2.585663	-3.857473	4.452604
2.336514	-2.649367	5.488712
5.604489	-0.086901	-1.428116
4.990821	-1.537091	-1.184410

```
4.397233  0.949689  3.786027
4.066172  -0.365909  2.988001
1.697469  4.069185  2.178539
2.699657  5.226274  1.652192
METADYNAMICS COLLECTIVE VARIABLES
DEFINE VARIABLES
3
BNSWT 1  3  8  24  2.80  SCF  1.0  KCV  10.0  MCV  500
COOR_RF  INDAT  4  91  6  14  1.40  SCF  8.0  KCV  1.0  MCV  500
COOR_RF  INDAT  3  91  6  14  1.60  SCF  6.0  KCV  5.0  MCV  500
END DEFINE
METASTEPNUM
16000
HILLS  SHIFT  RCUT  2.0  1.0  =  0.03  0.001
LAGRANGE  TEMPERATURE
150
LAGRANGE  TEMPCONT
150  150
MAXSTEPNUM  INTERMETA
500
MINSTEPNUM  INTERMETA
400
METASTORE  [NO TRAJECTORY]
```

```
10  5  10000

MOVEMENT  CHECK

0.00015D0

MONITOR

400

END  METADYNAMICS

& END
```

Bibliography

[1] P. P. Kumar, A. G. Kalinichev, and R. J. Kirkpatrick. Dissociation of carbonic acid: gas phase energetics and mechanism from ab initio metadynamics simulations. *J. Chem. Phys.*, 126:204315, 2007.

[2] A. Stirling and I. Papai. H_2CO_3 forms via HCO_3^- in water. *J. Phys. Chem. B*, 114(50):16854–16859, 2010.

[3] X. Liu, X. Lu, R. Wang, and H. Zhou. In silico calculation of acidity constants of carbonic acid conformers. *J. Phys. Chem. A*, 114(49):12914–12917, 2010.

[4] P. M. Haugan and H. Drange. Sequestration of CO_2 in the deep ocean by shallow injection. *Nature*, 357:318–20, 1992.

[5] W. Hage, K. R. Liedl, A. Hallbrucker, and E. Mayer. Carbonic acid in the gas phase and its astrophysical relevance. *Science*, 279(5355):1332–1335, 1998.

[6] H. A. Al-Hosney and V. H. Grassian. Carbonic acid: an important intermediate in the surface chemistry of calcium carbonate. *J. Am. Chem. Soc.*, 126 (26):8068–8069, 2004.

[7] A. Ridgwella and R. E. Zeebeb. The role of the global carbonate cycle in the regulation and evolution of the earth system. *Earth and Planetary Science Letters*, 234:299–315, 2005.

[8] O. Hoegh-Guldberg, P. J. Mumby, A. J. Hooten, R. S. Steneck, P. Greenfield, E. Gomez, C. D. Harvell, P. F. Sale, A. J. Edwards, K. Caldeira, N. Knowlton, C. M. Eakin, R. Iglesias-Prieto, N. Muthiga, R. H. Bradbury, A. Dubi, and M. E. Hatziolos. Coral reefs under rapid climate change and ocean acidification. *Science*, 318:1737–1742, 2007.

[9] J. C. Orr, V. J. Fabry, O. Aumont, L. Bopp, S. C. Doney, R. A. Feely, A. Gnanadesikan, N. Gruber, A. Ishida, F. Joos, R. M. Key, K. Lindsay, E. Maier-Reimer, R. Matear, P. Monfray, A. Mouchet, R. G. Najjar, G.-K. Plattnerand, K. B. Rodgers, C. L. Sabine, J. L. Sarmiento, R. Schlitzer, R. D. Slater, I. J. Totterdell, M.-F. Weirig, Y. Yamanaka, and A. Yool. Anthropogenic ocean acidification over the twenty-first century and its impact on calcifying organisms. *Nature*, 437(26):681–686, 2005.

[10] S. Solomon, D. Qin, M. Manning, Z. Chem, M. Marquis, K. B. Averryt, M. Tignor, and H. L. Millers. IPCC, 2007: Summary for policymakers. In: climate change 2007: the physical science basis. Contribution of working Group I to the fourth assessment report of the intergovernmental panel on climate change. Technical report, Intergovernmental Panel on Climate Change, 2007.

[11] I. Kurtz, J. Kraut, V. Ornekian, and M. K. Nguyen. Acid-base analysis: A critique of the stewart and bicarbonate-centered approaches. *Am. J. Physiol.*

Renal. Physiol., 294:F1009–F1031, 2008.

[12] D. Kikeri, M. L. Zeidel, B. J. Ballermann, B. M. Brenner, and S. C. Hebert. pH Regulation and response to AVP in A10 cells differ markedly in the presence vs. absence of $CO_2 \cdots HCO_3^-$. *Am. J. Physiol. Cell Physiol.*, 259:C471–C483, 1990.

[13] D. N. Silverman and R. McKenna. Solvent-mediated proton transfer in catalysis by carbonic anhydrase. *Acc. Chem. Res.*, 40(8):669–675, 2007.

[14] H. S. Harned and R. Davis. The ionization constant of carbonic acid in water and the solubility of carbon dioxide in water and aqueous salt solutions from 0 to 50 degree. *J. Am. Chem. Soc.*, 65(10):2030–2037, 1943.

[15] T. Shedlovsky and D. A. MacInnes. The first ionization constant of carbonic acid, 0 to 38 degree, from conductance measurements. *J. Am. Chem. Soc.*, 57 (9):1705–1710, 1935.

[16] D. A. MacInnes and D. Belcher. The thermodynamic ionization constants of carbonic acid. *J. Am. Chem. Soc.*, 55(7):2630–2646, 1933.

[17] A. L. Soli and R. H. Byrne. CO_2 system hydration and dehydration kinetics and the equilibrium CO_2/H_2CO_3 ratio in aqueous NaCl solution. *Mar. Chem.*, 78(2-3):65–73, 2002.

[18] K. Adamczyk, M. Premont-Schwarz, D. Pines, E. Pines, and E. T. J. Nibbering. Real-time observation of carbonic acid formation in aqueous solution. *Science*, 326:1690–1694, 2009.

[19] T. Mori, K. Suma, Y. Sumiyoshi, and Y. Endo. Spectroscopic detection of isolated carbonic acid. *J. Chem. Phys.*, 130:204308, 2009.

[20] T. Mori, K. Suma, Y. Sumiyoshi, and Y. Endo. Spectroscopic detection of most stable carbonic acid, cis-cis H_2CO_3. *J. Chem. Phys.*, 134:044319, 2011.

[21] J. A. Tossell. Boric acid, carbonic acid, and N-containing oxyacids in aqueous solution: ab initio studies of structure, pKa, NMR shifts, and isotopic fractionations. *Geochimica et Cosmochimica Acta.*, 69(24):5647–5658, 2005.

[22] M. Eigen, K. Kustin, and G. Maass. Die geschwindigkeit der hydratation von SO_2 in wassriger losung. *Zeitschrift fr Physikalische Chemie*, 30:130–136, 1961.

[23] G. A. Mills and H. C. Urey. The kinetics of isotopic exchange between carbon dioxide, bicarbonate ion, carbonate ion and water. *J. Am. Chem. Soc.*, 62: 1019, 1940.

[24] F. J. W. Roughton. The kinetics and rapid thermochemistry of carbonic acid. *J. Am. Chem. Soc.*, 63:2930, 1941.

[25] C. Ho and J. M. Sturtevant. The kinetics of the hydration of carbon dioxide at 25 degree. *J. Biol. Chem.*, 238:3499, 1963.

[26] B. H. Gibbons and J. T. Edsall. Rate of hydration of carbon dioxide and dehydration of carbonic acid at 25 degree. *J. Biol. Chem.*, 238:3502, 1963.

[27] M. J. Welch, J. F. Lifton, and J. A. Seck. Tracer studies with radioactive oxygen-15. Exchange between carbon dioxide and water. *J. Phys. Chem.*, 73: 3351, 1969.

[28] Y. Pocker and D. W. Bjorquist. Stopped-flow studies of carbon dioxide hydration and bicarbonate dehydration in water and water-D2. Acid-base and metal ion catalysis. *J. Am. Chem. Soc.*, 99:6537, 1977.

[29] J. F. Marlier and M. H. O. Leary. Carbon kinetic isotope effects on the hydration of carbon dioxide and the dehydration of bicarbonate ion. *J. Am. Chem. Soc.*, 106:5054, 1984.

[30] X. Wang, W. Conway, R. Burns, N. McCann, and M. Maeder. Comprehensive study of the hydration and dehydration reactions of carbon dioxide in aqueous solution. *J. Phys. Chem. A*, 114:1734–1740, 2010.

[31] C. A. Wight and A. I. Boldyrev. Potential energy surface and vibrational frequencies of carbonic acid. *J. Phys. Chem.*, 99(32):12125–12130, 1995.

[32] M. T. Nguyen, G. Raspoet, and L. G. Vanquickenborne. How many water molecules are actively involved in the neutral hydration of carbon dioxide? *J. Phys. Chem. A*, 101(40):7379–7388, 1997.

[33] T. Loerting, C. S. Tautermann, R. T. Kroemer, I. Kohl, A. Hallbrucker, E. Mayer, and K. R. Liedl. On the surprising kinetic stability of carbonic acid (H_2CO_3). *Angew. Chem. Int. Ed. Engl.*, 39:891–894, 2000.

[34] C. S. Tautermann, A. F. Voegele, T. Loerting, I. Kohl, A. Hallbrucker, E. Mayer, and K. R. Liedl. Towards the experimental decomposition rate

of carbonic acid (H_2CO_3) in aqueous solution. *Chem.-A Eur. J.*, 8:66–73, 2002.

[35] K. Leung, I. M. B. Nielsen, and I. Kurtz. Ab initio molecular dynamics study of carbon dioxide and bicarbonate hydration and the nucleophilic attack of hydroxide on CO_2. *J. Phys. Chem. B*, 111:4453–4459, 2007.

[36] M. T. Nguyen, M. H. Matus, V. E. Jackson, V. T. Ngan, J. R. Rustad, and D. A. Dixon. Mechanism of the hydration of carbon dioxide: direct participation of H_2O versus microsolvation. *J. Phys. Chem. A*, 112:10386–10398, 2008.

[37] P. P. Kumar, A. G. Kalinichev, and R. J. Kirkpatrick. Hydrogen-bonding structure and dynamics of aqueous carbonate species from Car-Parrinello molecular dynamics simulations. *J. Phys. Chem. B*, 113:794–802, 2009.

[38] A. Stirling. HCO_3^- formation from CO_2 at high pH: ab initio molecular dynamics study. *J. Phys. Chem. B*, 115(49):14683–14687, 2011.

[39] M. Mucha, T. Frigato, L. M. Levering, H. C. Allen, D. J. Tobias, L. X. Dang, and P. Jungwirth. Unified molecular picture of the surfaces of aqueous acid, base, and salt solutions. *J. Phys. Chem. B*, 109(16):7617–7623, 2005.

[40] M. Subir, J. Liu, and K. B. Eisenthal. Protonation at the aqueous interface of polymer nanoparticles with second harmonic generation. *J. Phys. Chem. C*, 112(40):15809–15812, 2008.

[41] N. E. Levinger, L. C. Rubenstrunk, B. Baruah, and D. C. Crans. Acidification of reverse micellar nanodroplets by atmospheric pressure CO_2. *J. Am. Chem. Soc.*, 133(18):7205–7214, 2011.

[42] E. S. Shamay, V. Buch, M. Parrinello, and G. L. Richmond. At the water's edge: nitric acid as a weak acid. *J. Am. Chem. Soc.*, 129(43):12910–12911, 2007.

[43] T. Lewis, B. Winter, A. C. Stern, M. D. Baer, C. J. Mundy, D. J. Tobias, and J. C. Hemminger. Does nitric acid dissociate at the aqueous solution surface? *J. Phys. Chem. C*, 115(43):21183–21190, 2011.

[44] J. Bernard, M. Seidl, E. Mayer, and T. Loerting. Formation and stability of bulk carbonic acid (H_2CO_3) by protonation of tropospheric calcite. *ChemPhysChem*, 13(13):3087–3091, 2012.

[45] L. Turi, W.-S. Sheu, and P. J. Rossky. Characterization of excess electrons in water-cluster anions by quantum simulations. *Science*, 309(5736):914–917, 2005.

[46] T. Frigato, J. VandeVondele, B. Schmidt, C. Schutte, and P. Jungwirth. Ab initio molecular dynamics simulation of a medium-sized water cluster anion: From an interior to a surface-located excess electron via a delocalized state. *J. Phys. Chem. A*, 112(27):6125–6133, 2008.

[47] A. E. Bragg, J. R. R. Verlet, A. Kammrath, O. Cheshnovsky, and D. M. Neumark. Hydrated electron dynamics: From clusters to bulk. *Science*, 306 (5696):669–671, 2004.

[48] R. Ludwig. Water: From clusters to the bulk. *Angew. Chem. Int. Ed. Engl.*, 40(10):1808–1827, 2001.

[49] J. V. Coe. Fundamental properties of bulk water from cluster ion data. *Int. Rev. Phy. Chem.*, 20(1):33–58, 2001.

[50] U. Buck and F. Huisken. Infrared spectroscopy of size-selected water and methanol clusters. *Chem. Rev.*, 100(11):3863–3890, 2000.

[51] I. K. Ortega, A. *Määttänen*, T. Kurtén, and H. Vehkamäki. Carbon dioxide-water clusters in the atmosphere of mars. *Comput. and Theor. Chem.*, 965 (2):353–358, 2011.

[52] V.-A. Glezakou, R. Rousseau, L. X. Dang, and B. P. McGrail. Structure, dynamics and vibrational spectrum of supercritical CO_2/H_2O mixtures from ab initio molecular dynamics as a function of water cluster formation. *Phys. Chem. Chem. Phys.*, 12(31):8759–8771, 2010.

[53] A. R. Ravishankara. Heterogeneous and multiphase chemistry in the troposphere. *Science*, 276:1058, 1997.

[54] T. L. Tarbuck and G. L. Richmond. Adsorption and reaction of CO_2 and SO_2 at a water surface. *J. Am. Chem. Soc.*, 128(10):3256–3267, 2006.

[55] V. Vaida. Perspective: Water cluster mediated atmospheric chemistry. *J. Chem. Phys.*, 135:020901, 2011.

[56] C. E. Kolb, R. A. Cox, J. P. D. Abbatt, M. Ammann, E. J. Davis, D. J. Donaldson, B. C. Garrett, C. George, P. T. Griffiths, D. R. Hanson, M. Kulmala,

G. McFiggans, U. Poschl, I. Riipinen, M. J. Rossi, Y. Rudich, P. E. Wagner, P. M. Winkler, D. R. Worsnop, and C. D. O Dowd. An overview of current issues in the uptake of atmospheric trace gases by aerosols and clouds. *Atmos. Chem. Phys.*, 10:10561, 2010.

[57] Y. Miller, J. L. Thomas, D. D. Kemp, B. J. Finlayson-Pitts, M. S. Gordon, D. J. Tobias, and R. B. Gerber. Structure of large nitrate−water clusters at ambient temperatures: Simulations with effective fragment potentials and force fields with implications for atmospheric chemistry. *J. Phys. Chem. A*, 113(46):12805–12814, 2009.

[58] M. Galib and G Hanna. Mechanistic insights into the dissociation and decomposition of carbonic acid in water via the hydroxide route: an ab initio metadynamics study. *J. Phys. Chem. B*, 115(50):15024–15035, 2011.

[59] M. I. H. Panhuis, C. H. Patterson, and R. M. Lynden-Bell. A molecular dynamics study of carbon dioxide in water: diffusion, structure and thermodynamics. *Mol. Phys.*, 94:963, 1998.

[60] T. Somasundaram, M. I. H. Panhuis, R. M. Lynden-Bell, and C. H. Patterson. A simulation study of the kinetics of passage of CO_2 and N_2 through the liquid/vapor interface of water. *J. Chem. Phys.*, 111:2190, 1999.

[61] T. Somasundaram, R. M. Lynden-Bell, and C. H. Patterson. The passage of gases through the liquid water/vapour interface: a simulation study. *Phys. Chem. Chem. Phys.*, 1:143, 1999.

[62] K. A. Sparks, J. W. Tester, Z. Cao, and B. L. Trout. Configurational properties of water clathrates: A monte carlo and multidimensional integration versus the lennard−jones and devonshire approximation. *J. Phys. Chem. B*, 103:6300, 1999.

[63] A. Demurov, R. Radhakrishnan, and B. L. Trout. Computations of diffusivities in ice and CO_2 clathrate hydrates via molecular dynamics and Monte Carlo simulations. *J. Chem. Phys.*, 116:702, 2002.

[64] R. Radhakrishnan and B. L. Trout. A new approach for studying nucleation phenomena using molecular simulations: application to CO_2 hydrate clathrates. *J. Chem. Phys.*, 117:1786, 2002.

[65] R. Radhakrishnan and B. L. Trout. Nucleation of crystalline phases of water in homogeneous and inhomogeneous environments. *Phys. Rev. Lett.*, 90:158301, 2003.

[66] S. R. P. da Rocha, K. P. Johnston, R. E. Westacott, and P. J. Rossky. Molecular structure of the water-supercritical CO_2 interface. *J. Phys. Chem. B*, 105:12092, 2001.

[67] S. R. P. da Rocha, K. P. Johnston, and P. J. Rossky. Surfactant−modified CO_2-water interface: a molecular view. *J. Phys. Chem. B*, 106:13250, 2002.

[68] H. Zhang and S. J. Singer. Analysis of the subcritical carbon dioxide−water interface. *J. Phys. Chem. A*, 115(23):6285–6296, 2011.

[69] D. Frenkel and B. Smit. *Understanding Molecular Simulation: from Algorithms to Applications*, volume 1. Academic press, 2001.

[70] D. C. Rapaport. *The Art of Molecular Dynamics Simulation.* Cambridge university press, 2004.

[71] L. Monticelli and D. P. Tieleman. Force fields for classical molecular dynamics. In *Biomolecular Simulations*, pages 197–213. Springer, 2013.

[72] C. J. Cramer. *Essentials of Computational Chemistry: Theories and Models.* John Wiley and Sons, 2013.

[73] D. Marx and J. Hutter. Ab initio molecular dynamics: Theory and implementation. *Modern methods and algorithms of quantum chemistry*, 1:301–449, 2000.

[74] M. E. Tuckerman. Ab initio molecular dynamics: Basic concepts, current trends and novel applications. *J. Phys. Cond. Matt.*, 14(50):R1297, 2002.

[75] B. Kirchner, P. J. di Dio, and J. Hutter. Real-world predictions from ab initio molecular dynamics simulations. In *Multiscale Molecular Methods in Applied Chemistry*, pages 109–153. Springer, 2012.

[76] R. Car and M. Parrinello. Unified approach for molecular dynamics and density-functional theory. *Phys. Rev. Lett.*, 55:2471–2474, 1985.

[77] A. Laio and M. Parrinello. Escaping free-energy minima. *Proc. Natl. Acad. Sci. USA*, 99:12562, 2002.

[78] C. Micheletti, A. Laio, and M. Parrinello. Reconstructing the density of states by history-dependent metadynamics. *Phys. Rev. Lett.*, 92:170601, 2004.

[79] B. Ensing, A. Laio, M. Parrinello, , and M. L. Klein. A recipe for the computation of the free energy barrier and the lowest free energy path of concerted reactions. *J. Phys. Chem. B*, 109(4):6676–6687, 2005.

[80] M. Iannuzzi, A. Laio, and M. Parrinello. Efficient exploration of reactive potential energy surfaces using Car-Parrinello molecular dynamics. *Phys. Rev. Lett.*, 90(23):238302, 2003.

[81] R. Martonak, A. Laio, M. Bernasconi, C. Ceriani, P. Raiteri, F. Zipoli, and M. Parrinello. Simulation of structural phase transitions by metadynamics. *Zeitschrift far Kristallographie*, 220:489–498, 2005.

[82] A. Laio and F. L. Gervasio. Metadynamics: A method to simulate rare events and reconstruct the free energy in biophysics, chemistry and material science. *Rept. Prog. Phys.*, 71:126601–126622, 2008.

[83] *CPMD V3.13.2.* Copyright IBM Corp 1990-2008, Copyright MPI fur Festkorperforschung Stuttgart 1997-2001. URL `http://www.cpmd.org/`.

[84] H. J. C. Berendsen, J. P. M. Postma, W. F. V. Gunsteren, and J. Hermans. In B. Pullman, editor, *Intermolecular Forces*, chapter Interaction models for water in relation to protein hydration, pages 331–342. Reidel, Dordrecht, 1981.

[85] S. L. Mayo, B. D. Barry D. Olafson, and W. A. Goddard. Dreiding: a generic force field for molecular simulations. *J. Phys. Chem.*, 94(26):8897–8909, 1990.

[86] A. D. Becke. Density-functional exchange-energy approximation with correct asymptotic behavior. *Phys. Rev. A*, 38(6):3098–3100, 1988.

[87] C. Lee, W. Yang, and R. G. Parr. Development of the colle-salvetti correlation-energy formula into a functional of the electron density. *Phys. Rev. B*, 37(2): 785–789, 1988.

[88] D. Vanderbilt. Soft self-consistent pseudopotentials in a generalized eigenvalue formalism. *Phys. Rev. B*, 41(11):7892–7895, 1990.

[89] K. Laasonen, A. Pasquarello, R. Car, C. Lee, and D. Vanderbilt. Car-Parrinello molecular dynamics with vanderbilt ultrasoft pseudopotentials. *Phys. Rev. B*, 47(16):10142–10153, 1993.

[90] G. Bussi, A. Laio, and M. Parrinello. Equilibrium free energies from nonequilibrium metadynamics. *Phys. Rev. Lett.*, 96:090601, 2006.

[91] B. Metz, O. R. Davidson, P. R. Bosch, R. Dave, and L. A. Meyer. IPCC, 2007: summary for policymakers. In: climate change 2007: the physical science basis. Contribution of working group III to the fourth assessment report of the intergovernmental panel on climate change. Technical report, Intergovernmental Panel on Climate Change, 2007.

[92] J. K. Terlouw, C. B. Lebrilla, and H. Schwarz. Thermolysis of $NH_4HCO_3^-$ a simple route to the formation of free carbonic acid (H_2CO_3) in the gas phase. *Angew. Chem. Int. Ed. Engl.*, 26:354–355, 1987.

[93] R. Ludwig and A. Kornath. In spite of the chemist's belief: carbonic acid is surprisingly stable. *Angew. Chem. Int. Ed. Engl.*, 39:1421–1423, 2000.

[94] P. L. Geissler, C. Dellago, D. Chandler, J. Hutter, and M. Parrinello. Autoionization in liquid water. *Science*, 291:2121–2124, 2001.

[95] J.-G. Lee, E. Asciutto, V. Babin, C. Sagui, T. Darden, and C. Roland. Deprotonation of solvated formic acid: Car-Parrinello and metadynamics simulations. *J. Phys. Chem. B*, 110:2325–2331, 2006.

[96] J. M. Park, A. Laio, M. Iannuzzi, and M. Parrinello. Dissociation mechanism of acetic acid in water. *J. Am. Chem. Soc.*, 128:11318–11319, 2006.

[97] K. E. Laasonen and M. L. Klein. Ab initio study of aqueous hydrochloric acid. *J. Phys. Chem. A*, 101(01):98–102, 1997.

[98] S. Raugei and M. L. Klein. Dynamics of water molecules in the Br^- solvation shell: an ab initio molecular dynamics study. *J. Am. Chem. Soc.*, 123(38): 9484–9485, 2001.

[99] D. Kim and M. L. Klein. Liquid hydrogen fluoride with an excess proton: ab initio molecular dynamics study of a superacid. *J. Am. Chem. Soc.*, 121(48): 11251–11252, 1999.

[100] V. Thomas, P. Maurer, and R. Iftimie. On the formation of proton-shared and contact ion pair forms during the dissociation of moderately strong acids: an ab initio molecular dynamics investigation. *J. Phys. Chem. B*, 114:8147–8155, 2010.

[101] E. Schwegler, J. C. Grossman, F. Gygi, and G. Galli. Towards an assessment of the accuracy of density functional theory for first principles simulations of water. ii. *J. Chem. Phys.*, 121(11):5400–5409, 2004.

[102] M. Galib and G. Hanna. The Role of hydrogen bonding in the decomposition of H_2CO_3 in water: mechanistic insights from ab initio metadynamics studies of aqueous clusters. *J. Phys. Chem. B*, 118(22):5983–5993, 2014.

[103] R. J. Buszek, J. S. Francisco, and J. M. Anglada. Water effects on atmospheric reactions. *Int. Rev. Phys. Chem.*, 30(3):335–369, 2011.

[104] K. R. Leopold. Hydrated acid clusters. *Ann. Rev. Phys. Chem.*, 62:327–349, 2011.

[105] T. Salmi, N. Runeberg, L. Halonen, J. R. Lane, and H. G. Kjaergaard. Computational vibrational and electronic spectroscopy of the water nitric oxide complex. *J. Phys. Chem. A*, 114(14):4835–4842, 2010.

[106] M. A. Allodi, M. E. Dunn, J. Livada, K. N. Kirschner, and G. C. Shields. Do hydroxyl radical-water clusters, $OH(H_2O)_n$, $n = 1$-5, exist in the atmosphere? *J. Phys. Chem. A*, 110(49):13283–13289, 2006.

[107] S. Aloisio, P. E. Hintze, and V. Vaida. The hydration of formic acid. *J. Phys. Chem. A*, 106(2):363–370, 2002.

[108] G. G. Erin, L. J. Kaushik, F. R. J. Michael, C. T. D. Adri, and J. A. W. Castleman. Effect of formic acid addition on water cluster stability and structure. *J. Phys. Chem. A*, 115(18):4657–4664, 2011.

[109] K. H. Weber, F. J. Morales, and F.-M. Tao. Theoretical study on the structure and stabilities of molecular clusters of oxalic acid with water. *J. Phys. Chem. A*, 116(47):11601–11617, 2012.

[110] A. D. Hammerich, B. J. Finlayson-Pitts, and R. B. Gerber. NOx reactions on aqueous surfaces with gaseous HCl: formation of a potential precursor to atmospheric Cl atoms. *J. Phys. Chem. Letters*, 3(23):3405–3410, 2012.

[111] R. Bianco, S. Wang, and J. T. Hynes. Theoretical study of the first acid dissociation of H_2SO_4 at a model aqueous surface. *J. Phys. Chem. B*, 109 (45):21313–21321, 2005.

[112] R. Bianco, S. Wang, and J. T. Hynes. Theoretical study of the dissociation of nitric acid at a model aqueous surface. *J. Phys. Chem. A*, 111(43):11033–11042, 2007.

[113] I. Smith. Single-molecule catalysis. *Science*, 315(5811):470–471, 2007.

[114] B. Wang and Z. Cao. How water molecules modulate the hydration of CO_2 in water solution: insight from the cluster-continuum model calculations. *J. Comput. Chem.*, 34(5):372–378, 2013.

[115] S. Wang, R. Bianco, and J. T. Hynes. Depth-dependent dissociation of nitric acid at an aqueous surface: Car-Parrinello molecular dynamics. *J. Phys. Chem. A*, 113(7):1295–1307, 2009.

[116] M. T. Nguyen, M. H. Matus, V. E. Jackson, V. T. Ngan, J. R. Rustad, and D. A. Dixon. Mechanism of the hydration of carbon dioxide: direct participation of H_2O versus microsolvation. *J. Phys. Chem. A*, 112(41):10386–10398, 2008.

[117] P. G. Blower, E. Shamay, L. Kringle, S. T. Ota, and G. L. Richmond. Surface behavior of malonic acid adsorption at the air/water interface. *J. Phys. Chem. A*, 117(12):2529–2542, 2013.

[118] P. G. Blower, S. T. Ota, N. A. Valley, S. R. Wood, and G. L. Richmond. Sink or surf: atmospheric implications for succinic acid at aqueous surfaces. *J. Phys. Chem. A*, 117(33):7887–7903, 2013.

[119] K. F. Wissbrun, D. M. French, and A. Patterson. The true ionization constant of carbonic acid in aqueous solution from 5 to 45 degree. *J. Phys. Chem.*, 58 (9):693–695, 1954.

[120] Since the simulation box was $11.4\times11.4\times28.4$ Å^3 with periodic boundary conditions in the x and y directions, the maximum meaningful distance for the RDF is approximately $\sqrt{[(11.4/2)^2 + (11.4/2)^2]} = 8.06$ Å. Therefore, all RDFs were truncated at this distance.

[121] J. T. Wootton, C. A. Pfister, and J. D. Forester. Dynamic patterns and ecological impacts of declining ocean pH in a high-resolution multi-year dataset. *Proc. Natl. Acad. Sci. U.S.A.*, 105:18848, 2008.

[122] R. A. Feely, C. L. Sabine, K. Lee, W. Berelson, J. Kleypas, V. J. Fabry, and F. J. Millero. Impact of anthropogenic CO_2 on the $CaCO_3$ system in the oceans. *Science*, 305:362, 2004.

[123] C. L. Sabine, N. Feely, R. A.and Gruber, R. M. Key, K. Lee, J. L. Bullister, R. Wanninkhof, C. S. Wong, D. W. R. Wallace, B. Tilbrook, F. J. Millero,

T. H. Peng, A. Kozyr, T. Onon, and A. F. Rios. The oceanic sink for anthropogenic CO_2. *Science*, 305:367, 2004.

[124] M. Heimann and M. Reichstein. Terrestrial ecosystem carbon dynamics and climate feedbacks. *Nature*, 451:289, 2008.

[125] T. Takahashi. The fate of industrial carbon dioxide. *Science*, 305:352, 2004.

[126] S. Solomon, G. K. Plattner, R. Knutti, and P. Friedlingstein. Irreversible climate change due to carbon dioxide emissions. *Proc. Natl. Acad. Sci. U.S.A.*, 106:1704, 2009.

[127] K. L. Lackner. Carbonate chemistry for sequestering fossil carbon. *Ann. Rev. Energy Environ.*, 27:193, 2002.

[128] O. Hoegh-Guldberg, P. J. Mumby, A. J. Hooten, R. S. Steneck, P. Greenfield, E. Gomez, C. D. Harvell, P. F. Sale, A. J. Edwards, K. Caldeira, N. Knowlton, C. M Eakin, R. Iglesias-Prieto, N. Muthiga, R. H. Bradbury, A. Dubi, and M. E. Hatziolos. Coral reefs under rapid climate change and ocean acidification. *Science*, 318:1737, 2007.

[129] S. Lindskog. Structure and mechanism of carbonic anhydrase. *Pharmacol. Ther.*, 74:1, 1997.

[130] D. W. Christianson and C. A. Fierke. Carbonic anhydrase: Evolution of the zinc binding site by nature and by design. *Acc. Chem. Res.*, 29:331, 1996.

[131] D. N. Silverman and R. McKenna. Solvent-mediated proton transfer in catalysis by carbonic anhydrase. *Acc. Chem. Res.*, 40:669, 2007.

[132] F. Lehmkuhler, M. Paulus, C. Sternemann, D. Lietz, F. Venturini, C. Gutt, and M. Tolan. The carbon dioxide−water interface at conditions of gas hydrate formation. *J. Am. Chem. Soc.*, 131(2):585–589, 2009.